

Development of a Thermally Sprayed Electro-thermal Anti-icing System for In-flight Ice Mitigation

Nima Hamed Nohbaradaran

**A Thesis in The Department of Mechanical, Industrial and Aerospace
Engineering**

**Presented in Partial Fulfillment of the Requirements for the Degree of
Master of Applied Science (Mechanical Engineering) Concordia University
Montreal, Quebec, Canada**

April 2022

©Nima Hamed Nohbaradaran, 2022

CONCORDIA UNIVERSITY
School of Graduate Studies

This is to certify that the thesis prepared

By: Nima Hamed Nohbaradaran

Entitled: Development of a Thermally Sprayed Electro-thermal Anti-icing
System for In-flight Ice Mitigation

and submitted in partial fulfillment of the requirements for the degree of

Master of Arts (Educational Technology)

complies with the regulations of the University and meets the accepted standards with respect to originality and quality.

Signed by the final Examining Committee:

_____Chair

Prof. Martin D. Pugh

_____Examiner

Dr. Pantcho P. Stoyanov

_____Supervisor

Prof. Ali Dolatabadi

_____Supervisor

Prof. Christian Moreau

Approved by _____

Professor Martin D. Pugh

November 2021

Professor Mourad Debbabi

ABSTRACT

Development of a Thermally Sprayed Electro-thermal Anti-icing System for In-flight Ice Mitigation

Nima Hamed Nohbaradaran

Ice formation and accumulation cause many inconveniences in daily routine. Drawbacks in infrastructures such as road structure, overhead telecommunication, wind turbines, and transportation are examples of icing consequences. In-flight icing, for instance, can bring about severe aerodynamic and mechanical problems. Formation, adhesion, and accumulation of ice disfigure the airflow on the aircraft's critical aerodynamic surfaces, decreasing the lift and increasing the drag force, and causing undesired circumstances. Hence, significant efforts have been devoted to developing methods to mitigate icing problems, including anti-icing, and deicing strategies. There are three types of ice protection systems, including passive, active, and hybrid systems frequently used in anti-icing mode, deicing mode, or both. Several inadequacies in these methods encourage researchers to investigate the feasibility of developing more efficient and reliable ice-opposing systems. Accordingly, based on the literature, designing, and producing efficient ice protection systems are needed, especially regarding safety, energy consumption, cost-efficiency, and long-lasting performance. The present work aims to study a specific active ice protection system fabricated by a thermal spray technique (electro-thermal heating) in harsh icing conditions. Moreover, this work will study this ice protection system's performance by integrating it into a unique architecture (empowering efficiency). Also, this work aims to briefly study performance of a passive ice protection system (nano-textured superhydrophobic coating) in anti-icing performance. Plasma spray technique as a versatile and cost-effective surface modification alternative is used as the manufacturing method in this study. Several coatings are developed and studied during this project to determine the most promising materials, processes, and parameters achieving the optimized active ice-mitigation system. Furthermore, the functionality of the established system is assessed using an icing wind tunnel. Besides, challenges and solutions for improving the desired performance of to-be-heated surfaces are discussed.

Acknowledgement

First and foremost, I would like to express my special thanks to Prof. Ali Dolatabadi and Prof. Christian Moreau, my amazing supervisors, for their assistance, ideas, feedback, and financial support during my MASc program. Without their help, this work would never have been possible. Their contribution to my life expands beyond their invaluable scientific input and academic advice. I learned from them inspiring lessons of professionalism, commitment, creativity, and compassion, among many other things.

Secondly, It is a great pleasure for me to acknowledge Green-SEAM network for supporting and providing me with the opportunity pursuing an outstanding research during my MASc program.

I am immensely thankful to my great friends in the Thermal Spray and Multi-phase Flow lab group, especially Dr. Navid Sharifi, Dr. Fadhel Ben Ettouil, Gilles Huard, Dr. Ali Akbarnouzari, Dr. Mehdi Jadidi, Robert Oliver, Alireza Rahimi, and Mazen Samara. I sincerely appreciate their helpfulness and willingness to provide helpful information for this study.

I am incredibly grateful to my lovely wife, Neshat, because this work could not have been completed without her endless understanding, patience, and encouragement, and I am fortunate to share my life with her. I appreciate her sacrifices for me.

I am forever indebted to my mom, Tahereh, my dad, Reza, and my brothers Navid and Farid for their unconditional love and ever-lasting support.

I wish to extend my sincere thanks to my mother-in-law, Mahnaz, and my father-in-law, Jalaladdin, for their love, prayers, and support.

Last but not least, many thanks to my friends Amir Mafinezhad, Mehrdad, Sara, Naghmeh, and Amirhossein, who were always there for me, especially in the most challenging moments.

Contents

List of Figures	vii
List of Tables	x
List of Abbreviations	xi
1 Introduction	1
1.1 In-flight Icing	2
1.2 In-flight Icing Preconditions	3
1.3 Ice Protection Systems	7
1.3.1 Active Ice Protection Methods	8
1.3.2 Passive Ice Protection Methods	10
1.3.3 Multi-functional (Hybrid) Ice Protection Methods	14
2 Literature Review	16
2.1 Background of Active Ice Protection Methods	16
2.1.1 Chemical Ice Protection Techniques	16
2.1.2 Mechanical Ice Protection Methods	18
2.1.3 Thermal Ice Protection Systems	22
2.2 Review of Passive Ice Protection Strategies	27
2.3 Multi-functional (Hybrid) Strategies	29
3 Fabrication Approaches	36
3.1 Thermal Spray Technology	37

3.1.1	Plasma Spray Techniques	38
3.2	Thermal Spray Application for Heater Fabrication	39
3.2.1	Conventional Heating Elements	39
3.2.2	Thermally Sprayed Resistive Heaters	40
4	Research Objectives	42
5	Materials and Methodology	44
5.1	Design and Preparation of Experiment Samples	44
5.1.1	Materials and Types of Equipment Selection	46
5.1.2	Coating Process	47
5.2	Coating Structure and Performance Characterization	49
5.2.1	Structural Imaging and Morphology Characterization	49
5.2.2	Electrical Characterization	49
5.2.3	Surface Temperature Measurement	52
5.2.4	Icing Tests	53
6	Results and Discussion	56
6.1	Coating Fabrication	56
6.1.1	Insulator Layer	57
6.1.2	Resistive Layer	59
6.2	Coating characterization	62
6.3	Electrical characterization	65
6.4	Thermal Analysis	68
6.5	Icing Test	72
6.5.1	Ice Accretion Test	74
6.5.2	Heated Anti-icing Test	76
7	Conclusion and Future Works	91
7.1	Future Works	92
	Bibliography	93

List of Figures

1.1	The importance of surface protection against icing in a broad spectrum of systems [1].	1
1.2	Ice formation in clouds and the subsequent possibility of aircraft icing [12].	5
1.3	(a) Clear, (b) Mixed, (c) Rime icing on airfoils [13].	5
1.4	Overview of strategies and approaches for prevention of ice nucleation and accretion [22].	8
1.5	Surface wettability characteristic [27].	11
1.6	Schematic for wettability of different surface structures [29].	11
1.7	Classification of the three mechanisms applied in development of ice-phobic coatings [18].	13
1.8	Schematic of the different categories of ice-phobic coatings [19].	14
2.1	Schematic of FPD deicing system [44].	18
2.2	Electro-expulsive Deicer located in the wing nose [46].	19
2.3	Impulsive coil in a leading edge (Eddy current) [49].	19
2.4	Ice shattering using the electro-expulsive separation system [23].	20
2.5	Cross-section of a pneumatic deicing boot deflated (top) and inflated (bottom) [52].	21
2.6	Electro-mechanical expulsion deicing system [53].	21
2.7	Ultrasound actuator placed inside the nose of leading edge [54].	22
2.8	Schematic of Engine Bleed Air ice protection method [55].	23
2.9	Illustration of an ETIPS operating in deicing mode [19].	24
2.10	Schematic of the integrated active-passive IPS: (A) thermo-electric heating wire, (B) piezo-electric actuators, and (C) icephobic surface (on the airfoil top surface) [88].	32
2.11	Comparison of various anti/deicing strategies, (a) ice accretion process over the hydrophilic surface, (b) passive strategy with superhydrophobic coating, c) active electro-thermal strategy, and (d) multi-functional ice protection strategy [16].	33

2.12	ICE-WIPS (Hybrid Ice-phobic Coating and Electro-thermal Heating) [90].	34
3.1	Classification of the thermal spray deposition techniques [94].	38
3.2	Schematic of a plasma spray process [95].	39
3.3	Several types of conventional heating elements [59].	40
5.1	Schematic representation of the designed cylindrical samples for the experiments.	45
5.2	Photomicrographs of (a) Metco 202NS and (b) Metco Amdry 9700 [101].	46
5.3	Schematic of the plasma spray process [102].	48
5.4	Plasma spray process equipment.	48
5.5	Schematic of four point probe method [103].	50
5.6	Schematic of designed circuit.	51
5.7	Electrical characterization process equipment.	52
5.8	types of power suppliers used in the experiments.	53
5.9	Schematic of the icing wind tunnel [104].	53
6.1	Major processing parameters that affect the coating microstructure [105].	57
6.2	One sample before and after the deposition of Zirconia layer.	59
6.3	Design of different heating elements.	60
6.4	Schematic of one of the masked samples.	60
6.5	Coated samples with five different geometries.	62
6.6	SEM micrograph of five samples with different width of FeCrAlY coating (figure 6.5).	63
6.7	SEM micrograph of a coated sample.	64
6.8	Voltage vs current for the FeCrAlY coatings.	67
6.9	Temperature profile of the sample coated in three different voltages and three different widths.	71
6.10	Performance test of the FeCrAlY resistive heaters for (a) one, (b) two, and (c) three strips	73
6.11	Schematic of icing wind tunnel test section.	74
6.12	Ice accretion on (a) hydrophilic, and (b) SHS coating.	76
6.13	Schematic of the heat generation circuit.	78
6.14	Required anti-icing power for heating only the middle strip.	79
6.15	Formation of runback ice on the unprotected regions.	79

6.16	Surface temperature while heating only the middle strip under icing condition.	80
6.17	Required anti-icing power for heating two strips.	81
6.18	Required anti-icing power for heating three strips.	82
6.19	Anti-icing performance of heating system with three heaters on.	83
6.20	Surface temperature under icing conditions when (a) one strip, (b) two strips, and (c) three strips are turned on.	84
6.21	Schematic of the prepared sample for the conventional heated anti-icing test.	85
6.22	Test section and the sample holder used in the icing wind tunnel.	86
6.23	Surface temperature while heating: (a) stabilized temperature before water spraying, and (b) stabilized temperature after 15 min of water spraying.	87
6.24	Temperature variation versus time for thermally-sprayed heater and cartridge heating element.	88

List of Tables

1.1	Circumstances for formation of different ice types [12].	6
1.2	In-flight icing risk [11].	6
2.1	Comparison of active ice mitigation techniques [19].	26
2.2	Comparison of ice mitigation techniques [25].	35
5.1	The plasma spray parameters used for the coating of substrates.	47
5.2	Summary of Proposed Methodology.	55
6.1	The plasma spray parameters used for the Zirconia coating.	58
6.2	The plasma spray parameters used for the FeCrAlY coating.	61
6.3	Properties of the (a) Zirconia and (b) FeCrAlY coatings	65
6.4	Electrical properties of the coated samples.	66
6.5	Electrical properties for the coated samples with different geometries.	69
6.6	Effect of applying SHS on the ice accumulation ratio.	75
6.7	Calibration of the power required for electro thermal anti-icing.	86

List of Abbreviations

AOI	Angle Of Impact
LWC	Liquid Water Content
MVD	Mean Volumetric Diameter
SLD	Super-cooled Large Droplets
IPS	Ice Protection System
SHS	Superhydrophobic Surface
SHP	Super-hydrophilic Surface
CA	Contact Angle
SA	Slide Angle
CAH	Contact Angle Hysteresis
FPD	Freezing Point Depressant
ADF	Aircraft Deicing System
AAF	Aircraft Anti-icing System
SPEED	Sonic Pulse Electro Expulsive Deicer
EIDI	Electro Impulsive Deicer
FAA	Federal Aviation Administration

EESS	Electro Expulsive Separation System
EMEDS	Electro Mechanical Expulsion Deicing System
ETIPS	Electro Thermal Ice Protection System
PDMS	Common Silicon Rubber
SAS	Superhydrophobic Surface
SLIPS	Slippery Liquid Infused Porous Surfaces
LE	Leading Edge
APS	Atmospheric Plasma Spray
SPS	Suspension Plasma Spray
SEM	Scanning Electron Microscope
IWT	Icing Wind Tunnel
DOE	Design Of Experiments
FST	Flame Spray Technology
ASTM	American Society of Testing and Materials

Chapter 1

Introduction

Icing is an ever-present phenomenon that undesirably impacts a broad range of daily activities. The inconveniences that the icing incidents bring to our daily routine cause severe problems. Icing can hold back industrial components' operation and decrease mechanisms' efficiency. In reality, its downsides can be seen in the aerospace industry, wind turbine operation, power transmission lines, and other infrastructural and energy systems (some of them can be seen in Figure (1.1)). As a general rule, icing happens when water droplets (usually super-cooled) impinge on a surface and create a deposition or coating of ice on such a surface [1]. For instance, in the aerospace and aviation industry, Ice formation on aircraft's critical aerodynamic surfaces involves or causes unexpected substantial losses or failures for human activities either on the ground or during flight [2]. The present study's primary goal revolves around this topic, which is discussed in the following sections.



Figure 1.1: The importance of surface protection against icing in a broad spectrum of systems [1].

1.1 In-flight Icing

In certain weather conditions, every moving airfoil is prone to icing. Defects on wind turbine blades, aircraft wings, open rotor engine blades, aircraft tail, are some examples of icing consequences. Hence, formation, adhesion, and accumulation of ice on top of unprotected surfaces are undesired occurrences [3]. In-flight icing for instance, can cause severe problems by disturbing the smooth air-flow on the frontal surfaces of an airplane, which increases drag force, and decreases thrust force; consequently, ice build-up brings about a loss in operational efficiency, and degraded safety margins [4]. Increase of drag force and weight requires to add extra power, which itself leads to an increase of the airplane's angle of attack, and even more ice formation is awaited. Ice accumulates on every exposed frontal surface of the airplane, not only on the wings, propeller, and windshield but also on the antennas, vents, intakes, and cowlings. It generates ruthless vibration in antennas and may cause them to break. A lightweight aircraft can become so iced up that it makes a nonstop flight impossible either in slight to severe circumstances. The airplane may stall at much higher speeds and lower angles of attack than usual. It can roll or pitch uncontrollably, and recovery may perhaps be impossible. Ice can also cause engine blockage by icing up the carburetor. Moreover, in the case of a fuel-injected engine, icing blocks the air source of the engine [5]. Icing-related problems associated with aircraft also cause significant losses. For example, in terms of personal injuries and damages, icing incidents cause \$96 million annual economic losses in the USA; moreover, the percentage of icing-related aircraft fatal accidents has been reported as high as 8.2% [6]. Stories are related to icing fall commonly into two categories: ground-level icing and in-flight icing, in which many participants, different regulations, and separate ice protection systems are designated for tackling each type. Concerning icing problems, various alternatives are employed to improve all-weather flying safety, including pre-flight precautions and in-flight courses of action, which comprised of deicing (removal of the ice) and anti-icing (protecting against ice formation) [7]. When super-cooled water droplets (liquid water at temperature below its freezing point) impinge on the airplane's frontal surfaces, ice starts forming and accumulating on the exposed surfaces. Considering airplane's altitude, relative velocity, and surrounding air circumstances, the freezing phenomenon may occur

immediately or after spreading [8]. As a result of successive impingement of super-cooled water droplets, ice accumulates over time and builds up relatively thick ice cover, raising subsequent problems [9].

1.2 In-flight Icing Preconditions

Presence of several key factors are required for aircraft icing to happen, including **Liquid Water Content (LWC)**, **Ambient Temperature** and **Mean Volumetric Diameter of droplet (MVD)**. The LWC is essential to assess the existing volume of water in the cloud for icing. The mass of the water in a cloud in a specified amount of air is measurable by rating the liquid water content (LWC). The measurement is generally defined by dividing the mass of water per volume of air ($\frac{g}{m^3}$). Measuring the LWC also determines the types of clouds that are going to form that helps to figure out the coping solution against icing. Temperature affects both the severity and the type of icing. Temperature decrease results in increasing the icing area. This rise up occurs in a short time when the temperature is between $-6^{\circ}C$ and $-12^{\circ}C$. Between temperature $-14^{\circ}C$ and $-20^{\circ}C$, the icing area increases slowly. The environmental temperature has significant influences on the icing area on an airfoil. Some calculations show that 43% of the airfoil leading edge area is iced when the temperature is $-20^{\circ}C$ [10]. The average droplet diameter distribution (MVD) influences the collection of water droplets by the air-frame. Icing typically consists of tiny droplets ranging in diameter from 10 to 50 microns. Sometimes airfoil surface encounters Super-cooled Large Droplets (SLD). Large super-cooled droplets can reach up to 100 microns. Once the ice has formed on a critical surface, it can only be removed using an ice protection system. In addition, if the ice protection system is working and removing ice from the leading edge, any ice aft of the protection system may quickly grow into a ridge. This will significantly disrupt the flow over the airfoil and may result in handling issues or performance degradation. Therefore protecting the whole surface of an airfoil also is of great importance.

Cloud type, airfoil geometry, airspeed and exposure duration are the other substantial factors that significantly affect icing circumstances. Once the ice is started to form and accumulate on the aircraft's critical aerodynamic surfaces, it does not matter to have a considerable ice

volume for an icing accident. Even a tiny layer of frost on a critical aerodynamic surface is enough to be the reason for altering the roughness on the airfoil leading edge, and this alteration is sufficient to deteriorate stall characteristics. From this point of view, preserving the critical surfaces of an airplane against ice formation is essential, and removing the accumulated ice is essential for a safe flight. Therefore, the necessity of keeping airplane surface results in developing and applying various ice protection techniques [11].

Based on the mentioned key factors, three ice types may form on critical aerodynamic surfaces, including rime, clear or glaze, and mixed ice. The glaze or clear ice typically forms at $-10^{\circ}C$ and lower temperatures. When water droplets impinge on the surface, they do not freeze immediately, resulting in the formation of runback flow and shed on the surface. This type of ice is recognized as glassy, transparent, and relatively smooth and dense ice. Rime ice as the second type typically forms at temperatures between $-15^{\circ}C$ to $-20^{\circ}C$. Unlike the clear ice, which consists of partially frozen super-cooled water droplets, rime ice is formed mainly due to frozen super-cooled water droplet's impingement, resulting in immediate ice formation upon impact the surface. Rime ice naturally is white and irregular. The high adhesion of glaze ice and its potentiality to form on various surface regions rather than only the point of impact make it a more dangerous type of ice. Between $-10^{\circ}C$ to $-15^{\circ}C$, mixed ice formation is possible (a combination of clear and rime ice), which is not considered a significant threat. Mixed ice has the characteristics of both in effect. It is formed quickly when ice particles are embedded in clear ice and form a rough accumulation of ice. It has been determined that Strati-form clouds have the most intense icing. The icing altitudes typically does not extend above 3,000 feet (a change in altitude of only a few thousand feet can remove the aircraft from icing conditions, even if it is still in cloud cover). Figure (1.2) shows the concentration and distribution of the super-cooled water droplets and ice crystals in different temperatures and altitudes [12].

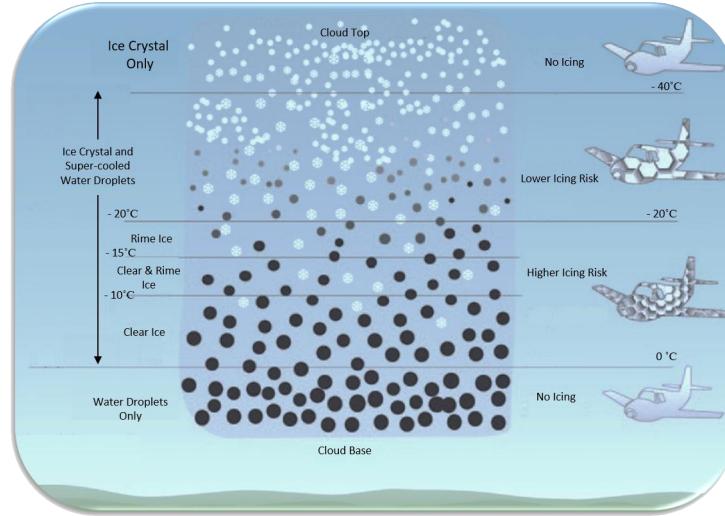


Figure 1.2: Ice formation in clouds and the subsequent possibility of aircraft icing [12].

Figure (1.3) shows ice on the cross-section of an airfoil, (a) clear ice, which is transparent and dense, (b) Mixed ice combined of clear and rime ice; (c) Rime ice, is opaque and milky

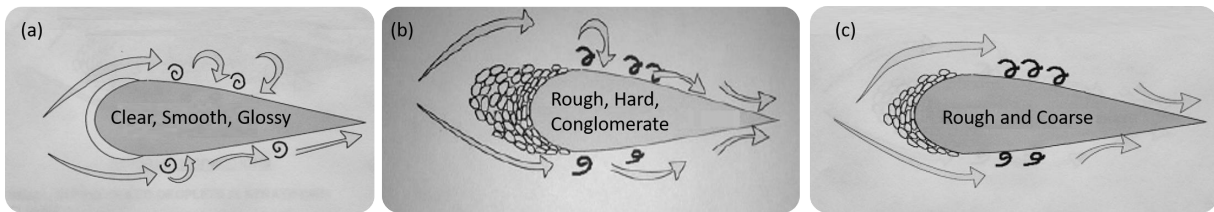


Figure 1.3: (a) Clear, (b) Mixed, (c) Rime icing on airfoils [13].

Overall, for icing occurrence, some specific conditions are necessary. First of all, icing happens at air temperature equal to 0°C or colder. However, it should be noted that icing may happen above freezing temperature if an airplane remains below the freezing temperature and when it moves in a region above freezing point because the aircraft's surface temperature can remain below the freezing point for some time. The second main reason for the icing incident is the presence of super-cooled liquid water droplets or wet snowflakes, mainly found at temperatures varying from 0°C to -20°C . Small amounts of super-cooled droplets may be found at a temperature ranging from -20°C to -40°C . While an aircraft enters in

the air, a super-cooled water droplet’s internal stability is destroyed due to impacting the surface of an aircraft, increasing its freezing temperature because of the phenomenon known as aerodynamic heating (the freezing temperature rise resulting from adiabatic compression and friction) [13]. Table (1.1) presents the summary of the parameters influencing the type of ice and icing risk. Clear ice, because of its high adhesion to the surface and severity is the most undesirable type of ice. It is more damaging to flight safety as it can affect many areas due to runback flow and can grow large enough to negatively affect an airplane’s aerodynamic characteristics [12].

Table 1.1: Circumstances for formation of different ice types [12].

Parameters	Glaze(Clear) Ice	Mixed Ice	Rime Ice
Temperature	$0^{\circ}C$ to $-10^{\circ}C$	$-10^{\circ}C$ to $-15^{\circ}C$	$-15^{\circ}C$ to $-40^{\circ}C$
Droplet Size	Large	Small to Large	Small
Liquid Water Content	High	Low to High	Low
Risk	High	Intermediate	Low

Finally, it is shown that icing risk restrictions are usually accepted in the presence of water droplets smaller than $50\ \mu\text{m}$; however, it may happen in the presence of larger droplets [14]. According to the hazards of in-flight icing, ice protection systems should be intended to keep aircraft surfaces free from ice formation and accumulation. An ice protection system should either avoid ice formation or support the aircraft to shed the ice in case of ice formation before growing up to a risky thickness. Table (1.2) represents the conditions that are naturally considered as an in-flight icing risk [11].

Table 1.2: In-flight icing risk [11].

Parameters	Icing Risk Condition
Liquid Water Content (LWC))	From 0.1 to $3\ \text{g}/\text{m}^3$
Temperature	From $+4^{\circ}C$ to $-40^{\circ}C$
Droplet Diameter (MVD)	Usually from $1\text{-}50\ \mu\text{m}$ but also up to $400\ \mu\text{m}$

Events related to icing fall commonly into two categories: ground-level icing and in-flight-icing, in which many stakeholders, different regulations, and separate ice protection systems are involved [7].

1.3 Ice Protection Systems

Concerning ice-protection systems, various alternatives are employed to improve all-weather flying safety, involving pre-flight precautions and in-flight courses of action, including *de-icing* (removal of the ice) and *anti-icing* (protecting against ice formation) [7]. There are three classifications of ice protection systems in terms of energy: *Passive* systems are used to prevent ice accumulation without any additional source of energy, *Active* systems which are required external energy to operate, and *Multi-functional (hybrid)* systems are the combination of other methods. These ice protection systems can be developed in anti-icing, deicing, or cooperation modes [15]. The conventionally used active ice protection techniques are categorized into *Chemical*, *Mechanical*, and *Thermal* systems [3]. Among all active strategies, surface heating (thermal approach) is the most desired, reliable, and energy-efficient method [16]. There are typical concerns about performance, efficiency, energy consumption, and environmental problems for active systems, which resulted in significant attempts to developing an alternative solution reducing the adhesion forces between the ice and the aerodynamic surface using an ultra-smooth, nano-structured coating with water and ice-repellent properties (ice-phobic surface) that boosts the ice shedding [17]. However in passive methods, the correlation between ice-phobicity and surface properties (roughness, chemistry, porosity) is still imprecise. This uncertainty leads these strategies not to be accepted as dependable ice protection systems. Therefore, regardless of ongoing researches on designing and engineering ice-phobic coatings, there is no standalone coating solution (passive strategy) to in-flight ice mitigation [18]. Based on these issues, the limitations and principal merits of active and passive techniques suggest using multi-functional (hybrid) ice protection systems for preserving aerodynamic surfaces ice-free in all icing episodes. Accordingly, several results indicated that combining the passive strategies (ice-phobic coatings) and the active strategies (particularly surface heating) can keep the entire airfoil surface free from

ice almost under all icing conditions [19]. Moreover, coatings have been proved to decrease thermal deicing’s power consumption up to 80% and lower the runback ice simultaneously [20]. Thus evidence shows that re-configuring individual ice protection systems towards being a part of a hybrid system is much more reliable and highly advantageous procedure to preserve critical surfaces free from ice [21]. A summary of currently active and passive Icing Protection System (IPS) and the classification of these methods are provided in Figure (1.4) [22].

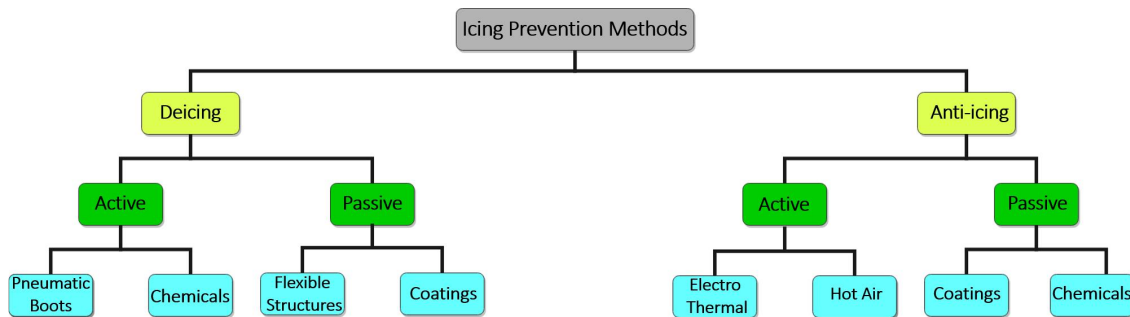


Figure 1.4: Overview of strategies and approaches for prevention of ice nucleation and accretion [22].

1.3.1 Active Ice Protection Methods

Ice protection systems are designed based on effective factors in the formation and accumulation of ice all at once, including cloud’s liquid water content (LWC), an average of droplets size (MVD), atmospheric conditions, airfoil geometry, aircraft velocity, and angle of impact (AOI) [19]. Conventional active ice protection systems can be separated into chemical methods, mechanical methods, and thermal methods. These methods protect different aircraft components, such as wings, leading-edge slats and spoilers, engine inlets, engine struts, radar domes, and vertical and horizontal stabilizers. Designing and implementing ice mitigation techniques require an in-depth understanding of flight physics, meteorology, and icing sensation. Many books, papers, and reports are available to date, including experimental and numerical studies of icing phenomenon and alternative solutions to cope with this issue. Some of these methods are commercially available, while many are immature and

need more investigation to be implemented on an industrial scale [23]. Some earlier anti-icing methods were improved, such as liquid de-icers (chemical methods), where changes in design have enabled this form of ice protection to be used today. At present, designers have many options for ice protection, each one with some advantages and disadvantages. However, because aircraft are used for specific roles and have a restricted ice tolerance, choosing ice protection systems becomes limited. Overall, all considerations have to be taken into account, including first cost, operating costs, reliability, weight, complexity, ease of maintenance, and, of course, guaranteed performance.

Generally, systems that try to prevent icing are so-called anti-icing systems, and systems to remove the ice are known as deicing systems. These systems, in turn, can be divided into distinct sub-categories. For instance, thermal systems can be divided into two main approaches: evaporating or wet water runback regimes. Ice protection can be effectively achieved in the evaporating regime by heating the critical surfaces to over 100°C to evaporate all the impinged super-cooled water droplets. The evaporating regime requires an extremely high-power input to the electric heating element for keeping the heated surface at a high temperature over 100°C under all icing conditions, which might also cause unexpected over-heating issues. In such systems, the choice is restricted to use the thermal system because the aerodynamic surfaces should be preserved cleaned at all times. On the other hand, wet water runback regime in which the impinged super-cooled water droplets are heated up to a “warmed” state (temperature higher than the water frozen temperature) to remain in the liquid phase. Then the liquid ridges are shed by natural forces like gravity or wind. However, there is a concern here, and it goes back to the possibility of runback ice formation. If ice’s temporary presence can be endured, applying protection methods would be more convenient and economical to only when required, and this arrangement is called deicing. Systems applying this approach operate intermittently by using heat or mechanical energy to remove the ice. Mechanical pulsating systems as another field of ice protection were used since ice can remain on aerodynamic surfaces for a short while. However, always clean aerodynamic shape is expected on completion of ice removal. In this context, the electrical-thermal system will be the most probable choice [24]. Active systems continuously need energy to operate. According to the typical active IPS, chemical substances are used as

an ice protection method. These materials create a thermal hysteresis between the melting point and the freezing point. Mechanical methods involve physically shattering the ice by using vibration or movement of the structure. Pneumatic techniques and ultrasonic deicing can be identified as the primary methods under this category. Thermal methods mainly include hot air injection, resistive heaters, and microwave heating [25].

1.3.2 Passive Ice Protection Methods

The wettability of a solid surface is related to the tendency of a liquid to maintain contact with that surface. A water molecule tends to stick to things, including itself, because of considerable surface tension, primarily due to its electrical dipole structure. Surfaces forming ionic or a hydrogen bond with water are identified as hydrophilic, while surfaces that do not partake in the water’s hydrogen bonding are so-called hydrophobic [26]. To quantitatively evaluate the wettability (hydrophilic or hydrophobic) of a surface, two parameters are involved: water contact angle (CA) and slide angle (SA). The contact angle (θ) is the angle conventionally measured through the liquid, where a liquid–vapor interface meets a solid surface, and the slide angle (θ_S) is the tilt angle required for a static droplet deposited on a surface to start rolling down. In theory, the wettability of an entirely smooth surface is defined by Young’s Equation (1.1),

$$\cos(\theta) = \frac{\gamma_{SA} - \gamma_{SL}}{\gamma_{LA}}, \quad (1.1)$$

where (θ) shows contact angle, γ_{SA} and γ_{SL} are the surface energies of the solid against air and liquid, and γ_{LA} is the surface energy of liquid against air. Any surface with $CA < 90^\circ$ is categorized as hydrophilic, while values of $CA > 90^\circ$ are considered hydrophobic. For a surface to be classified as superhydrophobic, $CA > 150^\circ$ and $SA < 10^\circ$ are generally required. Moreover, two factors are relevant to the evaluation of the water droplet mobility on a surface: the advancing contact angle (θ_a) at the front of the moving droplet and the receding contact angle (θ_r) at the back. Contact angle hysteresis (CAH) is subsequently defined as the difference between the advancing and receding contact angles. In case of having

a contact angle hysteresis smaller than 10° beside the above-mentioned features, the surface is determined as superhydrophobic. Figure (1.5) depicts hydrophilic, hydrophobic, superhydrophobic surfaces, and also the advancing contact angles (θ_a), receding contact angle (θ_r), and sliding angle of a tilted surface (SA) [27].

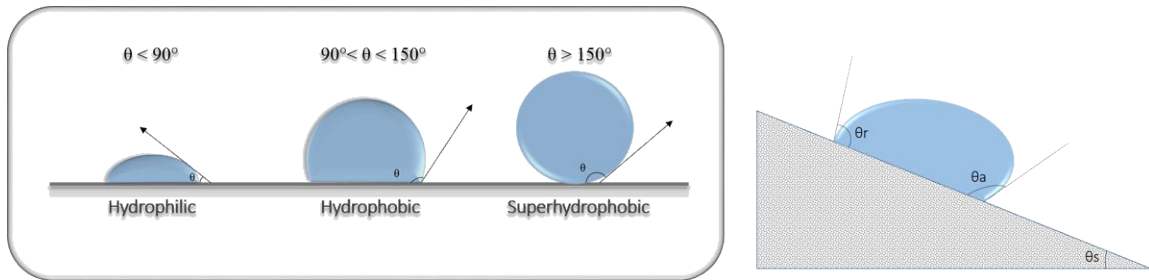


Figure 1.5: Surface wettability characteristic [27].

In both fundamental and practical terms, controlling the surface's wettability is a concern that is essential to consider. For instance, lotus leaves showing striking superhydrophobicity and self-cleaning characteristics became the inspiration for the fabrication of synthetic surfaces with comparable features, like creating superhydrophobic surfaces with low surface energy to take advantage of their remarkable properties [28]. Figure (1.6) shows some characteristics, including a hierarchical, micro, or nano-structure of superhydrophobic surfaces [29].

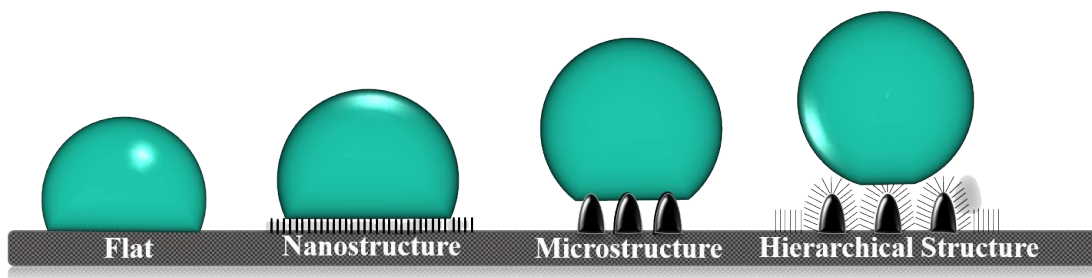


Figure 1.6: Schematic for wettability of different surface structures [29].

The high water-repellency capabilities of superhydrophobic surfaces, in conjunction with the same ice and water adhesion mechanisms, make them advantageous for forming anti-icing

or ice-phobic coatings. From this viewpoint, implementing these surfaces in the aviation industry is a potential solution for mitigating in-flight icing. Different production methods are applied to create artificial ice-phobic surfaces such as lithography, evaporation, sol-gel, etc. Various materials are used to make superhydrophobic surfaces (metals, polymers, semiconductors, nanotubes, nanoparticles) [28]. On the first consideration, ice-phobic surfaces are defined as surfaces with low adhesion strength between ice and a solid surface [29]. In general, water in its solid form should be prevented or delayed from being formed on critical surfaces. Otherwise, against ice formation, the accumulation rate on the surface should be slowed down, and the adhesion to the substrate should be reduced (can be easily removed). Ice-phobic surfaces are anticipated to be practical for a wide range of applications, including dams, solar panels, airplanes, wind turbines, and more. Therefore, the structural and chemical integrity of ice-phobic surfaces used in operation must be able to withstand erosion, wear, UV radiation, and other weathering conditions. Furthermore, these surfaces must be practicable, inexpensive, environmentally friendly, and mechanically durable. To figure out the best strategies for developing ice-phobic surfaces, these various characteristics should be classified. In other words, the correlation between ice-phobicity and surface characteristics (roughness, chemistry, porosity) is still imprecise. This uncertainty is due to the different definitions of ice-phobicity. Various poorly understood test methods evaluate the ice-phobicity of a surface, which provokes these ambiguities. Essentially, three parameters play a decisive role in designing an ice-phobic surface: **Topography** (determines the wettability state of the surface), **Elasticity** (determines flexibility and surface energy level), and **Liquid Extent**, which provides a smooth liquid interface that reduces droplet retention and ice adhesion strength (a lubricant with a low freezing point infuses the micro or nano-porous surface). Figure (1.7) presents a schematic of ice-phobic coatings classification based on these distinctive surface characteristics: elasticity (soft vs. hard), topography (smooth vs. rough), and liquid extent (dry vs. wet) [18]. Developing new materials with the desired ice-phobicity requires an accurate understanding of ice repellency in all environments. Despite all the progress made, no single surface has shown the ideal ice-phobicity [30]. As a rule, four key-features define the ice-phobicity excellence of a surface: (1) lower temperature to start ice nucleation, (2) delay in ice accretion time, (3) smaller ice adhesion strength at the

ice-solid interface, and (4) long-lasting durability. The required key-features are vary based on the type of application for ice-phobic surfaces. In the aerospace industry, low freezing temperatures, low ice adhesion, and long-term durability are the most critical requirements [1].

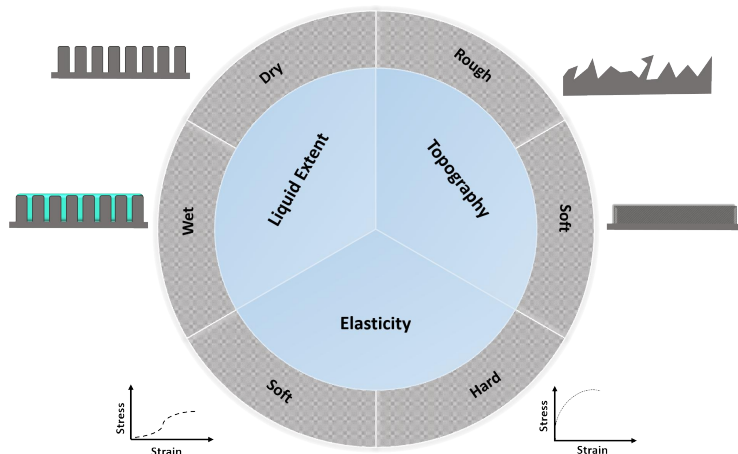


Figure 1.7: Classification of the three mechanisms applied in development of ice-phobic coatings [18].

Despite the continued innovation in developing ice-phobic surfaces, ice-phobic coatings have not yet been certified for aerospace applications due to the complexity of icing conditions, solid-ice interaction, and mechanical properties [31]. From another perspective, results indicate that ice-phobic coatings alone may not be adequate for de-icing and anti-icing purposes [32]. It specifies that icing problems’ diversity causes various challenges, and icing conditions can only be controlled in individual circumstances. For example, heat exchangers may be designed to operate within limited temperature and humidity changes. In contrast, ice build-up occurs in natural environments over a wide range of temperatures, humidity degrees, and other weather conditions. Although it is typical for laboratory experiments to analyze a single aspect of icing, practically ice-phobic materials need the ability to withstand a wide range of possible conditions [33].

As things stand now, standard ice-phobic coatings can be divided into several main classifications that exist naturally or are produced artificially. A classification of the main well-accepted ice-phobic surfaces is shown in Figure (1.8). However, these technologies might not be precisely compared because of preferred parameters and the different test methods. Nev-

ertheless, the presence of shortcomings is still felt in the fabrication of consistent ice-phobic surfaces, and this is why other solutions should be considered. Employing multi-functional ice protection systems is an example of these solutions. Using an active ice protection systems (electro-mechanical or electro-thermal) combined with ice-phobic coatings (passive strategies) has proven as reliable multi-functional ice protection methods [19]. Current industry strategies for tackling icing problems consist of various techniques such as active heating, chemical deicing fluids, and mechanical removal. These processes can be inefficient, environmentally unfavorable, expensive, and time-consuming. However, they would be advantageous as complementary systems to overcome the limitations seen in passive ice protection strategies [33].

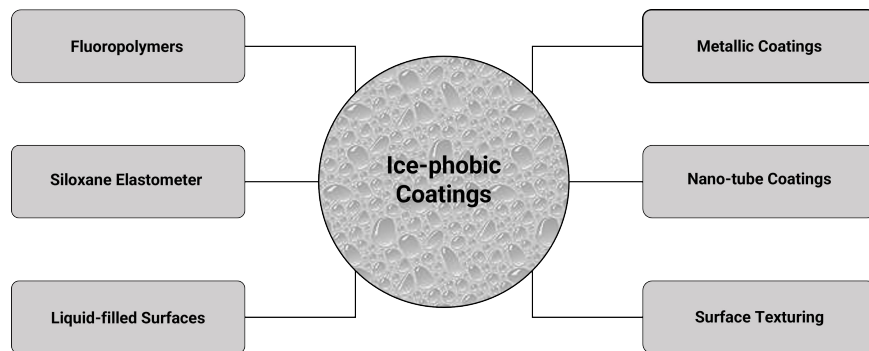


Figure 1.8: Schematic of the different categories of ice-phobic coatings [19].

1.3.3 Multi-functional (Hybrid) Ice Protection Methods

Primarily active ice protection systems (chemical, mechanical and thermal) were applied for in-flight ice mitigation. These methods are characterized based on the physical principle they used to remove the ice [34]. Secondly, concerns about performance, efficiency, energy consumption, and active systems’ environmental problems result in significant attempts to developing alternative solutions. In this regard, applying electrical power as a more efficient and cleaner energy source has been considered a severe issues for an all-electric aircraft [35]. These ice removal techniques are mainly divided into electro-thermal and electro-mechanical systems. Hybrid systems that employ multiple ice protection strategies have been established

to decrease required energy for in-flight ice mitigation. The electro-thermal model is used to stop droplets from freezing in the area near the leading edge, while the electro-mechanical system is regularly pushed to produce ice shedding in the unheated section at the back of the airfoil [36]. Besides the conventional active ice protection systems, many studies are focused on exploring the possibility of using water-repellent coatings to delay or even prevent ice formation on aerodynamic surfaces. However, passive systems could not still provide all the requirements for being admitted as dependable in-flight ice mitigation techniques. Hybrid mechanisms combining passive and active methods have been proved to be more efficient, environmentally friendly, less expensive, and time-saving systems [37]. The aim of this study is also to introduce the multi-functional deicing system. This system would integrate electro-thermal heating and superhydrophobic coating into a unique architecture to have a more durable ice protection system with less power consumption.

Chapter 2

Literature Review

This section deals with the background of our study. At first, selected technologies for active and passive ice protection systems are reviewed. Afterward, a synopsis of the multi-functional ice mitigation systems and their figures of merit are pointed up.

2.1 Background of Active Ice Protection Methods

After the Second World War, significant consideration was given to in-flight icing hazards, and the necessity of developing more efficient protection systems was better understood, which resulted in the improvement of earlier anti-icing methods. Initial costs, manufacturing, operating costs, reliability, weight, complexity, ease of maintenance, and guaranteed performance are always the primary and essential requirements for an ice protection system to be certified. This is the reason for restriction in choice and development of ice-opposing systems [24]. In general, active ice protection systems require energy to operate. Based on energy consumption type, they can be separated into **chemical** methods, **mechanical** methods, and **thermal** methods, which are briefly defined in Chapter 1 [38].

2.1.1 Chemical Ice Protection Techniques

The idea of using chemicals for ice protection originates from the polar animals observed in nature. Scientists discovered particular antifreeze proteins in the body of animals that

survive species in polar regions. These biochemical proteins decrease the freezing point in animal's blood and protect them against icing [39]. Chemical techniques for deicing and protecting aircraft surfaces are using freezing point depressant (FPD) fluids. These liquids are commercially offered. Several chemicals such as chloride salts, acetate compounds, glycol-based solutions can also be placed in this category. However, these chemicals are short-term options because they lose their properties over time. In several instances, they also have shown the capability to corrode the protected surface [40]. Besides, chemicals usually contain harmful ingredients, making them environmentally toxic [41]. With chemical techniques, frost, ice, snow or slush is removed from an aircraft using a heated aircraft deicing fluid (ADF) and aircraft anti-icing fluid (AAF). Chemical substances are applied to a surface to protect it from the buildup of frozen contaminants for a limited period. Four types of chemical fluids are used for aircraft deicing or anti-icing that are categorized based on physical and chemical properties, and their use is aircraft specific. However, the basic structure of all types is the same. All types are usually glycol-based (lower the freezing point and prevent ice contamination at temperatures below freezing). They are typically mixed with water to wash (leaching) the lead or copper from pipes, wetting agents that allow the liquid to spread more easily across any solid surface, corrosion inhibitors to protect the aircraft skin and dye from visually identifying the fluid type. These fluids are formulated to remove ice, snow, and frost from aircraft's exterior surfaces (deicing). The composition of anti-icing fluids is comparable to deicing fluids, and the only difference is the polymeric thickeners, which are added to anti-icing fluids to prevent for a more extended time. Laser-drilled titanium porous panels distribute the FPD liquid to the aircraft leading edge. The FPD liquid usually is delivered to the propellers and windshield using a slinger ring and spray bar [42]. In general, the FPD liquid flow is pumped into the surface-ice interface to weaken the ice bonding and make ice removal of the surfaces easier by aerodynamic forces [43].

Figure (2.1) shows the simple conventional procedure of FDP distribution in anti-icing or deicing. Porous panels are inserted as a cuff over the leading edge of protected zones. Liquid pumped into the cavity exudes through the surface to provide a protective film [44].



Figure 2.1: Schematic of FPD deicing system [44].

2.1.2 Mechanical Ice Protection Methods

As the second major group of active IPS, mechanical methods involve physically shattering the ice using vibration or structure’s movement. Pneumatic techniques and ultrasonic deicing can be identified as the primary methods under this category. Running active IPS always requires on-board power and needs frequent careful maintenance. A review of modern and most-common active IPS technologies is given in the following [23]. Sonic Pulse Electro-expulsive Deicer (SPEED) system is an acceleration-based deicer for aircraft ice protection. NASA Lewis and ARPA’s SBIR program developed the system in cooperation. The idea of developing the Electro-impulsive deicing (EIDI) concept results in the advent of SPEED with a significant improvement in the actuator coil and electronics. In this system, impulsive loads with rapid acceleration are directly applied to actuator coils located behind the aircraft’s leading edge. This speedy acceleration causes de-bonding and shedding the ice layers efficiently. In terms of deicing power efficiency, SPEED is recognized as the most accessible advanced system. Later, to provide an autonomous mode of operation, a Icing Onset Sensor was added to the primary system. This sensor monitors the ice accretion beginning and the amount of accumulation and commands the deicer to fire. This technology was introduced by IDI company (Innovative Dynamics Inc.). After extensive tests in wind tunnels and in-flight conditions, this method was certified by FAA in 2000. The design is covered by U.S. Patent Number 6,102,333. reduced power consumption; erosion resistant, low-cost design, reliable and maintenance-free, and fault-tolerant operation are underlined by IDI to disclose their SPEED system [45]. Figure (2.2) shows a schematic of the Electro-expulsive deicing

system [46].

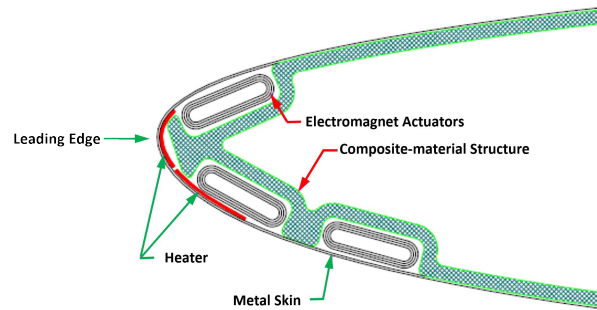


Figure 2.2: Electro-explosive Deicer located in the wing nose [46].

In England, in 1973, another important ice protection method (Electro-impulse Method) was patented [47]. Extensive tests were done on NASA Twin Otter aircraft in the wind tunnel and in-flight conditions. In this method, a sudden electromagnetic repulsive force in the skin throws ice in all directions because of promptly discharge the high-voltage capacitors through the coils installed inside the skin of the aircraft leading edge. Electromagnetic interference, structural fatigue and passenger response to the noise are some disadvantages of this method. Using this method is allowed on only one airplane and only on its tail. Helicopter rotors and turbine engine inlets could be protected against icing by this method [48].

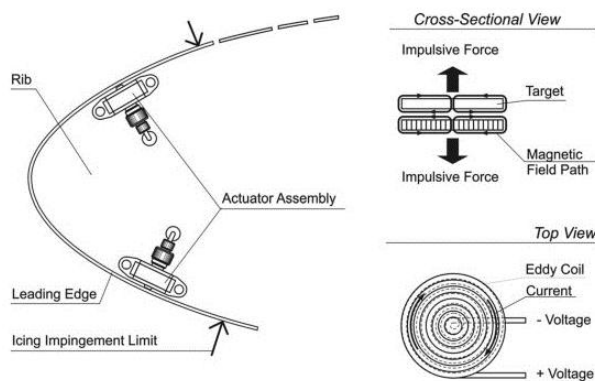


Figure 2.3: Impulsive coil in a leading edge (Eddy current) [49].

In 2002 Dennis Newton, in his work, introduced the Electro-impulsive as a reliable, effective, efficient and light-weight system with an improved design [49]. An Electro-impulse

system can be seen in Figure (2.3). Another certified active method is the Electro-expulsive Separation System (EESS), which lies on two main parts: the EESS Controller and the EESS Expulsive Boot. Also, ice detection sensors, electrical cabling, indicators, and controllers are used as additional elements. Figure (2.4) illustrates that there are two conductors in this system. Both the top and bottom conductors are embedded in an elastomer substance. Passing rapidly current through two conductors generates a magnetic field producing either attractive or repulsive forces around conductors, which causes them to push apart. Passing an enormous pulse of current in a brief time (millisecond) causes the conductors to jump about 500 μm , resulting in ice bond breakage [23]. According to Leonard Haslim of NASA's Ames, ice shrinkage into tiny particles in this method would not harm aircraft components. Meanwhile, the power consumption is reduced by 1000 compared to the electro-thermal ice removal, and the weight is one-tenth the weight of Electro-Thermal Ice Removal Systems [50].

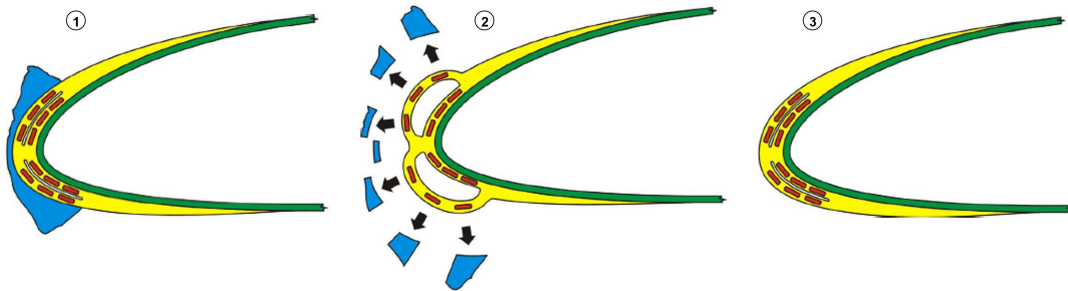


Figure 2.4: Ice shattering using the electro-expulsive separation system [23].

Another widely deicing method used in the aerospace industry is the pneumatic deicing boots system, invented by Goodrich company in 1923. The pneumatic deicing boots system's operation is based on supply-blooded air extracted from the airplane engines into the boots. This system comprises fabric-reinforced layers of synthetic rubber and several air chambers between the layers. Inflating and deflating the boot air chambers in this system results in mechanical ice removal from leading edges. The chambers' inflation and deflation shatter the ice from the surfaces shed then by aerodynamic forces. The thickness of pneumatic boots is usually less than 1.9 mm, and a low power is required for deicing. However, the formation of ice bridging in pneumatic boot systems is always possible. Ice bridging forms on top of

the boot, and its removal is complicated and difficult. The ice bridging problem has been partially resolved by modifying the speed of inflation and deflation [51]. Pneumatic deicing boot before and after inflation is shown in Figure (2.5) [52].

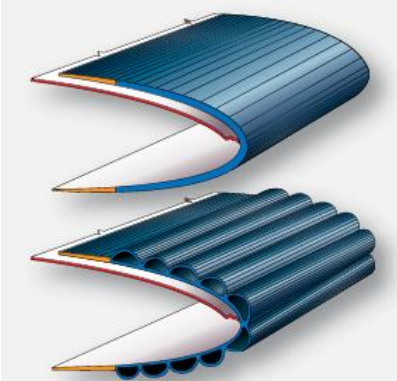


Figure 2.5: Cross-section of a pneumatic deicing boot deflated (top) and inflated (bottom) [52].

COX Inc developed another electro-mechanical ice protection system based on the latest technology known as Electro-Mechanical Expulsion Deicing System (EMEDS). There are actuator coils in this system embedded in a row on the leading edge. A massive current delivers into actuators in microsecond intervals. Consequently, an opposing electromagnetic field has been generated that causes a rapid change in the actuator’s shape results in acceleration-based debonding of accumulated ice on the erosion shield. A schematic of this system is shown in Figure (2.6) [53].

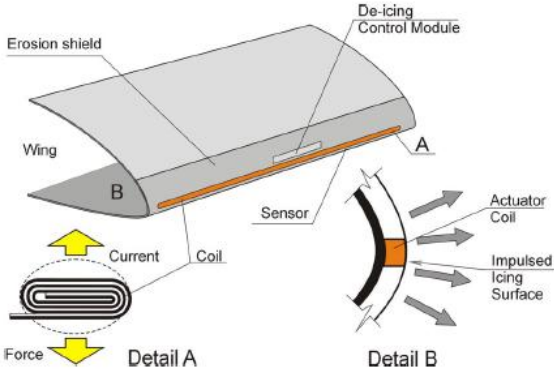


Figure 2.6: Electro-mechanical expulsion deicing system [53].

Another approach of mechanical ice removal is using ultrasonic technology. Glenn Research Center in NASA initially developed this method. This approach can be used in the

aeronautical industry and is compatible with air-frame ice protection, automobile windshield ice protection, and ice buildup protection for marine vessels. Sound waves in this method break the adhesive bond between two materials by forming a large enough stress field at the interface. This stress field causes debonding at the interface of ice and substrate. However, most of the research is dedicated to debonding ice from aluminum surfaces; future studies may also include unique substrates like composite, glass, and steel. However, this technology is limited in the laboratory state thus far, but this alternative will soon be available commercially. Figure (2.7) depicts a schematic of this technology [54].

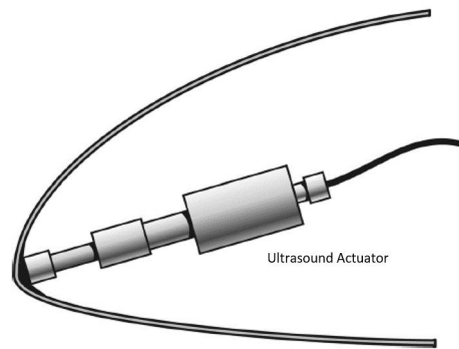


Figure 2.7: Ultrasound actuator placed inside the nose of leading edge [54].

2.1.3 Thermal Ice Protection Systems

As the last active IPS, the heat is applied on aerodynamic surfaces (thermal method). Thermal methods mainly include hot air injection, resistive heaters, microwave heating. This technology is used to prevent ice accumulation by maintaining the surface temperature above the freezing point. Among all these strategies, Engine Bleed Air and Electro-thermal systems are the most predominant ice opposing techniques regarding their efficiency and reliability. Both systems are established based on heating the critical zones of aircraft, which are prone to icing. Engine Bleed Air ice protection technique is primarily employed in aerospace rather than the Electro-thermal technique. However, this mechanism needs long and complex piping systems with switches and vents, making the system heavy with accordingly high fuel consumption. Air temperature control is impossible; thus, the air temperature degree is almost between [200 to 250] °C, and there is high pressure inside

the system. Later regarding this concern, applying electrical power as a more efficient and cleaner source of energy has considered an all-electric aircraft, and it led to the precedence of electro-thermal systems. Re-freezing is still a problem in Bleed Air System [25]. In Figure (2.8) a simple ice protection procedure of engine inlets and wing leading edges by Hot Air Injection (Bleed Air) system is depicted [55].

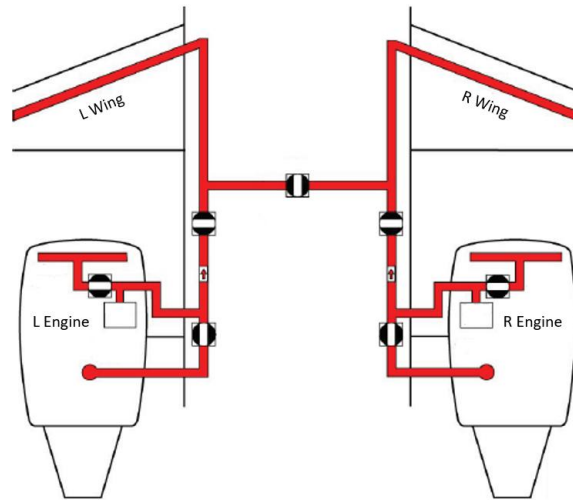


Figure 2.8: Schematic of Engine Bleed Air ice protection method [55].

The Electro-thermal system's idea is to pin the resistive heating element under the surface required to be protected from ice. Electrical heating elements deliver the energy to operate either in anti-icing or deicing mode. The structural design of an electro-thermal ice protection system (ETIPS) is typically based on a multi-layered stack of materials. Each stack may vary in material properties and thickness according to the design and applications [56]. These systems use resistance heaters in different forms like wire, film, or foil for heating and deicing an airplane or wind-turbine blades. The electro-thermal heaters heat the to-be-protected area once an electrical current is applied to them [43]. The electro-thermal systems act as anti-icing when the heaters work nonstop to prevent ice formation and as deicers when the heaters work intermittently to remove the ice accumulated on the critical surfaces [57]. The running of a modern electro-thermal ice protection system in deicing mode is depicted in Figure (2.9). A parting strip (heater C) is maintained active during the entire cycle. Then according to the distinct cycle, the rest of the heaters are activated. This cycle initiates a liquid water film formation at the interface between the ice and the protected surface;

consequently, ice's ability to remain attached to the surface is significantly reduced. Once a critical amount of water film is formed, the ice block is shed under aerodynamic forces [19].

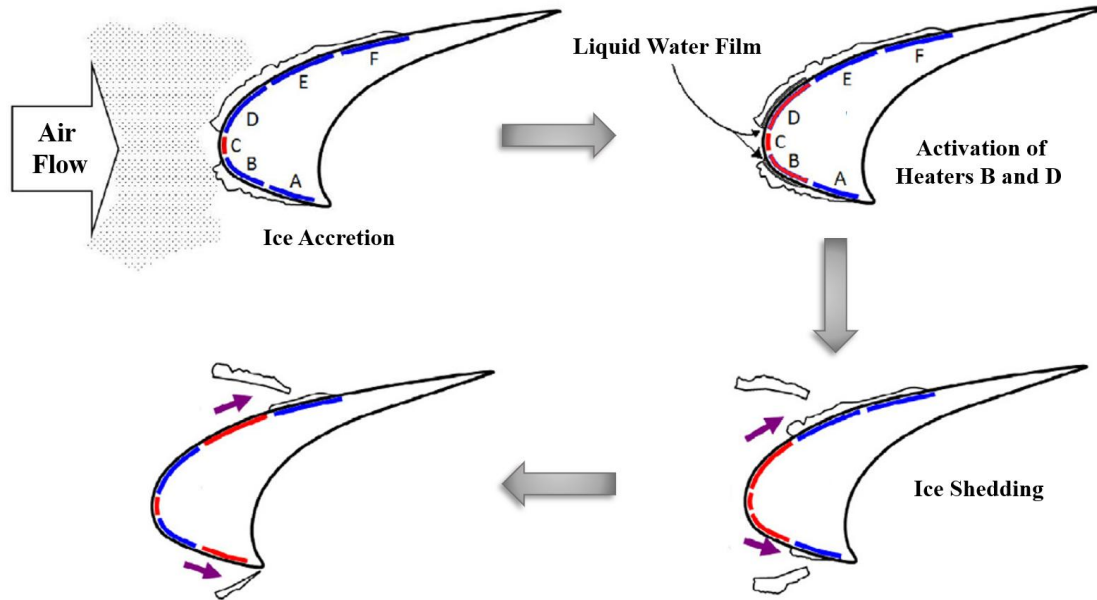


Figure 2.9: Illustration of an ETIPS operating in deicing mode [19].

Despite the effectiveness of the active ice protection systems in delaying ice formation and reducing ice adhesion, delivering guaranteed anti-icing or deicing methods still require further development. For instance, it could be noted that innovation in production methods here can be mentioned as a developing technique. For example, in the structural design of an electro-thermal ice protection system (ETIPS), electrical elements are embedded in the vicinity of to-be-heated surfaces to provide the anticipated amount of heat applied to these surfaces. Accordingly, there are different heating elements, such as metal heating elements, thick film heaters, thermally sprayed heaters. For instance, on the subject of ice mitigation, thermally sprayed resistive materials right on surfaces can tackle the restrictions of other heating elements by tailoring the geometry of them to the application [58]. Furthermore, they have shown better performance in the homogeneity of temperature distribution because of the intimate contact between the heating element and the substrate. Also, the heat transfer rate is maximized by minimizing the distance between the heater and the to-be-heated surface. These are also reliable for industries because even at high temperatures, their life span is well

long compared with other types because of immunity from thermal shocks, which notably affects heaters on ceramic substrates [59]. In effect, this technique offers a fast and flexible way of fabricating standard heater solutions for different shape surfaces [60].

Another alternative to heat super-cooled water droplets impinging on aerodynamic surface is microwave electromagnetic energy transmitted to the droplets. This method was disclosed for the first time in 1982 by Hansman [25]. Another system is microwave frequency IPS. This system also is energy efficient and very easy to maintenance. The only concerns of this technique are safety matters [61]. As another thermal ice protection technology, infrared heating does not require any installation on the blades to transfer thermal energy because, in this system, energy is emitted through the air. This system delivers energy from the power resource to a distant object. The infrared system, as a result, does not have additional roughness due to the installations, which is a tremendous advantage for the efficiency of the ice mitigation process. This system also can be used in both deicing or anti-icing mode. The mechanism of this system is established based on the significant capability of ice to absorb infrared radiation. The ice is melted by absorption of the heat radiated in the air and sheds by aerodynamic forces. However, it should be noted that there is a limitation in material selection in this method because only materials that do not absorb the range of radiation could be used in the structure; otherwise, there is always a risk of fire. For instance, lubricants, oils and many other components in the nacelle can quickly overheat; thus, the technology necessitates particular safety precautions [62].

In large airplanes, it should be noted that the required energy consumption by using joule heating would rise dramatically by increasing the dimension of the aerodynamic surfaces. Therefore, heating the whole critical surfaces is undesired; on the other hand, heating smaller areas (ice nucleation region) may cause significant challenges. Primarily, it initiates the form of so-called runback ice (water flow running back from the heated or protected zones to unprotected areas and refreezes there). Runback ice may cause severe problems and detrimentally affects operation and safety [63]. Ultimately, The application of thermally-sprayed resistive heaters seems to be the best method of thermal ice protection. This thermal ice mitigation method has been studied several times by various authors, although in terms of in-flight ice relief strategies, the subject is almost felt to be neglected.

However the inadequacies of active IPS techniques over the time have drawn increasing attention to passive anti-icing alternatives due to their low installation cost and almost zero energy consumption [64]. A summary of current active IPS, their advantages and disadvantages as well as their applications are provided in Table (2.1).

Table 2.1: Comparison of active ice mitigation techniques [19].

Method	Description of Technology	Deicing Potential	Anti-icing Potential	Advantages and Disadvantages
Freezing point depressants	- Ice removed by pumping FPD through porous outer skin in-flight and spraying heated FPD on the ground - If a thin layer of FPD is remains on the aircraft surface, short-term anti-icing C:Can be achieved	YES	YES	- Can be used on the ground and in-flight - Layer of FPD on the aircraft can result in detrimental effects to aircraft performance - Fluids can be toxic and cause environment concerns
Engine bleed air	- Hot engine air redirected to the leading edge, heating the surface and melting the accreted ice - If no ice is present, it can prevent droplets from freezing and evaporate droplets on the surface	YES	YES	- Reduction in engine efficiency - Not available on piston and turboprop-powered airplanes - High system weight due to required internal piping
Electro-thermal (embedded heaters)	- Heating coils placed in the leading edge can melt accumulated ice when supplied with electrical energy - Can prevent the impinging droplets from freezing	YES	YES	- Large power consumption, about 1.5–2 W/cm ² - Limited to critical areas - Surfaces must be thermally conductive
Pneumatic boots	- Rubber boots installed on the leading edge inflate with air to break accumulated ice into chunks	YES	NO	
Pneumatic impulse	- Rubber boots are embedded in a metal or polymer system on the outside of the leading edge - When inflated, the boots expand rapidly, expelling any ice build-up	YES	NO	- Protective layers consisting of metal or polymers are required to prevent the tubes from being exposed to rain erosion, ice pellet impingement and other forms of surface damage - Can remove ice at temperatures as low as 55 °C
Electro-impulse	- High-voltage capacitors on the inside of the leading edge are rapidly discharged which generates an electromagnetic repulsive force in the skin causing fracture of ice bonded to the surface	YES	NO	- Used to de-ice power transmission lines - May cause electromagnetic interference with other aircraft systems components - Can cause structural fatigue - No longer in use for aerospace
Electro-expulsive separation	- Magnetic fields are generated about the two parallel layers of conductors, producing forces that push the conductors apart. When current is passed into the system, the rapid acceleration of the conductors breaks the bond the ice has formed with the surface	YES	NO	- Short response time (ms) - Low power consumption (Tested on Cessna Sky-master and installed on Raytheon business jet)
Ultrasound technology	- When supplied with current, piezoelectric actuators on the inside of the B25leading edge produce ultrasonic waves that travel through the aircraft skin, generating shear stresses at interface between the ice and surface. These shear stresses debond and break apart the ice layer	YES	YES	- Piezoelectric actuators require a lower power density than other methods for ice delamination - Actuator count required based on the size of surface needing protection - Bond strength to the surface may be fatigued after billions of cycles.
Microwave	- Microwave energy transferred through aircraft leading edge and converted to heat which melts the bond that ice has formed with the surface	YES	YES	- Intended for use on turboprop aircraft - Can cause interference with other electronics - More energy intensive than other systems

2.2 Review of Passive Ice Protection Strategies

The definition of passive ice protection methods was discussed in detail in the previous chapter. It was concluded that passive anti-icing surfaces or ice-phobic surfaces turn to a subject that attracts much attention. The purpose of this chapter is to provide a description of the origin and development of these surfaces. The passive method's popularity refers to their significant economic, energy implications and appropriate safety margins in ice prevention. However, the nature of ice-phobicity concept is particularly complicated. In practice, the extensive range of icing scenarios results in different definitions of ice-phobicity, which subsequently brings many challenges in designing ice-repellent surfaces. For instance, with their hierarchical structure, superhydrophobic surfaces are not always ice-phobic. Results are proved that surfaces with high ice repellency under certain conditions can act ultimately adversely in another environment. Therefore, additional studies are still required to realize such surfaces' potentiality in different icing conditions and based on their desired application. It is crucial to comprehend the nature of ice repellency in all environments to identify the limitations of solutions and design new materials with robust ice-phobic properties [30]. Thomas Young described the equilibrium behaviour in a droplet on an ideal surface in 1805 [27]. In the early 1900s, the metallurgical community described deviations in the droplet's contact angle on a solid surface that affect the adhesion and mobility of a liquid on such a surface. They called that "hysteresis" [65]. However, in earlier times, Gibbs's work on surfaces' thermodynamic properties included metallurgical community claims. The work was about the frictional resistance to a displacement at the liquid-solid interface, which was later named contact angle hysteresis (CAH) [66]. Subsequent developments have led to the Wenzel [67], and Cassie-Baxter equations to understand non-ideal surfaces further [68]. All these theories jointly have determined the surface properties considered necessary to produce highly efficient water repellent surfaces [69]. In the 1900s, the discovery of natural rubbers and the subsequent development of synthetic polymers resulted in the significant development of water-repellent surfaces [70]. Common silicone rubber (PDMS) and polytetrafluoroethylene (PTFE) (commercially called Teflon) are two examples of results from the development of synthetic polymers with water-repellency properties (low surface energy).

This breakthrough was later updated by identifying porosity. Modifying surface porosity affected PTFE properties and made it breathable and more water-repellent. It was an innovation in the high-performance textile industry. Modifying surface wettability by these polymers can be done on various materials because these polymers can be applied on surfaces as coatings. Development in creating low-energy surfaces caused more accurate control on chemistry and repellency of certain materials' surfaces [71]. In the late 1990s, improvements in visualization and fabrication techniques created the possibility of a more detailed investigation of occurrences in nature, including detecting water-repellent phenomena. For instance, the ability to visualize and imitate the lotus leaf structure enabled manufacturing synthetic superhydrophobic surfaces (SHSs) with hierarchical structure and low surface energy. Superhydrophobic surfaces show very high water contact angles ($CA > 150^\circ$) and low ($CAH < 10^\circ$) [72]. However, there is another issue related to these complex surfaces with the water-repellent feature. Later it was discovered that under harsh environmental conditions, voids between surface topography could serve as vulnerabilities. This problem resulted in manufacturing another water-repellent surface known as slippery liquid-infused porous surfaces (SLIPS). In this method, a lubricant is infiltrated inside a textured solid surface. These surfaces are stable under high pressure, showing virtually no contact line pinning and are called omniphobic [73]. Many beneficial properties have been obtained by producing non-wettable surfaces, such as fluid-flow drag reduction, heat transfer enhancement, and self-cleaning ability [74]. Assumption of similarity mechanisms of ice and water adhesion suggests that surface-roughness-induced superhydrophobicity can be used as ice-phobic material. However, results are indicated that superhydrophobic coatings alone may not be adequate for deicing and anti-icing purposes because the force required to detach a piece of ice depends on the receding contact angle and the initial size of the interfacial crack, while the force needed to repel a water droplet, additionally depends on contact angle hysteresis. Therefore, even surfaces with very high receding contact angle (superhydrophobic surfaces) may have strong adhesion to ice [32]. For example, in-flight icing depends on external circumstances, not only the surface morphology, and a thin layer of ice is formed, the coating would no longer be functional. Using a hybrid coating or active ice protection system for aerospace applications is one of the solutions that has taken much attention [75].

As a rule, four key-features define the ice-phobicity performance of a surface: (1) lower temperature to start ice nucleation, (2) delay in ice accretion time, (3) smaller ice adhesion strength at the ice-solid interface, and (4) long-lasting durability. The influence of these key-features varies according to the type of application for ice-phobic surfaces [1]. The diversity of icing problems causes various challenges, and icing conditions can only be controlled in specified circumstances. For example, heat exchangers may be designed to operate within limited temperature and humidity source. In contrast, ice build-up occurs in natural environments over a wide range of temperatures, humidity degrees, and other weather conditions. Although it is typical for laboratory experiments to analyze a single aspect of icing, practically ice-phobic materials need the ability to withstand a wide range of possible conditions [33]. Therefore, the industry for tackling icing problems still utilizes active ice protection systems (chemical, mechanical and thermal). However, these mechanisms can be inefficient, environmentally unfavourable, expensive, and operationally time-consuming. Thus, it would be helpful if surfaces could passively impede ice formation or simplify ice removal [76]. Among all techniques, superhydrophobic surfaces (SHSs) are of high interest due to their remarkable ability to get rid of water. However, research has revealed that durability and humidity tolerance during ice removal is still a big challenge. Despite the continuous improvement of passive ice-repellent materials, each of them has certain limitations. For instance, Sun et al., in their work, used SHS surfaces to reduce the amount of fluids in airplane deicing. They also proposed to use biological or bio-mimetic antifreeze proteins in combination to have more environmentally friendly solution [77]. There are a limited number of studies about the integration of ice-phobic materials with current active technologies; however, it seems important consideration should be paid to these techniques. The inadequacies and principal merits of these methods call to substitute the individual anti-icing systems, which led to the design of multi-functional (hybrid) systems [78].

2.3 Multi-functional (Hybrid) Strategies

The limitations and principal merits of the passive and active IPS methods were addressed in the prior sections. Active ice protection systems (chemical, mechanical and thermal) are

applied for in-flight ice mitigation. These methods are characterized based on the physical principle they used to remove the ice [34]. Concerns about performance, efficiency, energy consumption, and active systems' environmental problems result in attempts to develop alternative solutions. In this regard, applying electrical power as a more efficient and cleaner energy source has been taken into serious consideration for an all-electric aircraft [79]. However, applying electric power for the whole leading edge, especially in large aircraft, requires a massive amount of energy, which is still a significant challenge in aircraft design. In particular, this stands out during take-off and landing, which have the highest potential risk of icing, and that was the main reason why attention was drawn to clean and energy-efficient passive methods [80]. However, as mentioned earlier, passive methods alone are not sufficient for aircraft deicing or anti-icing demands as demonstrated in the early work achieved by Anderson in 1997 [75].

Electrical ice removal techniques are mainly divided into electro-thermal and electro-mechanical systems. These systems, at first, have been established to decrease the amount of required energy for in-flight ice mitigation. The electro-thermal approach is used to stop droplets from freezing in the area near the leading edge, while the electro-mechanical system is regularly pushed to produce ice shedding in the unheated section at the back of the airfoil [36]. Besides the conventional active ice protection systems, many studies are focused on exploring the possibility of using water-repellent coatings to delay or even prevent ice formation on aerodynamic surfaces. However, passive systems could not still provide all the requirements for being admitted as dependable in-flight ice mitigation techniques. With this in view, hybrid mechanisms combining passive and active methods are proven to be more efficient, environmentally friendly, less expensive, and time-saving systems but how these systems work [35]. As the most accepted method, Prevention of ice formation and accretion over the aerodynamic surfaces can be efficiently achieved by manipulating active approaches to heat the critical surfaces electrically. There are two main regimes in this connection: the evaporative regime in which the heat is provided to over $100^{\circ}C$ on the surface to evaporate all the impinged super-cooled water droplets [81], and wet-water runback regime in which the surface is heated up to a temperature higher than the water frozen temperature to keep the impinged super-cooled water droplets in the liquid phase [82]. It is evident that an

extremely high-power input to the electric heating element is required in the evaporative regime to preserve the surface at a high temperature over 100 C. Although this method ensures the surface remains free from ice, it requires high power consumption. Moreover, it might also cause undesired over-heating issues to the surface. On the contrary, the wet-water runback regime is much safer and energy-saving. In this method, the existing water mass runback over the leading edge and is shed by boundary layer airflow. However, the driven water mass may freeze again downstream of the heated zone where the surface wetness factor coupled with the runback rivulet flow structure is deficient. Consequently, thermal systems would be inefficient and massive energy should be spent to solve this concern [83]. A much stronger convective heat transfer exists on an airfoil leading-edge (LE) stagnation line due to aerodynamic forces' zero velocity. Therefore higher energy input is required in the region near the blade leading edge, compare to the downstream regions. On the other hand, Papadakis et al. in their work showed that super-cooled droplets impinge the surface mainly in the region near the blade leading edge. Therefore it is essential to heat the stagnation region rather than the other surface regions. The only remaining challenge is preventing the refreezing of the runback surface water without consuming a considerable amount of power. The traditional solution to stop refreezing the downstream flow at the back of the surface is to extend the heated area's size, which keeps runback water in the liquid phase. Such a solution requires massive power to heat the whole surface [84].

Waldman et al. [85] and Liu et al. [86] revealed that ice adhesion strength over ice-phobic surfaces is much smaller than hydrophilic surfaces. They showed that water or ice-water mixture runback much faster over ice-phobic surfaces, which cause them to be repelled from the surface by the same magnitude of aerodynamic forces. Sharp roll-off and faster water droplets movement over the superhydrophobic surfaces is another promising solution to prevent runback ice formation. A combination of superhydrophobic coating (Passive IPS) and active leading edge (LE) heating method then established a cheaper ice protection strategy with higher efficiency [16].

Figure (2.2) is a sample of an electro-mechanical hybrid system. In this system, to prevent ice formation and accumulation, a running-wet electro-thermal heater is placed at the leading edge. In case of runback water freezing, piezoelectric actuators start to work and mechan-

ically shed the formed ice [46]. Because of the lowered ice adhesion on superhydrophobic surfaces, another hybrid method could be suggested, which is more efficient than the previous model. Such a system enables the melted ice to move faster downstream and pushed away by the aerodynamic forces. Piezoelectric actuators produce a dynamic mechanical shear in this condition and require less energy to operate [87]. A schematic of the hybrid IPS layout integrated active-passive IPS: (A) thermo-electric heating wire, (B) piezoelectric actuators, and (C) ice-phobic surface is presented in Figure (2.10) [88].

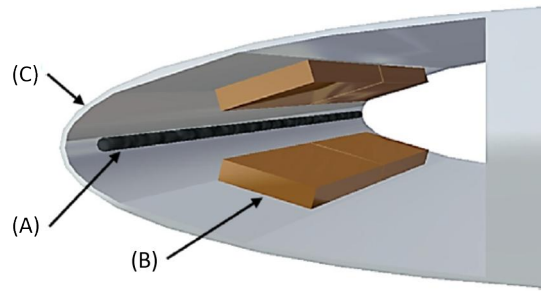


Figure 2.10: Schematic of the integrated active-passive IPS: (A) thermo-electric heating wire, (B) piezoelectric actuators, and (C) icephobic surface (on the airfoil top surface) [88].

As mentioned earlier, near an airfoil leading edge, aerodynamic shear forces in the region would become very small. It can even vanish at the stagnation line because the wind's local velocity would be zero there and not workable to shed water droplets anymore. As another instance of hybrid system worthiness, Figure (2.11): (a) presents the dynamic ice accretion process over the hydrophilic surface without any anti/deicing actions. After the super-cooled water droplets impinge onto the surface, a portion of the impacted water droplets turns into ice. The remaining portion of the impacted water mass was found to form a thin water film flow first and then runback flow over the iced surface. Figure (2.11): (b) shows a passive strategy with superhydrophobic coating. This coating was found to reduce ice accretion significantly; moreover, the accretion area was found significantly reduced. However, it is still far from sufficient to prevent ice formation. Figure (2.11): (c) shows the active electro-thermal strategy. When the water moved to a further downstream region beyond the area protected by the electric heating element, the runback surface water was found to be frozen into ice. The irregular-shaped ice structures accreted over the airfoil's rear surface would

cause severe adverse effects on the aerodynamic and structural performances. In summary, by using the heating strategy only, it was also incapable of preserving the entire surface free from ice. Finally, Figure (2.11): (d) presents a multi-functional ice protection strategy (combining both heating and superhydrophobic coating). During the icing experiment's entire duration, the airfoil area remained completely free from ice, showing an outstanding anti/deicing performance compared to that of the other methods. In this experiment, results showed that a hybrid strategy (a combination of electric-heating and ice-phobic surface coating) substantially requires less power consumption (up to 90% saving) for wind turbine ice mitigation in comparison to the conventional strategy [16]. As shown in Figure (2.11), using multi-functional equipment (hybrid systems) for ice-mitigation would be more efficient than fabrication surfaces that only passively repel super-cooled water droplets. Moreover, these systems have also shown better performance compared to an individual electro-thermal IPS [89].

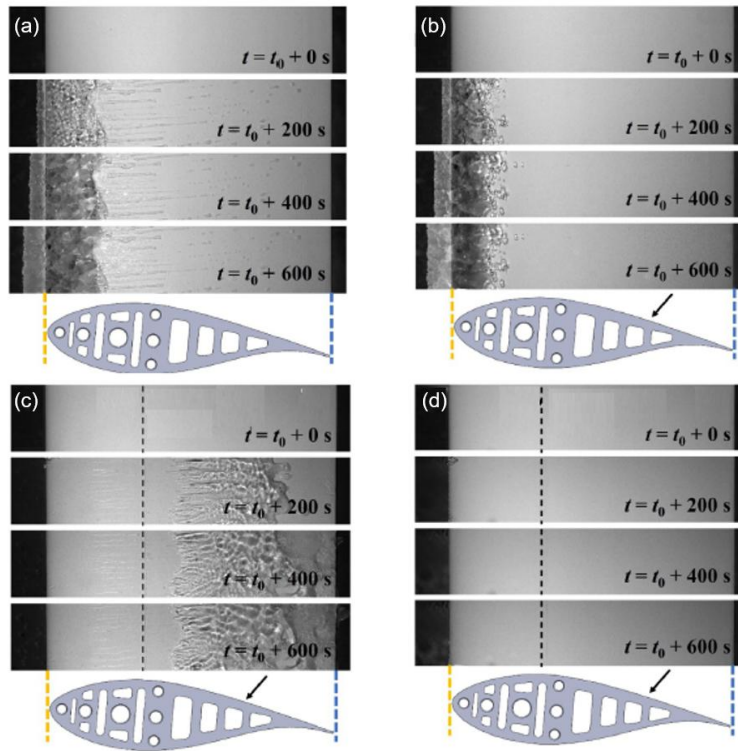


Figure 2.11: Comparison of various anti/deicing strategies, (a) ice accretion process over the hydrophilic surface, (b) passive strategy with superhydrophobic coating, (c) active electro-thermal strategy, and (d) multi-functional ice protection strategy [16].

Recently a hybrid anti-icing system (ICE-WIPS) has been developed by the Japan Aerospace Exploration Agency (JAXA). This system includes an ice-phobic coating and electro-thermal heating, which is proven to reduce power consumption by more than 70% in dry-icing conditions and 30% in wet-icing circumstances. A Schematic description of the system is presented in Figure (2.12), impacted Super-cooled water droplets form ice at first. These accumulated ice mass become melted by running an electro-thermal heating unit at the leading-edge region. Afterward, due to the local airflow around the wing, melted ice or water film moves downstream and usually refreeze at the surface's tail. Applying ice-phobic coating then supports the shedding of the ice or a water film from the surface. In this system, the energy consumption is remarkably reduced by restricting the to-be-heated area to the leading-edge region. However, the ice-phobic coatings' durability is a critical worry, mainly in harsh icing conditions that cause severe erosion of ice-phobic coatings. Therefore, regular coating repairs are consistently necessary [90].

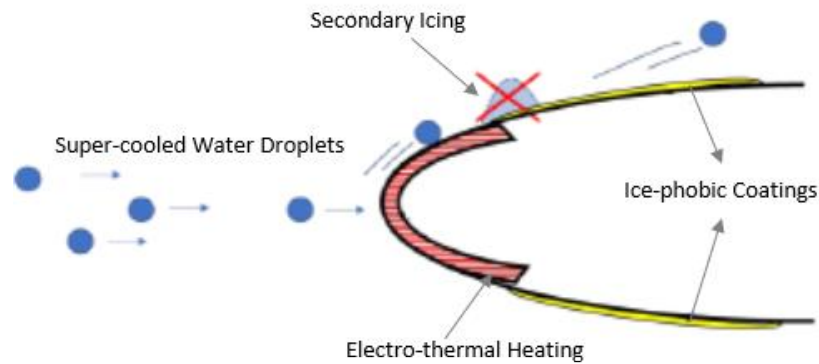


Figure 2.12: ICE-WIPS (Hybrid Ice-phobic Coating and Electro-thermal Heating) [90].

Various solutions have schemed in this connection, resulting in more durable coatings such as employing different coating fabrication methods or using different ice-opposing materials with more durability. However, in this study, these issues are not considered the primary target, but the focus would be on improving conventional anti-icing systems to a more efficient and safer one considering safety and commercial standards. The next chapter will discuss the fabrication method that can be used to develop such conventional systems. Table (2.2) presents a comparison of conventional ice mitigation techniques, which are can be utilized in combination as hybrid systems. [25].

Table 2.2: Comparison of ice mitigation techniques [25].

Techniques	Protection Type	Retrofitting	Lightning Protection	Control Issues	Effectiveness	Cost	Energy Consumption
Hydrophobic Coatings	Anti-icing	Yes	No	N/A	Limited	Low	N/A
Ice-phobic Coatings	Anti-icing	Yes	No	N/A	Limited	Low	N/A
Biscous Coatings (non water soluble)	Anti-icing	Yes	No	N/A	Momentaneous & Degrading	Low	N/A
Biochemicals	Anti-icing	Yes	No	N/A	Momentaneous & Degrading	Low	Medium
Black Paint	Anti-icing	Yes	No	N/A	Very Limited	Very Low	N/A
Pneumatic	De-icing	No	No	Medium	Very Limited	High	Very Low
Expulsive	De-icing	No	No	Medium	Effective	High	Very Low
Hot Air	Both	No	No	High	Effective	Very High	Medium-High
Outside Resistive heaters	Both	Yes	Yes	Medium	Effective	Very High	Low-Medium
Inside Resistive heaters (in the resin)	Both	No	Yes	Medium	Very Effective	High	Low-Medium
Inside Resistive heaters (outside the resin)	Both	No	Yes	Medium	Effective	Medium	Low-Medium
Microwave	De-icing	Yes	Yes	Very High	–	Medium	Low
Infrared	De-icing	Yes	Yes	Very High	–	Medium	Medium-High
Ultrasonic Waves	De-icing	Yes	No	Low	Very Effective	Medium	Low
Operational Stop	None	Yes	No	High	Limited	N/A	N/A

Chapter 3

Fabrication Approaches

Based on previous chapters' content, understanding of the icing phenomenon more in depth, or developing new fabrication strategies would be a solution to produce more reliable ice-opposing systems in the future. It is worthy to mention that efficient hybrid ice protection mechanisms might be cheaper, environmentally friendly, and entirely efficient. Using the active ice protection systems (electro-mechanical or electro-thermal) can be recognized as the most common ice protection method. Among these two types of systems, electro-thermal heating has proven the most efficient and reliable IPS type. In this connection, different types of systems are suggested either theoretically or, in some cases implemented practically. Efforts are made to address the existing shortcoming of these systems and improve them to meet the desired goals as far as possible. One solution is finding better production ways and implementing alternatives to develop these systems differently. For instance, various production methods are applied to create the desired structure. Various materials could be used to make these systems if the primary requirements are provided. For example, as a novel, flexible, versatile, and cost-effective method, thermal spray technology is considered as another process to create demanded structures. Utilizing this method also is an excellent way to tackle significant limitations involve with heating strategies. This chapter describes how we can produce our proposed ice protection system by using the plasma spray technique. Moreover, according to the expected function, the reason for this choice and the advantages are stated.

3.1 Thermal Spray Technology

A variety of fabrication methods are applied to produce artificial (bio-mimetic) surfaces, lithography, deposition, stretching, etching, evaporation, thermal spraying, sol-gel, and the like are some of the examples of these fabrication methods. Various materials are manipulated to make functional surfaces (metals, polymers, semiconductors, nano-tubes, nanoparticles). Thermal spraying techniques have proven to be a sufficient method in almost every aspect of surface fabrication [91]. Thermal spray processes comprise a combination of coating methods in which metallic or non-metallic coatings are deposited by a heat source to melt the feedstock. High-temperature gas is used to supply kinetic energy to the molten particles that impinge the substrate surface and rapidly cool down to form a stable topcoat with the desired thickness to provide the functional coating. Covering thermal sources and jet configurations bring about lots of different deposition processes, each one producing coatings with distinct micro structures and physical properties [92]. Metals, alloys, ceramics, plastics, and composites are coating materials used for thermal spray. The coating properties are typically characterized by measuring its porosity, oxide content, macro and micro-hardness, bond strength, and surface roughness, etc. Typically, thermal spraying processes can be classified into various categories according to temperature and velocity of the sprayed particles [93]. Figure (3.1) presents a classification of the thermal spray techniques [94].

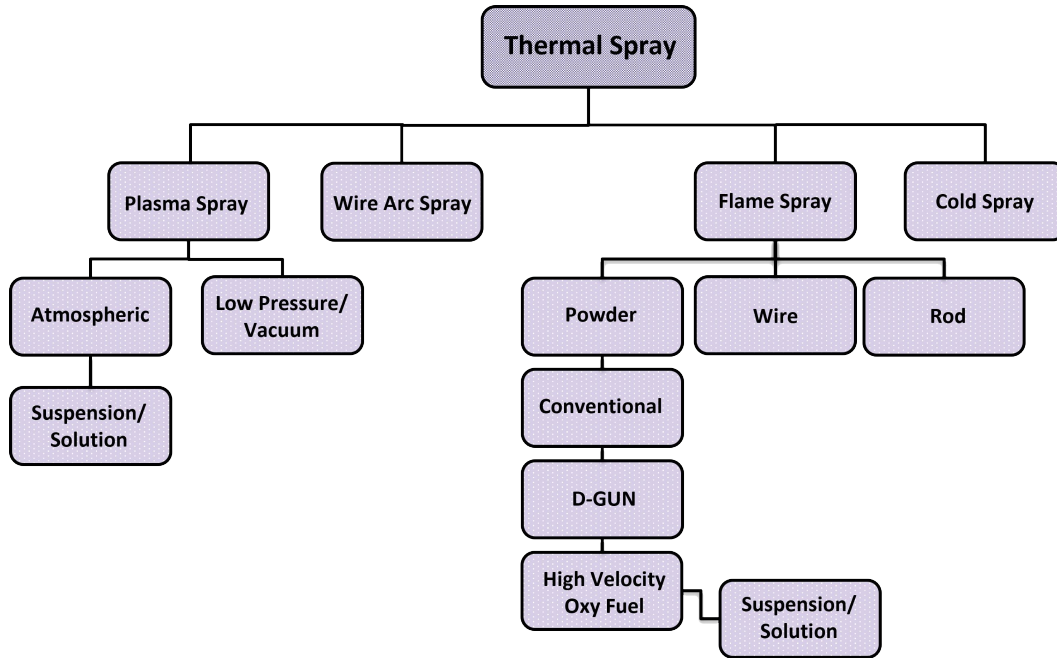


Figure 3.1: Classification of the thermal spray deposition techniques [94].

In this study atmospheric plasma spray (APS) is used for coating fabrication. Plasma spraying technique is a flexible, versatile and scalable process to produce coatings in the several applications.

3.1.1 Plasma Spray Techniques

Plasma spray processes can provide precise surface morphology with the desired mechanical properties. Some of the benefits of this method incorporate the ability to deposit a wide variety of materials on different substrates. This method of coating is cost efficient as compared to the other methods of surface alteration. APS coating process also can be used without applying a considerable amount of heat to the substrate. Using thermally sprayed coatings as heating elements for dealing with in-flight and other types of icing has been previously reported. Figure (3.2) shows a schematic representation of thermal spray process [95].

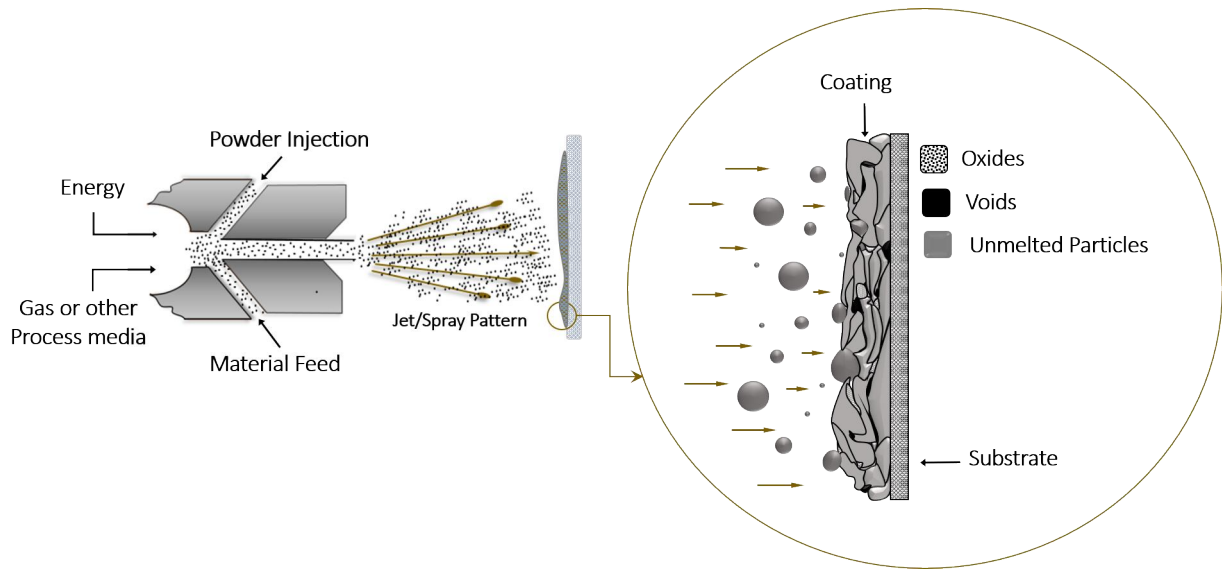


Figure 3.2: Schematic of a plasma spray process [95].

3.2 Thermal Spray Application for Heater Fabrication

In the following, the advantages of plasma spraying in the fabrication of heating elements are presented. The primary purpose of thermal spray technologies has been to deposition protective coatings, which improve or restore the surface of a solid material. One application of this method, which has recently received much attention, is utilizing thermally sprayed metals as heaters [96]. Heating surfaces is required in several of processes and systems such as scientific instrumentation, industrial apparatus, medical equipment, etc. Usually, electrical elements are embedded in the vicinity of these surfaces to provide the anticipated amount of heat on these surfaces [60].

3.2.1 Conventional Heating Elements

A heating element is composed of both electrically conductive and insulating materials, designed to serve a heating purpose. A heating element is more than the heating alloy alone. It is an assemblage of parts that includes a framework of insulating material as well as lead connectors, in the case of an open coil heater. For example, the heating alloy is typically held or suspended by a mica or ceramic insulator. Wire terminals safely connect the heater coils to the circuit. The core of an electric heater is the heating element alloy converting

electrical energy into heat [97]. Some conventional heating elements are shown in Figure (3.3) [98]. Accordingly, heating elements should be appropriately tailored to their particular applications. However, it is not always doable because of several intrinsic limitations associated with heating element geometry and physical location. Therefore, finding alternative solutions is a priority to overcome these limitations. One approach to cope with these issues is using thermal spray techniques to produce resistance heating elements suitable for applying considerable heat flux to solid surfaces. Several restrictions are resolved by replacing common heating elements with thermally sprayed heaters outlined subsequently [59].



Figure 3.3: Several types of conventional heating elements [59].

3.2.2 Thermally Sprayed Resistive Heaters

As earlier mentioned, thermally sprayed electrical elements deposited directly on surfaces can tackle common heating elements' restrictions by tailoring them to the application's geometry. Regarding temperature, for instance, it is reported that thermally sprayed heater is superior to other technologies like thick film technology, micro-hot plates, etc. Thermally sprayed heaters furthermore have shown better performance in uniform temperature distribution. The intimate contact between the heating element and the substrate helps in getting a homogeneous temperature distribution. Moreover, the rate of heat transfer is improved by minimizing the distance between the heater and the to-be-heated surface. They are also reliable for industrial use because even at high temperatures, their life span is well long compared with other heating element types because of their resistance to thermal shocks, which notably affects heaters on ceramic substrates [59]. There are some other significant particularity for thermally sprayed heaters over other heating approaches, including the capability

to coat large surfaces with complex shapes quickly and with various materials [99]. Recently, Battelle's Heath-coat technology uses a high-conductivity, carbon nanotube heating coating that conforms to the aircraft's skin and utilizes intelligent sensors and controls to reduce ice accumulation without compromising flight performance. This innovative anti-icing and de-icing solution's small size, weight, and power envelope are unmatched in the industry [100]. High-temperature resistive heaters have shown the ability to overcome the constraint of conventional heaters (usually 3D-geometry coil). They either comprise an air gap or a weighty insulator thickness between the to-be-heated material and the heater restraining the heat transfer's reaction time and efficiency. Likewise, this geometry is difficult to adapt to space-limited applications. As mentioned earlier, an elegant way of avoiding such problems is to thermally spray resistive elements directly on the surface to be heated. This technique offers a fast and flexible way of fabricating convention heater solutions for arbitrary shape surfaces. Resistive heaters have been fabricated using thermal spray by various authors. Safety, practicability, performance efficiency, durability, cost-efficiency, and environmental issues are the significant concerns that have always been given priority in aviation industries. In this context, improvements of in-flight ice mitigation strategies are still needed. Current systems have limitations, especially in terms of system design and fabrication methods (a place where other solutions should be considered). This thesis tries to define a more optimal anti-icing system for in-flight icing incidents. The next chapter presents the motivation and objective of the project.

Chapter 4

Research Objectives

This work aims to put forward a practical and cost-effective method to develop an ice protection system to address the weaknesses of typical deicing and anti-icing applications in aerospace industries. Furthermore, the present study analyzes an alternative fabrication method (thermal spray technique) to manufacture heating elements for aerospace applications, taking into account the anti-icing performances, durability, maintenance challenges, and cost-efficiency. Additionally, the contribution of a passive mechanism (nano-textured superhydrophobic coating) and an active method (electro-thermal heating) working in a synergic operational mode. Moreover, this work aims to investigate this multi-functional system's performance by integrating it into a unique architecture. Throughout this project, several sub-objectives have been set to reach the primary goal in the following way:

- An experimental study on the feasibility of developing an active ice protection system (electro-thermal anti-icing) ,focusing on the reduced power consumption in the harshest in-flight icing conditions.
- Using plasma sprayed iron-based powder (FeCrAlY) as resistive heaters right on the aerodynamic surface to tackle conventional heating elements' restrictions by tailoring them to the component geometry. This strategy is expected to lead to some significant improvements such as increasing the applicable temperature, better performance regarding the homogeneity of temperature distribution, increasing the heat transfer rate by minimizing the distance between the heater and the to-be-heated surface, and

resolving intrinsic limitations associated with heating element geometry and physical location .

- Developing the surface morphology by using superhydrophobic coatings to effectively repel water droplets, delay ice nucleation, and significantly , eliminate ice adhesion. Operating this strategy is expected to reduce the required energy consumption, deicing time and most efficient ice protection strategy. Having a cheaper and more environmentally friendly system is expected.
- Implementing only a small resistive heater chord instead of traditional heating of the whole front side of the wing leading edge. This structure acted in a minimal zone to prevent ice formation at the stagnation line.
- Design a particular structure by heating the unprotected areas when needed to prevent rapid runback ice formation at uncovered regions.
- Improving the temperature control of heating processes at any time required.
- Decrease in the time it takes for the heater to reach the target temperature needed to prevent icing, increasing safety significantly.

Chapter 5

Materials and Methodology

In this chapter, a detailed plan of the research methodology is presented. The required facilities and equipment are described along with their respective procedures. This research project comprises ten steps, including, (1) preparation of experiment samples (introduction to the type of substrates and how they are prepared before spraying), (2) presenting the powder feed-stocks that were used in each of the coatings, (3) deposition of coatings (insulation layer and heater layer) by using APS, (4) deposition of ice-phobic layer by using a commercial superhydrophobic coating, (5) analysis of the micro-structure of the coatings, (6) electrical characterization of the coated samples, (7) analysis the thermal performance of the coated samples, (8) evaluation the performance of the coated samples as a hybrid ice protection system in an Icing Wind Tunnel (IWT), (9) Identify of common electrical cartridge heating element, and repeat the electrical and thermal analysis for the system and (10) the way of setting up and testing the thermal anti-icing system by using conventional thermal ice protection system and fabricated anti-icing system system. These steps are discussed in detail below.

5.1 Design and Preparation of Experiment Samples

Several experimental methodologies were used for static measurement of physical properties (mechanical, electrical, and thermal) of the heaters' performance, and these measurements were incorporated into the simulation and actual analysis. Based on the results

obtained from previous published studies, a cylindrical aluminum tube was selected as the substrate for the deposition of the coatings. Aluminum was chosen because it is the fuselage's primary structure material, including the leading edges. The cylindrical shape was chosen to be as close as possible to the leading edge's form (airfoil geometry). A plasma sprayed layer of zirconium oxide was deposited on the aluminum tubular substrate to electrically insulate the resistive heater from the substrate. additionally, zirconium oxide also has a very low thermal conductivity that helps to prevent the transfer of heating energy into the substrate (thermal insulator). A plasma sprayed layer of FeCrAlY as a resistive heating element was deposited on the insulator layer. The resistive system is designed with a unique geometry that consists of parallel strips deposited at equal intervals on the insulator surface. Thermal spray masking tape was used to define the layout of this mechanism. The two layers was deposited by APS. In icing test one layer of a commercial superhydrophobic coating was deposited on top of the resistive heater to assess the effect of using a superhydrophobic layer on deicing time and reducing energy consumption (role of passive ice protection system).The measurement of electrical properties of the coating as well as icing tests were subsequently assessed .

Figure (5.1)) (a) shows the schematic of the designed sample structure for the icing test to evaluate the effect of using hydrophobic surfaces in deicing or anti-icing process, and (b) represents the schematic of the designed cylindrical samples for the heated anti-icing experiments.

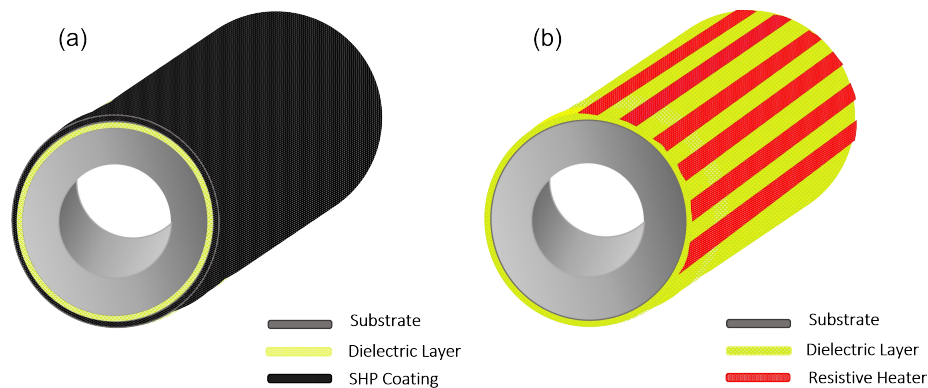


Figure 5.1: Schematic representation of the designed cylindrical samples for the experiments.

5.1.1 Materials and Types of Equipment Selection

A 10-cm (4-inch) long, 2.54-cm (1-inch) OD, and 0.65-cm (1/4-inch) wall thickness of high-strength 2024 aluminum tubes (METAL-PROS, Ottawa, Ontario, Canada) were used as the substrates. A cylindrical hi-density cartridge heater (diameter: 1.27 cm (1/2-inch), length: 11.4-cm (4.5inch), was used as an internal heater (Omega Environmental, QC, Canada). Yitria stabilized zirconium oxide powder (Metco 202NS) with a nominal particle size distribution of $(-90 \pm 16) \mu\text{m}$ and FeCrAlY iron-based alloy (Metco Amdry™ 9700) (Metco Oerlikon, Fort Saskatchewan, Canada) with a nominal particle size distribution of $(-45 \pm 11) \mu\text{m}$ were used to deposit the insulating and heating layer respectively. A radial injection plasma torch 3MB (Sulzer Metco, USA). Amdry T-3325, thermal spray masking tape (Metco Oerlikon, Fort Saskatchewan, Canada), providing the desired geometry. High temperature and high thermally conductive paste (Omega Environmental, QC, Canada) for continuous use between -40 and 200 °C.

Before deposition, the cylindrical aluminum substrates were grit-blasted for surface decontamination and enhance coating adhesion by increasing the surface roughness. In order to decrease the tensile stresses generated during cooling and solidification of the zirconia molten droplets, the substrates were preheated before spraying. Figure (5.2) (a) and (b) shows the morphology of the zirconia and FeCrAlY powders respectively [101].

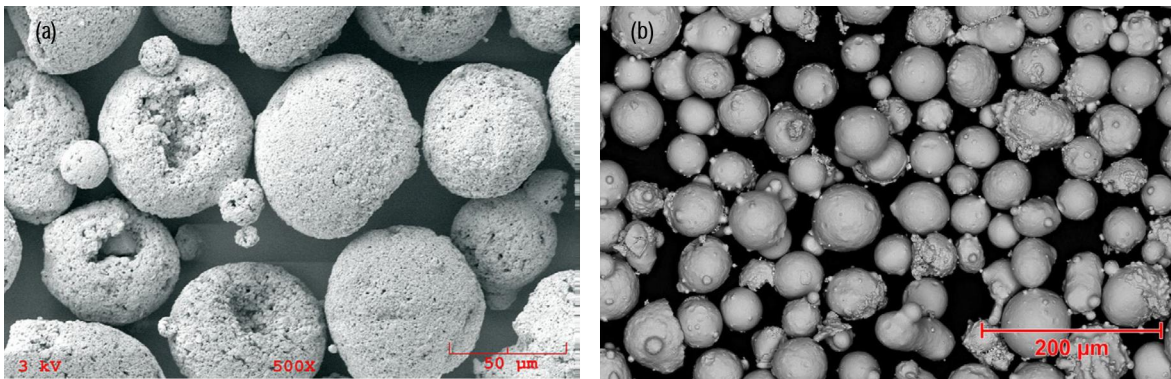


Figure 5.2: Photomicrographs of (a) Metco 202NS and (b) Metco Amdry 9700 [101].

5.1.2 Coating Process

The samples were coated by Zirconia and FeCrAlY using the reference parameters delivered by Metco, but some differences were applied to meet a better result, such as supplying more power, decreasing the powder feed rate, and modifying spray distance. Table (5.1) present the spray parameters for the coating deposition.

Table 5.1: The plasma spray parameters used for the coating of substrates.

Current (A)	Voltage (V)	Primary gas (Ar) (l/min)	Secondary gas (H2) (l/min)	Powder feed rate (g/min)	Spray distance (cm)	Number of passes
Insulator (Zirconia powder)						
500	64	39.4	6.6	45	64	12
Heating element (FeCrAlY powder)						
500	65	43.8	6.57	20	127	8

The Thermal Spray Laboratory at Concordia University is equipped with a 3MB (Sulzer Metco, USA) plasma torch and controller system that is fully operational and used to produce the coatings in this research. Figure (5.3) shows a schematic of the plasma gun and coating process [102].

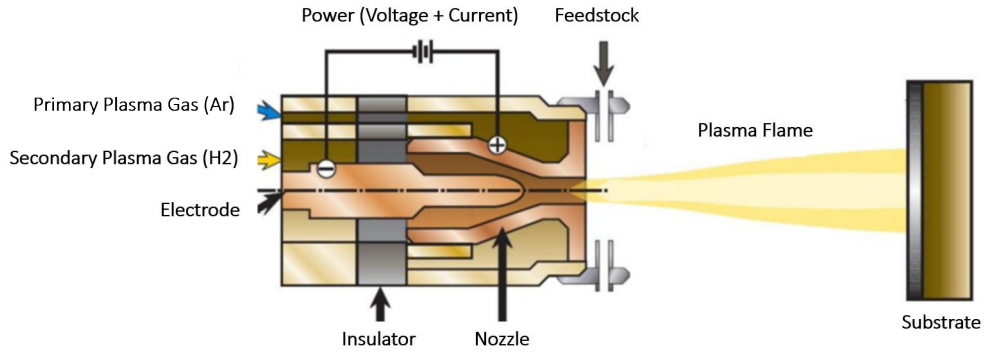


Figure 5.3: Schematic of the plasma spray process [102].

After analyzing the coated samples and finding the proper spray parameters and the appropriate powder type, Several samples were prepared and coated for the electrical, thermal, and icing tests. Figure (5.4) shows the setup used for the spraying of the substrate.

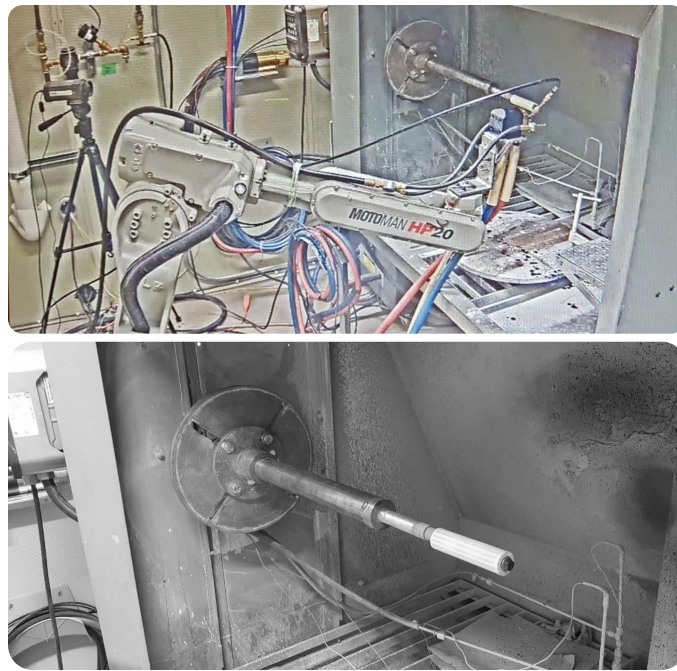


Figure 5.4: Plasma spray process equipment.

An optical spray sensor (Tecnar Accuraspray 4.0) were used to measure the temperature and velocity of the in-flight particles during spraying. An infrared camera (FLIR 42701-1201 A320 Thermal Imaging Camera) was also used for monitoring the substrate's surface

temperature during spraying. A design of the experiment (DOE) to efficiently reduce the time and cost of experiments assessed each process parameter's effect.

5.2 Coating Structure and Performance Characterization

5.2.1 Structural Imaging and Morphology Characterization

After the deposition process, according to ASTM guidelines, standard metallography procedures, including cutting, mounting, grinding, and polishing, was done to prepare the sprayed samples for cross-sectional imaging. A Secotom 15 precision cutting machine (Struers, Cleveland, OH, USA) was used to cut the coated samples. Then samples were cold-mounted in an epoxy resin (Epofix, Struers, Cleveland, OH, USA) for microstructural characterization. A Tegramin automated grinding and polishing system (Struers, Cleveland, Ohio, USA) was used to comprehensively grind and polish the samples to get a mirror-like surface suitable for further analysis. Optical microscopy primarily was utilized to evaluate the coating thickness, cross-sectional structure, and bonding quality. The coatings' morphology was investigated by Scanning Electron Microscopy (SEM) (Hitachi S-3400N VP) afterward. Samples were covered with a thin layer of gold to prevent the accumulation of static electric charges on the non-conductive zirconia coating. The collected images were analysed by the ImageJ software for image processing (developed at the LOCI, University of Wisconsin) to evaluate the coating porosity, and oxidation. The LEXT OLS4000 Confocal Laser Microscope (Olympus, Toronto, Canada) also used to measure the coatings' local and overall roughness.

5.2.2 Electrical Characterization

Defining the electrical properties of the coatings has a high level of importance since the amount of heat generated by a heating element (deicing element) coating for a given current is directly related to its electrical resistance. Electrical resistivity is a property of a material

that indicates how well it opposes and resists the flow of electricity. The following equation describes the relationship between resistance and resistivity of a specimen:

$$R = \frac{\rho \times L}{A} = \frac{\rho \times L}{wt} \quad (5.1)$$

In which ρ is the resistivity ($\Omega \cdot m$), R is the electrical resistance (Ω), L is the specimen length (m), A is the specimen cross-section area (m^2), w is the specimen width (m) and t is the specimen thickness (m). In this experiment, the four-point electrical probe technique was used to determine the specimens' electrical properties. This technique is handy due to eliminating the wire resistance and any contact resistance that might cause errors in the resistance calculation. As shown in the schematic of this method (Figure (5.5)) [103]. Four wires were attached to the sample's top face for doing the four-point probe test

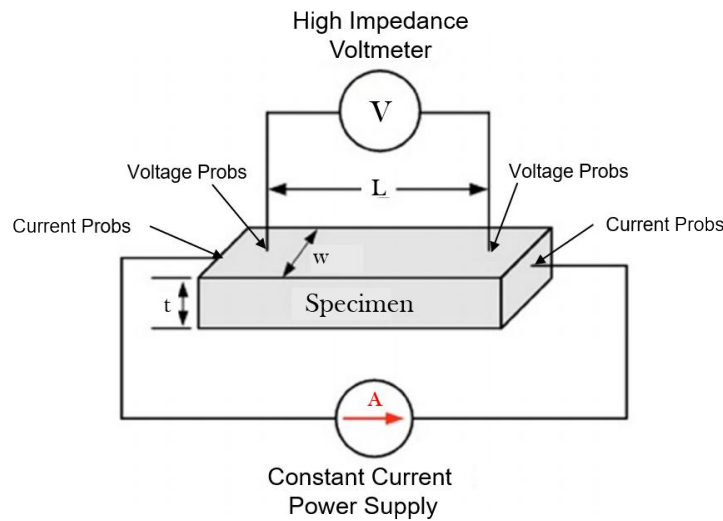


Figure 5.5: Schematic of four point probe method [103].

A constant current was applied to the sample through the current probes connected to a power supply. A voltmeter was connected to the sample using voltage probes for measuring the voltage drop between these two locations. The voltmeter is in parallel to the circuit and has a high resistance so that almost no current passes through the voltmeter, To avoid affecting the reading on the ohmmeter. The voltmeter was used to measure the voltage drop along the samples while different electrical currents were applied. Therefore, the resistance

was calculated using the equation (5.2), and we can calculate the resistivity from equation (5.1).

$$R = \frac{V}{I} \quad (5.2)$$

Based on the objectives of the study, samples with several heating configurations were fabricated. Therefore, we needed to calibrate the sample in different forms to evaluate its performance. The electrical characterization was done in seven configurations between three strips (three heating elements). First, the characterization for each strip was done separately, then the experiment was repeated for the three strips at the same time. Finally, this was done for two out of the three available strips (in turn for all strips). Therefore we had a total of seven configurations. In this way, both the correct operation of the system and its controllability were evaluated. Figure (5.6) illustrates this strategy more precisely.

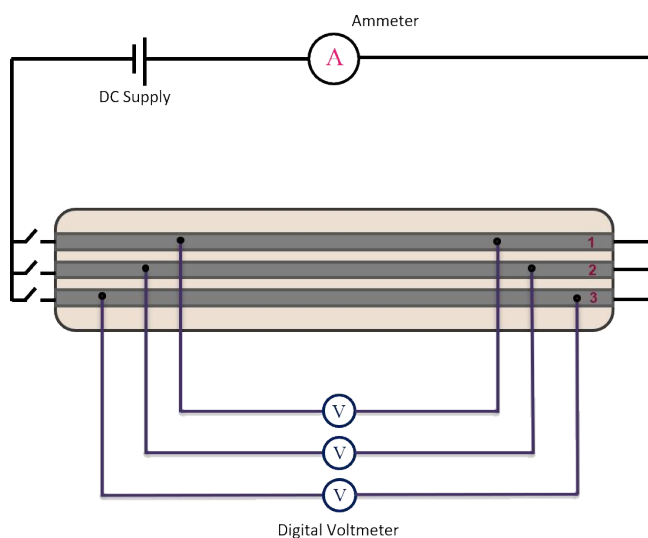


Figure 5.6: Schematic of designed circuit.

Figure (5.7) shows the types of equipment and setup of the experiment used for electrical characterization. For the both thermally-sprayed anti-icing experiments and anti-icing experiment, using the conventional heating strategy (use of electrical heating element to heat the substrate from behind the surface).

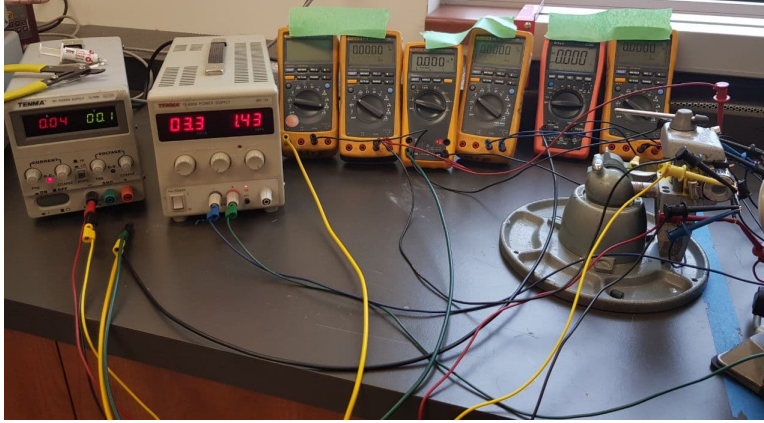


Figure 5.7: Electrical characterization process equipment.

5.2.3 Surface Temperature Measurement

This step involved measuring the surface temperature of coated samples to verify the correct performance of the system. The measurement was done at ambient temperature without force convection. First, the surface temperature of each heating element was recorded. Then, this record was repeated for each designed mode. To this aim, the surface temperature and its uniformity were monitored using an infrared camera (FLIR 42701-1201 A320 Thermal Imaging Camera). In order to guarantee the consistency of the results, each temperature measurement was repeated several times. In addition, the generated power was calculated using equation (5.4).

$$P = VI = RI^2 \quad (5.3)$$

In which P is the electrical power generated (watt), R is the electrical resistance (Ω), I is the current intensity (A), V is the voltage drop between two specimen's probes (volt). Temperatures along the coating surface were also measured by a thermocouple type K (KMQSS-062U-36, Omega, Canada) attached to the surface of the coated samples. Finally, temperature uniformity was measured while the samples were connected to a power supply. For providing the required power, two power supplies were used in the experiments. Figure (5.8) presents these two power suppliers including, (a) TEMNA 72-6908, POWER SUPPLY, BENCH, 35V, 175W) and (b) (TEMNA 72-7695, POWER SUPPLY, BENCH,

36V; Power Supply Output, Type: Adjustable).

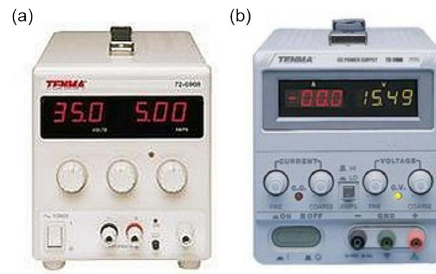


Figure 5.8: types of power suppliers used in the experiments.

5.2.4 Icing Tests

All icing tests were implemented using the closed-loop icing wind tunnel (IWT) at Concordia University (see Figure (5.9)) [104]. The test section of the wind tunnel has a square-shaped cross-section (10 cm wide). The IWT can generate a maximum air velocity of 45 m/s and a minimum air temperature of - 20 °C.

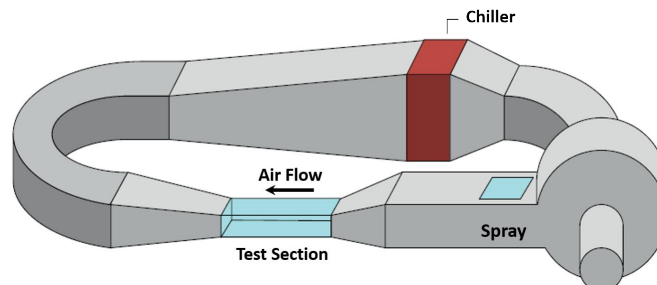


Figure 5.9: Schematic of the icing wind tunnel [104].

Substantially, four key-features define the ice-phobicity properties of a surface: (1) lower temperature to start ice nucleation, (2) delay in ice accretion time, (3) smaller ice adhesion strength at the ice-solid interface, and (4) long-lasting durability [1]. In the present study, two groups of tests were done assessing the anti/deicing performance of the fabricated samples.

Ice Accretion Tests

The first group of experiments comprised ice accretion and heating deicing tests. Several key factors are required for aircraft icing to happen, including liquid water content (LWC), free stream temperature, mean volumetric diameter of the droplet (MVD), and air stream velocity [11]. Primarily to evaluate the effect of the SPS superhydrophobic coatings compared to an unprotected surface on ice accretion, different sets of operating circumstances were performed to characterize typical in-flight icing scenarios in the IWT. These conditions comprised of different liquid water content (LWC) and water droplet median volume diameter (MVD) that affect the icing risk. In two air temperatures $(-3 \pm 1)^\circ\text{C}$ and $(-10 \pm 1)^\circ\text{C}$ conduction were investigated, which typically results in the formation of clear ice and a mixture of glaze and rime ice respectively. An air atomizing spray nozzle was used to inject the water droplets into the air stream. The size distribution and the spray pattern were adjusted by using the air-flow and water flow controllers. Icing blade technique (recommended by SAE International) was employed to measure the LWC value. For the icing tests, cold distilled water was used, which was maintained to a temperature lower than 4°C to guarantee the arrival of super-cooled water droplets to the test section. The total accumulated ice throughout the experiment was determined by weighing the samples before and after each test. Ice accretion on the uncoated sample and coated samples were recorded to investigate their anti-icing performance.

Heated Anti-icing Tests

The second group of experiments included placing the cylindrical heating element inside the tube samples to assess the potential contribution of combining minimum leading-edge electric heating and superhydrophobic coating for icing mitigation. The first set of tests considered the effect of combining the superhydrophobic coating and heating on deicing time. The superhydrophobic coating was placed in different icing conditions for a specific time. After the observation of the ice layer, the water spray was stopped. Then the electrical heating element inside the sample was turned on to absolute power. The time for the samples to become completely ice-free was recorded as the deicing time. Another test was used to

quantify the expected heat input to provide an ice-free surface using a multi-functional strategy compared to traditional techniques. This experiment was performed in distinct air-stream velocity and temperature. The results were recorded for all designed conditions to evaluate the required electrical power to maintain the superhydrophobic coatings ice-free compared to the uncoated sample. Besides, the effect of applying heat only on a smaller region was also tested. A summary of the proposed methodology of the present study is described in Table (5.2)

Table 5.2: Summary of Proposed Methodology.

PHASE 01	PHASE 02	PHASE 03	PHASE 04
Samples Preparation and Materials Selection	Coating Proces	Characterization	Icing Performance Evaluation
<ul style="list-style-type: none"> • Sample Fabrication • Insulator Coating (ZrO2) • Sample's Masking • Resistive Layer (FeCrAlY) • SHP Layer 	<ul style="list-style-type: none"> • Design of Experiment • Spraying • Optimization of the Deposition Parameters • Particle Diagnosis • Metallography 	<ul style="list-style-type: none"> • SEM • Confocal Laser • Microscopy • Image Processing 	<ul style="list-style-type: none"> • Sample Fabrication • Insulator Coating (ZrO2) • Sample's Masking • Resistive Layer (FeCrAlY) • SHP Layer

Chapter 6

Results and Discussion

The results are presented and discussed in this chapter concerning the aim of the research, which was to develop a novel ice protection system. The findings are presented under the following significant headlines: deposition of an insulator layer on substrates using plasma spraying, deposition of FeCrAlY layer by plasma spraying, morphology and structural characterization, electrical characterization, thermal analysis, and icing tests. However, it should be pointed out that this study focuses on the assessment of the fabricated system's anti-icing capability. The effect of heating element geometry on developing controllability of the heating energy is also of great importance. After all tests on heating performance were done on thermally-sprayed samples, all the tests were repeated by using a commercial heating element at the back of the substrate. All tests were done in the same condition to assess the advantages of using the new anti-icing system.

6.1 Coating Fabrication

All samples were manufactured using the Plasma Spraying technique. Before starting the deposition all the samples were prepared. For preparation, the samples were grit blasted to clean the surface as well as increasing the roughness of the surface, resulting in a more efficient deposition. Moreover, it removes the chemicals involved, accuracy for patterning, and longevity for the surface. As mentioned in the previous chapter, two coating layers were deposited on the substrate, that the process parameters to control and create the micro-

texture of the coatings is defined as follows.

6.1.1 Insulator Layer

It was discussed earlier that several process parameters could significantly affect the microstructure of coatings using plasma spraying. Figure (6.1) lists a few parameters that can significantly impact a coating's microstructure [105]. Then, in the current study, the deposition process parameters were modified to achieve the desired structures by depositing molten particles on a preheated substrate.

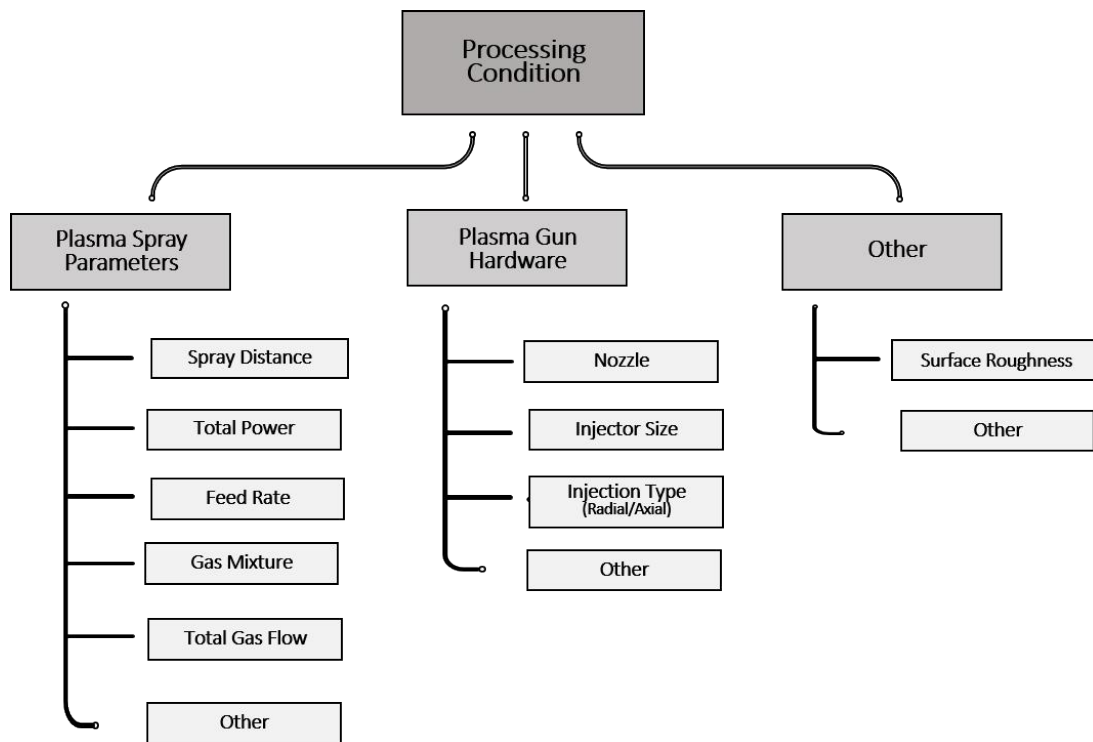


Figure 6.1: Major processing parameters that affect the coating microstructure [105].

These parameters were reminded because they are also applied in the current study. Hence, these considerations were adjusted according to the manufacturer's recommendation and desired microstructure of the test. As stated earlier, there were two coating layers deposited by atmospheric plasma spray. The substrates were preheated to approximately 100°C by the plasma instantly before coating for all samples. It was accompanied by sand-blasting in

providing the proper adhesion required. For the APS process, the surface temperature of the coatings was monitored by the infrared camera and kept below 200°C. Based on the previous studies and results, the optimum thickness for the deposited insulating layer is between 120-200 µm, for which the test parameters were adjusted accordingly [60]. On this point, Table (6.1) presents the spray parameters of the Zirconia layer (first layer) as an insulator coating.

Table 6.1: The plasma spray parameters used for the Zirconia coating.

Surface preparation	
Substrate	Aluminum
Surface preparation	Coarse grit blasting
Plasma parameters	
Plasma gun	3MB
Gas mixture	Argon-Hydrogen
Argon (primary plasma gas) flow rate (L/min)	39.4
Hydrogen (secondary plasma gas) flow rate (L/min)	6.6
Arc current intensity (A)	500
Arc Voltage (V)	64
Plasma nozzle	G (Oerlikon metco)
Spraying parameters	
Spray distance (mm)	64
Plasma gun traverse speed (m/s)	1
Feedstock parameters	
Feed rate (g/min)	45
Carrier gas	Argon
Carrier gas flow rate (L/min)	5.9

The insulation layer was deposited on 10 samples. All selected samples were deposited under the same spraying conditions. Figure (6.2) shows a sample before and after deposition of the Zirconia layer.

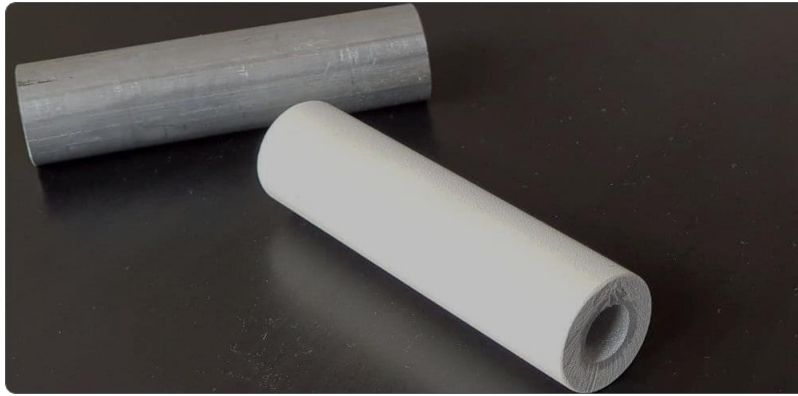


Figure 6.2: One sample before and after the deposition of Zirconia layer.

6.1.2 Resistive Layer

In the second phase of experiments, ceramic coated substrates were coated using the FeCrAlY powder (Amdry 9700). As previously mentioned, the resistive system (heating element) is designed with unique geometry for this study. The strips deposited at equal intervals on top of the insulator layer. For this goal, thermal spray masking tapes were used to define the layout of the heating elements. Furthermore, the masking tape uses pressure-sensitive silicone adhesives that allow the product to continuously withstand temperatures up to 260 °C (500 °F). Moreover, it also prevents slippage at high temperatures during the plasma spray process. In the first place, fabrication of these geometries was done to reduce costs and energy consumption by decreasing the required cross-section of the to-be-heated surface. Next, it is designed to investigate the capability of developing a multi-functional ice protection system to reduce power consumption in the glaze and rime ice regime. Finally, another outstanding significant objective of this design is to examine the possibility of controlling the heating of the desired surface whenever and wherever necessary. Throughout the design process, different cross-sections were fabricated to compare the expected capabilities

of the different designs and explore the possibility of creating a variety of cross-sections based on the needs in various circumstances. One of the most critical features of thermal spray methods was demonstrated in this part. Six geometries were fabricated as shown in Figure (6.3).

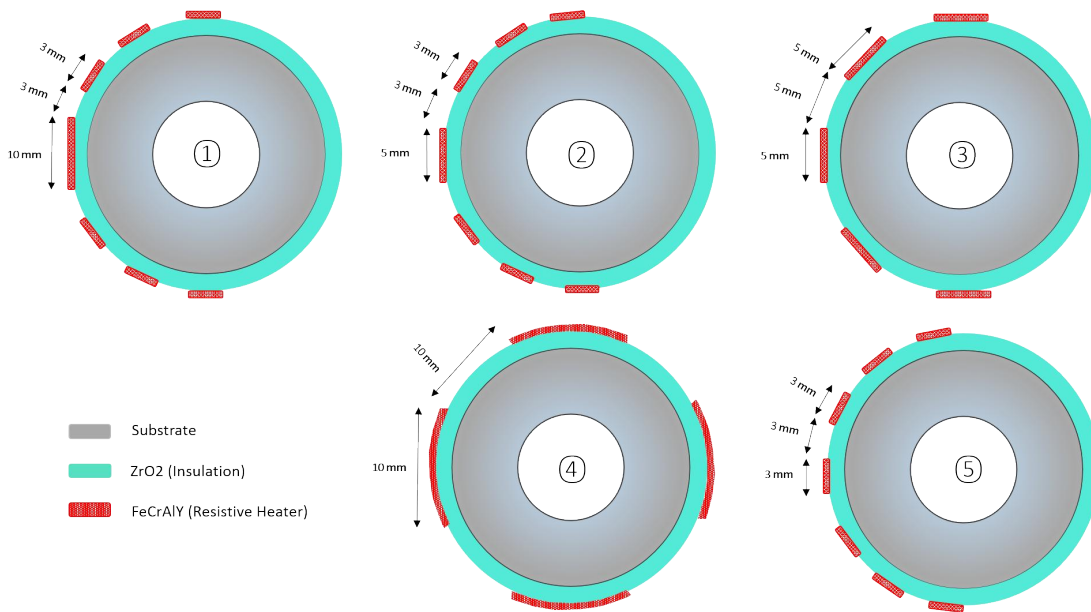


Figure 6.3: Design of different heating elements.

As an example, sample 5 is shown in Figure (6.4). On top of the insulator layer, a design-specific mask was applied for getting the desired heating element geometry. In accordance, studies and results have indicated that the optimum thickness for the deposited FeCrAlY

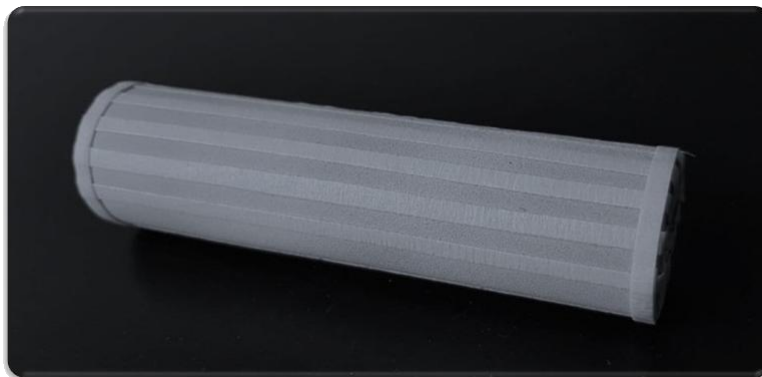


Figure 6.4: Schematic of one of the masked samples.

layer (heating element) is 60-80 μm , which has led to adjustments to the test parameters. In this regard, Table (6.2) shows the spray parameters for a coating of resistive strips. These parameters were chosen based on the manufacturer suggestions.

Table 6.2: The plasma spray parameters used for the FeCrAlY coating.

Surface preparation	
Substrate	Zirconia layer
Surface preparation	-
Plasma parameters	
Plasma gun	3MB
Gas mixture	Argon-Hydrogen
Argon (primary plasma gas) flow rate (L/min)	73
Hydrogen (secondary plasma gas) flow rate (L/min)	2.5
Arc current intensity (A)	500
Arc Voltage (V)	50
Plasma nozzle	GH (Oerlikon metco)
Spraying parameters	
Spray distance (mm)	127
Feedstock parameters	
Feed rate (g/min)	20
Carrier gas	Argon
Carrier gas flow rate (L/min)	4.4

As noted earlier , Air Plasma Spray technique was used to deposit metallic coatings on top of Zirconia layer. Figure (6.5) shows the prepared samples after deposition of metallic coatings (FeCrAlY) on top of the insulator layer. After masking the samples based on the designed cross-section the spray processes were performed. Different designs were fabricated to evaluate their performance in terms of local heating.

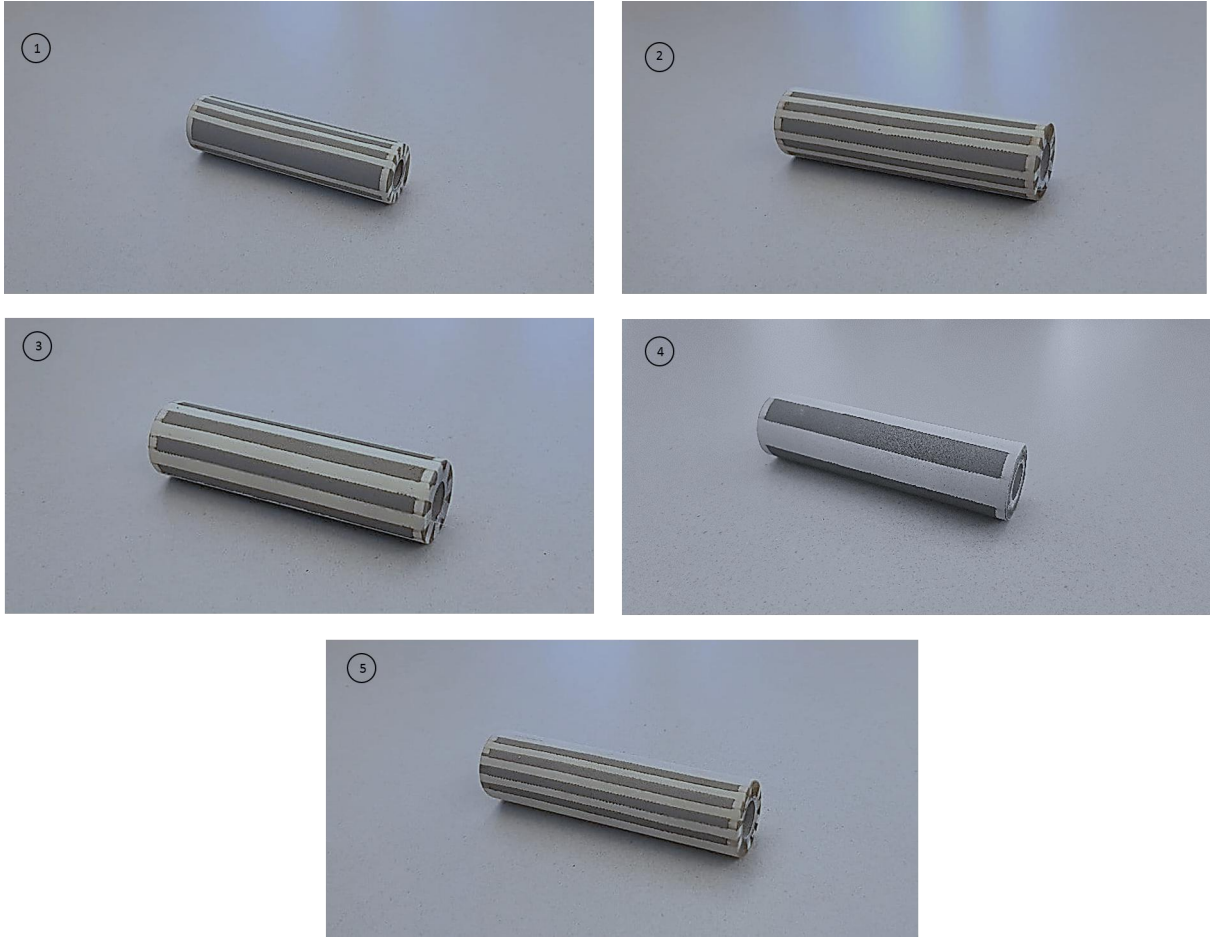


Figure 6.5: Coated samples with five different geometries.

6.2 Coating characterization

A cutting machine was used to cut multi-layered samples of the coatings, which were then mounted in epoxy resin for micro-structural analysis. Samples were coated with a thin layer of gold to prevent static electric charges on the non-conductive Zirconia coating for SEM characterization. Images were analyzed using Java-based image processing program (ImageJ) to measure porosity and oxidation of deposited coatings (a significant factor in this study). SEM micrographs of coating structure are shown in Figure (6.6). There are two different layers in the micrograph. A metallic layer (FeCrAlY) on top is the heating element. Ceramic layer (Zirconia) as an intermediate layer (insulator) and substrate (Aluminum tubing). The top coating layer (FeCrAlY) is on average 60-90 μm , and the zirconia

layer is approximately 150-200 μm . The parameters setting such as powder flow rate, current, stand-off-distance directly influence the properties and performance of the fabricated coating. After characterization of the coatings, the results indicate that microstructure for plasma-sprayed was satisfactory.

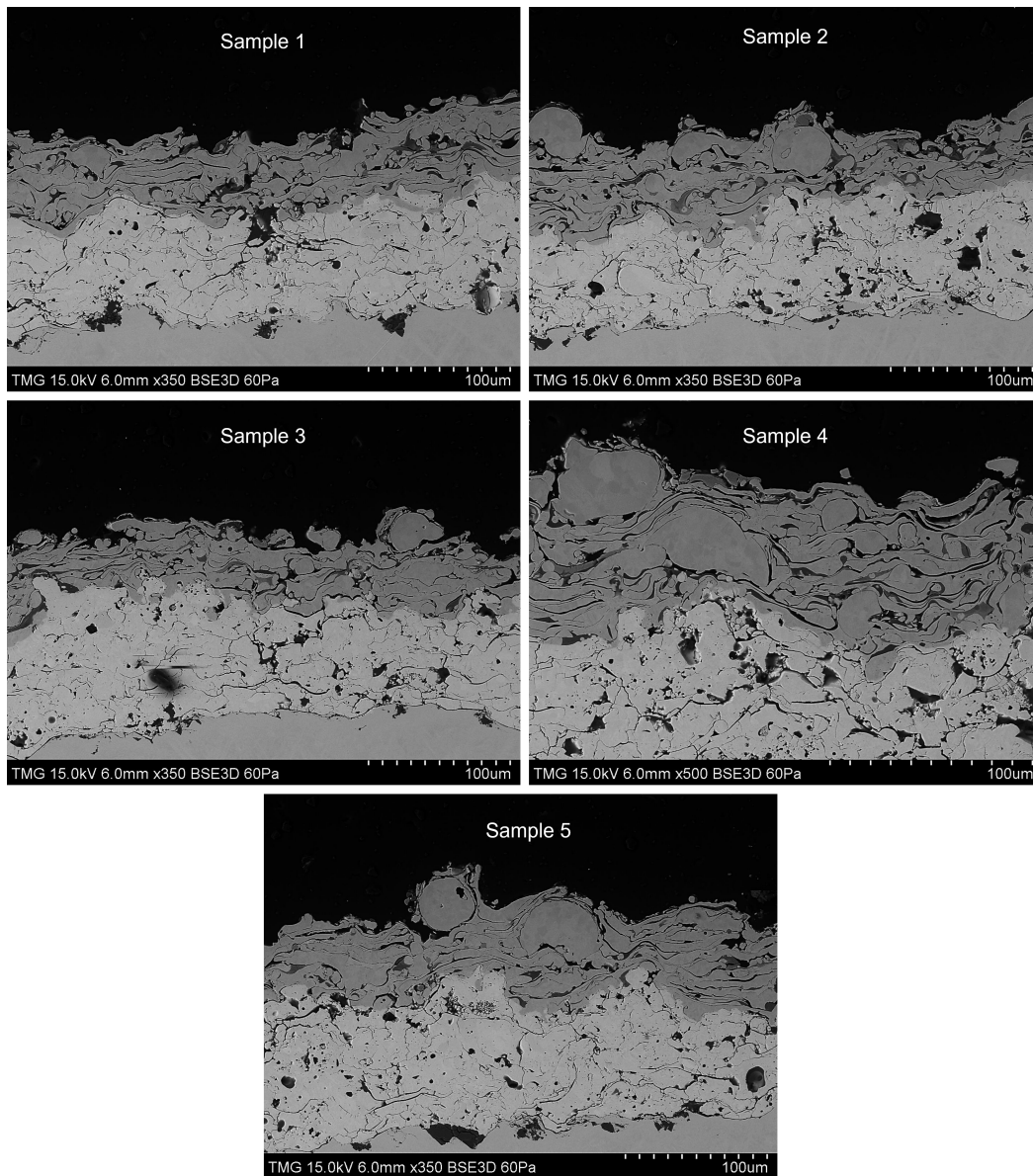


Figure 6.6: SEM micrograph of five samples with different width of FeCrAlY coating (figure 6.5).

All selected samples were deposited under the same spraying conditions and indicating the same texture. The SEM micrographs in Figure (6.7) represent the microstructure of coating.

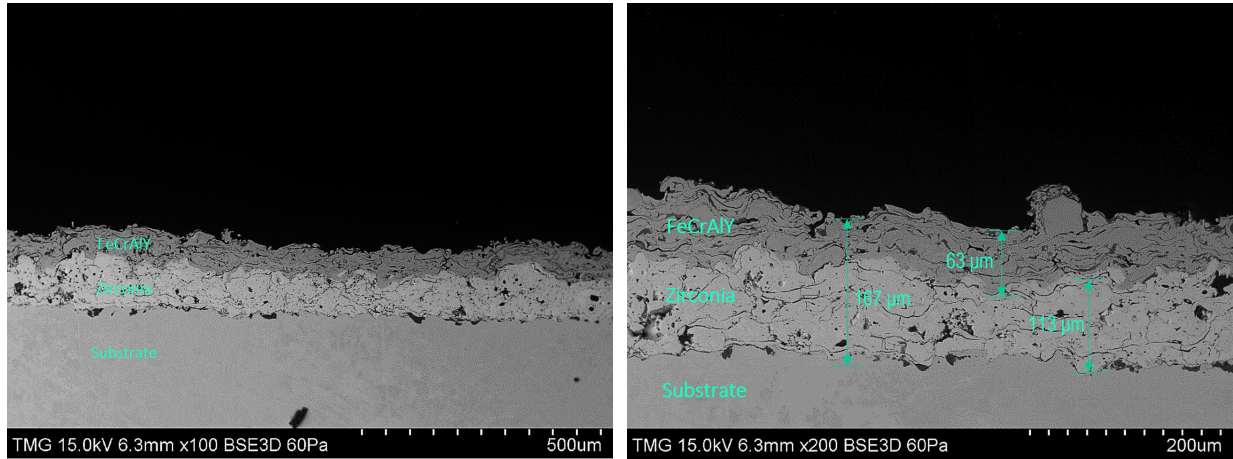


Figure 6.7: SEM micrograph of a coated sample.

As earlier mentioned, thermal spray technology poses the possibility to make large active coatings. Plasma spray coatings' microstructure and properties are largely dependent not only on the powder properties but also on the parameterization of the process itself. Typically, the effects of plasma spraying parameters on coating properties are studied, including phase content, powder deposition efficiency, deposition rate, microstructure roughness, porosity, and micro-hardness. Based on the goal of this study. Table (6.3) (a) presents the coating properties of Zirconia based on the stated spray parameters. In addition, FeCrAlY coating's properties were evaluated. Table (6.3) (b) presents the coating properties of FeCrAlY based on the stated spray parameters.

Table 6.3: Properties of the (a) Zirconia and (b) FeCrAlY coatings

(a) Zirconia Coating Characteristics									
Sample	Weight Before coating (g)	Weight After coating (g)	Weight gain (g)	Deposition Efficiency (%)	Average Deposition Efficiency (%)	Thickness Before Coating (μm)	Thickness After Coating (μm)	Thickness Difference (μm)	Average Deposition Rate ($\mu\text{m/Pass}$)
1	103.8	110.4	6.6	85.3	85 ± 0.8	25.5	127.5	153.0	12 ± 0.7
2	105.0	111.5	6.5	84.7		25.6	122.6	148.2	
3	104.2	110.7	6.5	84.5		25.6	120.6	146.2	
4	104.9	111.5	6.6	85.8		25.5	112.7	138.2	
5	105.4	112.0	6.6	85.6		25.6	123.6	149.1	

(b) FeCrAlY Coating Characteristics									
Sample	Weight Before coating (g)	Weight After coating (g)	Weight gain (g)	Deposition Efficiency (%)	Average Deposition Efficiency (%)	Thickness Before Coating (μm)	Thickness After Coating (μm)	Thickness Difference (μm)	Average Deposition Rate ($\mu\text{m/Pass}$)
1	110.4	112.5	2.1	80.5	80 ± 0.8	25.7	99.1	73.4	8 ± 0.8
2	111.5	113.6	2.1	79.3		25.8	94.0	68.2	
3	110.7	112.9	2.2	82.3		25.7	101.9	76.1	
4	111.5	113.6	2.1	78.2		25.7	89.7	63.9	
5	112.0	114.1	2.1	80.1		25.8	98.0	72.2	

6.3 Electrical characterization

This section is consisted of measuring the surface resistance of the coated samples using the four-point probe technique. In Table (6.4), the applied voltages (3, 6, and 9 V) and resulting currents along the surfaces of the coatings and some other electrical properties (resistance, resistivity, and intensity) for each type of coating are given. Prescribed voltages were applied to the coated samples, as a result, the required power could be supplied as intended, and more uniform heat distribution is achieved along with the coating and better control on the heating procedure is earned. After finding the resistance of the coated samples, the resistivity of the coatings was calculated. In contrast to resistance, resistivity is an intrinsic property of materials, independent of their shape and dimensions. Thus, two coatings sprayed with

the same spray parameters but with different dimensions should have the similar resistivity. Nevertheless, changing control parameters and powder size may affect the percentage of coating oxidation and porosity, leading to a different resistivity value. Since coatings are always associated with porosity and oxidation, their intrinsic properties, such as electrical resistivity, are usually different from bulk and pure materials. The resistivity values for the coatings sprayed samples (Middle strip in all) are shown in Table (6.4) comparing the resistivity values for coated samples, one finds that the difference between them is negligible.

Table 6.4: Electrical properties of the coated samples.

Sample	Voltage (V)	Current (A)	R (Ω)	Length (cm)	Width (mm)	Thickness (μm)	ρ ($\mu\Omega\cdot\text{m}$)	ρ average ($\mu\Omega\cdot\text{m}$)	Intensity (kW/m^2)
1	3	3.0	0.9	10	10	73 \pm 0.4	7.4	6 \pm 0.8	9
	6	5.9	1.0				6.6		35
	9	9.5	0.9				6.8		86
2	3	1.4	2.1	10	5	68 \pm 0.2	7.1	7 \pm 0.1	4
	6	2.9	2.0				7.1		17
	9	4.2	2.1				7.3		38
3	3	1.3	2.2	10	5	76 \pm 0.1	8.5	8 \pm 0.2	4
	6	2.8	2.1				8.3		16
	9	4.4	2.0				8.2		39
4	3	3.3	0.9	10	10	63 \pm 0.9	7.1	6 \pm 0.5	9
	6	5.7	1.0				6.2		34
	9	9.5	0.9				6.3		86
5	3	0.8	3.5	10	3	72 \pm 0.3	7.9	8 \pm 0.4	2
	6	1.5	3.8				8.7		9
	9	2.1	4.1				8.8		19

For each coated sample V-I graph is represented in Figure (6.8). As expected, the current is linearly related to the voltage, which corroborates the equation ($R = \frac{V}{I} = \frac{\Delta V}{\Delta I}$) in all cases. The slope of the curve represents the coating's resistance. From Figure, it is apparent that FeCrAlY coatings with a wider cross-section have a lower resistance value than coatings with a thinner cross-section. This confirms that resistance is directly proportional to electrical resistivity and length, as well as inversely proportional to cross-section ($R = \frac{\rho L}{A} = \frac{\rho L}{tw}$) in which parameter t and parameter w are the cross-section thickness and width, respectively. The samples were also tested at various temperatures for their resistance (25°C to 250°C).

In all cases, it performs that the resistance of the FeCrAlY coating during the temperature range is almost constant. Therefore, it can be concluded that the variation of resistance in this range of temperature is negligible.

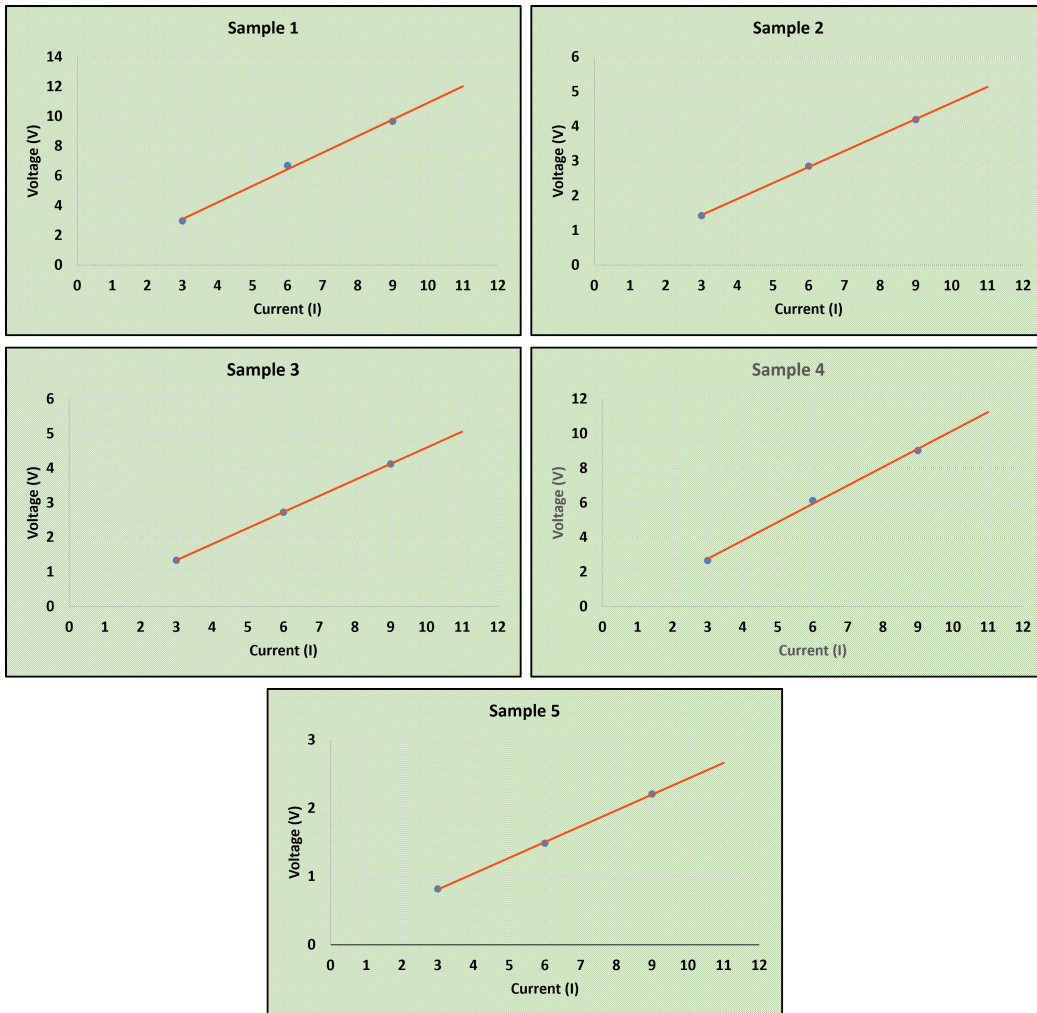


Figure 6.8: Voltage vs current for the FeCrAlY coatings.

As discussed earlier, different geometries were created to reduce the required area to-be-heated in the future which is not possible in traditional heating elements. In addition, The feasibility of developing a multi-functional ice protection system with a focus on solving the available system’s deficiencies was another reason for designing these geometries. This design also explored the possibility of controlling the temperature of the surface whenever and everywhere necessary. Therefore the tests were repeated for all the coated samples with different geometries to ensure their required performance. The method was assessed using an infrared camera (study the change in surface temperature and heating element performance during the heating process). In addition, it was examined in different conditions how well the supplied heat could be controlled. Further investigation of the electrical properties of different coated samples was undertaken.

6.4 Thermal Analysis

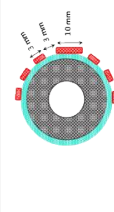
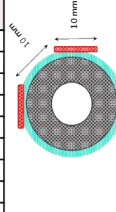
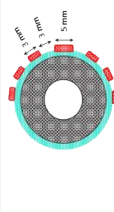
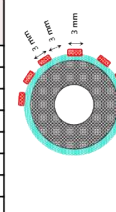
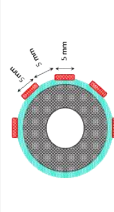
Three different voltages (3, 6, and 9 V) were applied to the coated samples for each set of experiments and surface temperature was measured using thermocouple and infrared camera . The law of intensity is determined by the equation (6.1) is used to calculate power in which R is equal to resistance, P is power, and V is voltage.

$$P = \frac{V^2}{R} \quad (6.1)$$

Tests were conducted for all samples with different heating elements configurations. All tries were done for one strip at first. Furthermore, tests were repeated for heating two and three strips simultaneously to investigate the system’s ability to work correctly. In other words, as discussed earlier, this strategy enables us to control our heating method; moreover, the system’s capability to provide the required amount of heat in more than one region was revealed. Table (6.4), in previous section presented the resulting current and the generated power per unit area known as intensity. For the different coatings, as expected, results indicate that the intensity of all the coatings’ power increases with increasing voltage. It was

also confirmed that the coatings' resistivity remains relatively constant at all temperatures as anticipated. Therefore, the sample with a smaller width of resistive coating would have a higher temperature for a given voltage than the other coated sample. Table (6.5) includes the results of supplying different voltages into the system (subsequent currents and power intensity, which were produced accordingly). Results showed a more uniform heating distribution, and the heating procedure is controlled to a greater extent. A variety of geometries, resulting in reducing the required surface area, were employed to reduce costs and energy use. Another achievement we could infer from testing these geometries was developing a multi-functional ice protection system that focuses on solving the individual systems' shortcomings. Tests were repeated six times for all the coated samples with different geometries to ensure the repeatability.

Table 6.5: Electrical properties for the coated samples with different geometries.

	Sample 1							Sample 4					
	Strips	Width (mm)	Resistance (Ω)	Voltage (V)	Current (Amp)	Intensity (kw/m^2)		Strips	Width (mm)	Resistance (Ω)	Voltage (V)	Current (Amp)	Intensity (kw/m^2)
	Top	3	3.9	3	0.7	2		Top	10	0.8	3	3.3	10
	Middle	10	0.9		3.0	9		Middle	10	0.9		3.3	9
	Bottom	3	3.3		0.9	2		Bottom	10	1.0		2.9	8
	Top	3	3.7	6	1.6	9		Top	10	0.9	6	6.0	36
	Middle	10	1.0		5.9	35		Middle	10	1.0		5.7	34
	Bottom	3	3.7		1.6	9		Bottom	10	1.0		5.5	33
	Top	3	4.0	9	2.2	19		Top	10	0.9	9	9.2	83
	Middle	10	0.9		9.5	86		Middle	10	0.9		9.5	86
	Bottom	3	3.9		2.3	20		Bottom	10	0.9		9.7	88
	Sample 2							Sample 5					
	Strips	Width (mm)	Resistance (Ω)	Voltage (V)	Current (Amp)	Intensity (kw/m^2)		Strips	Width (mm)	Resistance (Ω)	Voltage (V)	Current (Amp)	Intensity (kw/m^2)
	Top	3	3.1	3	0.9	2		Top	3	3.6	3	0.8	2
	Middle	5	2.1		1.4	4		Middle	3	3.5		0.8	2
	Bottom	3	3.3		0.9	2		Bottom	3	3.3		0.9	2
	Top	3	3.1	6	1.8	11		Top	3	4.0	6	1.4	9
	Middle	5	2.0		2.9	17		Middle	3	3.8		1.5	9
	Bottom	3	3.0		1.9	11		Bottom	3	4.8		1.2	7
	Top	3	2.9	9	3.0	27		Top	3	4.0	9	2.2	19
	Middle	5	2.1		4.2	38		Middle	3	4.2		2.1	19
	Bottom	3	3.6		2.4	22		Bottom	3	3.9		2.3	20
	Sample 3												
	Strips	Width (mm)	Resistance (Ω)	Voltage (V)	Current (Amp)	Intensity (kw/m^2)							
	Top	5	2.1	3	1.3	4							
	Middle	5	2.2		1.3	4							
	Bottom	5	1.9		1.5	4							
	Top	5	2.2	6	2.6	15							
	Middle	5	2.1		2.8	16							
	Bottom	5	2.3		2.5	15							
	Top	5	2.1	9	4.1	37							
	Middle	5	2.0		4.4	39							
	Bottom	5	1.9		4.5	40							

As a next step, the heaters were switched on, and enough time was allowed for their operation to stabilize the temperature profile. Three different voltages (3, 6, and 9 V) were applied to the coated samples with different widths (3, 5, and 10 mm) for each set of experiments. In order to ensure a steady state, we used a thermocouple and infrared camera. The steady-state condition was achieved when apparatuses showed stable temperature readings. The temperature profile of the samples coated for three different voltages and three different widths was measured. The thickness of the coating was equal in all models. Figure (6.9) illustrates the temperature profile of the sample coated in three different voltages and three different widths. The graph shows that the slope, especially in the beginning, is sharp, and the surface temperature rises very rapidly. The surface temperature in the highest supplied voltage (9 V) reaches 150°C in just less than 50 sec, and it goes to 210°C in about 120 sec. The 6 V curve indicates that the slope is smoother, and the temperature increases more slowly over time than the 9 V curve. In this case, the surface temperature increased from 26°C to 150°C in about 80 seconds. After 120 s, the temperature is approximately 190°C . In the 3 V, the temperature of 150°C is reached in around 100 seconds. In about 120 seconds, the temperature also reaches 170°C . The different cases show that the temperature profiles, especially after 90 s, have a more smooth slope; however, the time it takes to reach the temperature of 150°C is different for different supplied voltages. The samples with the applied higher voltage always have a higher temperature and reaches a specific temperature earlier. For the wider coatings (5mm and 10 mm), it should be noted that increasing the cross-section area results in decreasing the coating resistance.

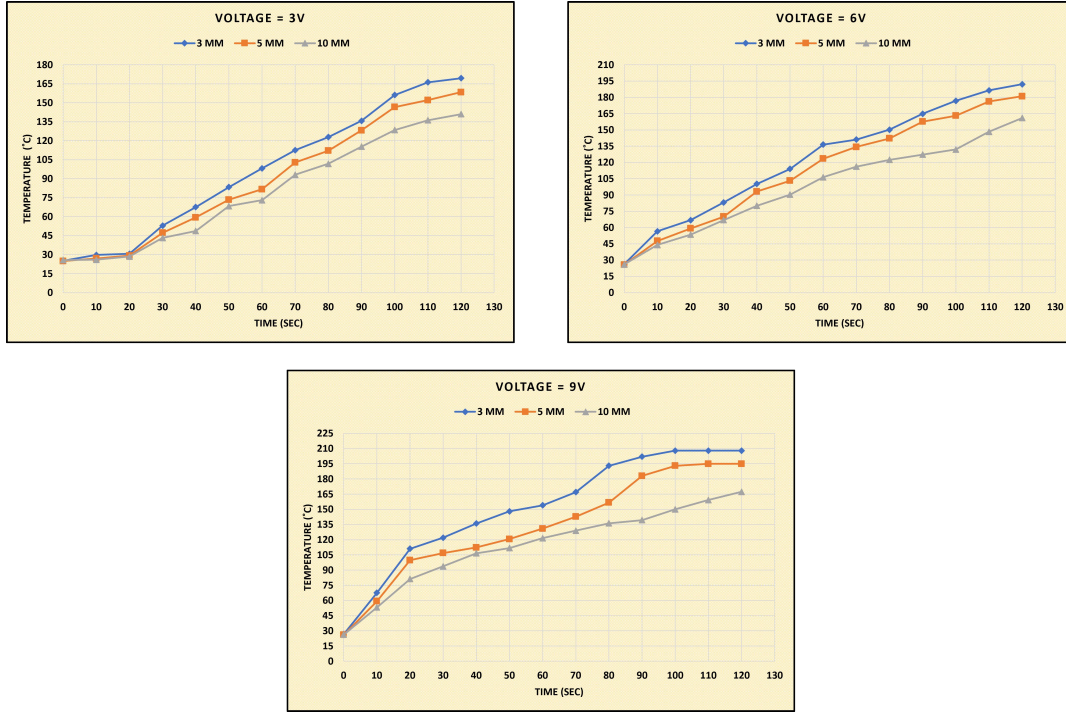


Figure 6.9: Temperature profile of the sample coated in three different voltages and three different widths.

With the same thickness of the coatings, the 3 mm wide coating appears to have better performance as a heating element due to higher surface temperatures higher power intensity, and a shorter steady-state time. Additionally, the surface temperature distribution resulted from a coating thickness of (70 ± 10) μm while the coating was connected to a power source was very uniform. Accordingly, the thickness was found to be properly chosen. In all these cases different constant voltages were applied to the samples (3, 6, and 9 V). It should be noted that the power generated using coating is lower in thinner coatings if instead of applying constant voltages, constant currents be applied to the coated samples, as $(P = \frac{V^2}{R} = RI^2)$. Each of these strategies might be proper depending on several factors like the application of the heating element, where it is used, the amount of needed power, uniformity, level of importance, and other limitation. The next step was to investigate the controllability of the heating elements. In this experiment, different voltages (3, 6, and 9 V) were applied to the coatings again. This time, however, two and three heating strips were powered simultaneously. As long as all heating strips were at the same width, the current passed through all heaters equally and the temperature changes grew similarly for all heat-

ing elements. But if the width of the heating elements is different the current pass through the coatings would be different because of changing resistance and the temperature profile will be altered. As a result, we were able to heat multiple heating elements at the same time, and we could control the heat output to each heating strip whenever needed. With this method, it is easy to control both the place and the time of heating. For instance, to prevent in-flight icing, as mentioned previously, we only need to heat the stagnation area of the leading edge. However, it is important to note that in different angles of attack there is a different stagnation region, and we need to heat the different zone of the leading edge at the right times. Using this technique, it is possible to heat a specific area at a specific time without having to heat the whole surface, which translates into a more efficient consumption of energy. Furthermore, homogeneous temperature distribution can be achieved on surface as a result of the intimate contact between the plasma-sprayed coatings (the heating elements) and the substrate. Essentially, the coating system would heat and melt ice more efficiently than conventional electric heating systems. However, applying more power did not result in any noticeable changes in the ice's melting times from one point on. Figure (6.10) in the next page illustrates the surface temperature distributions that result from heating on the different coatings.

6.5 Icing Test

Testing was done under two different conditions to assess the ice protection system's reliability and performance. In the first group of tests, the samples were evaluated for the performance against icing (ice accretion test) to determine the effect of superhydrophobic coating on anti-icing performance (demonstrate passive ice protection capacity). The second group of tests examined the anti-icing performance (heated anti-icing test) for the conventional thermal ice protection systems and the designed thermally-sprayed heating system. Then the results were compared to see the difference between the two systems' anti-icing performance. Finally, the test was include using superhydrophobic and heating concurrently as a multi-functional ice protection system (integration of passive and active method). The

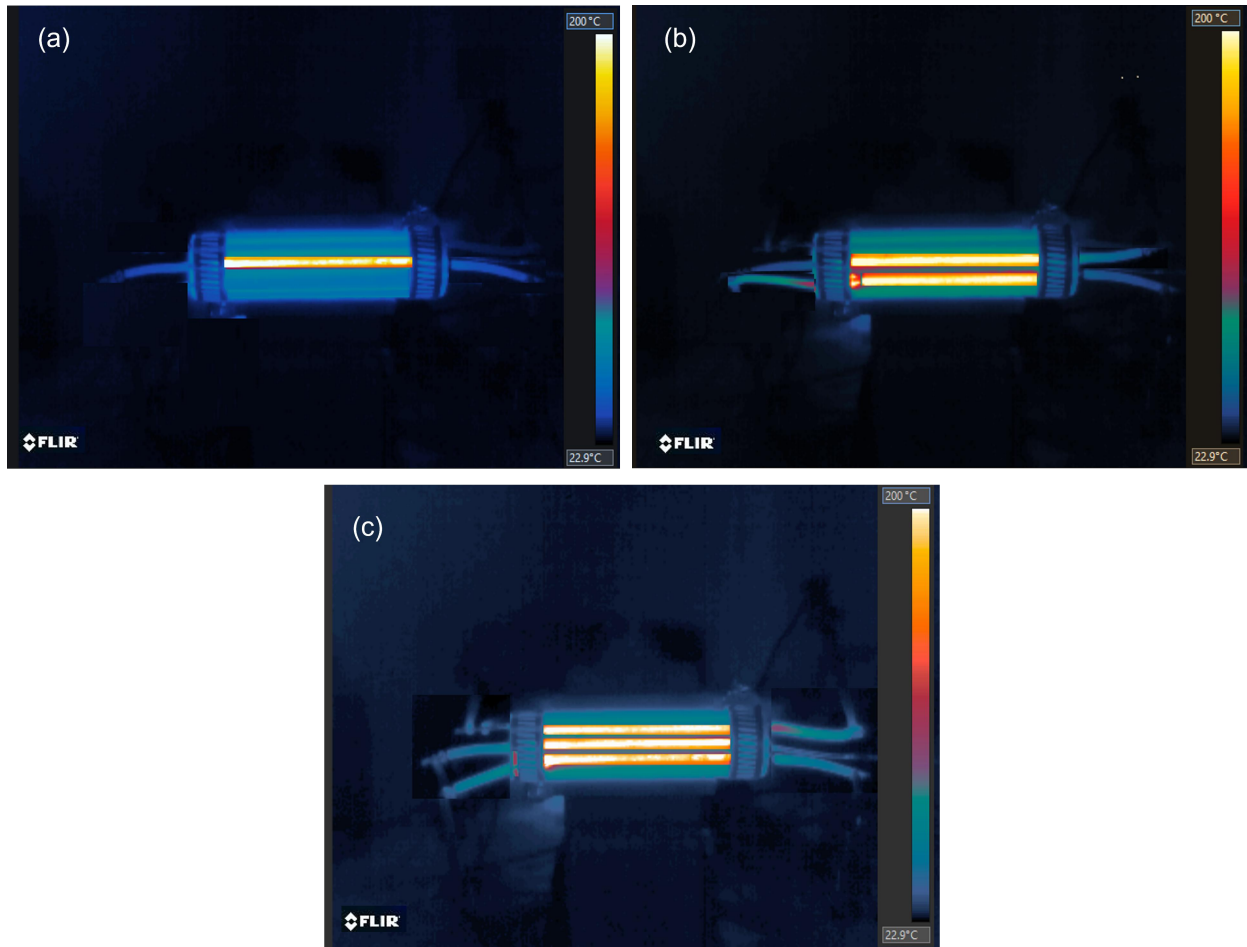


Figure 6.10: Performance test of the FeCrAlY resistive heaters for (a) one, (b) two, and (c) three strips

heating system's controllability was also evaluated (the ability to heat the leading edge at different angle of attacks while take-off or landing using coatings with a particular design). The test section of the wind tunnel has a square-shaped cross-section with a width of 10 cm. Test sections can achieve air speeds of up to 45 m/s and temperatures as low as -20°C with air speeds of up to 40 m/s. The maximum operating temperature of the wind tunnel increases with increasing air velocity since the residence time of the air in the chiller decreases when the air velocity increases. Cold distilled water was used for the spray. In order to obtain super-cooled water droplets, the water temperature was maintained below 4°C during icing tests. The water droplets were injected into the air stream using an air atomizing spray nozzle placed after the fan. By adjusting the airflow and water flow, the spray pattern can be tailored. The liquid water content in the test section can be varied between 0.2 g/m^3

to 1 g/m^3 . All the tests performed resulted in a spray with a median volume distribution (MVD) of $30 \mu\text{m}$ with an LWC of 0.5 g/m^3 and the velocity equal to 25 m/s . . Figure (6.11) shows the test section and the sample holder used in the icing wind tunnel. The details of these tests are discussed in the following sections.

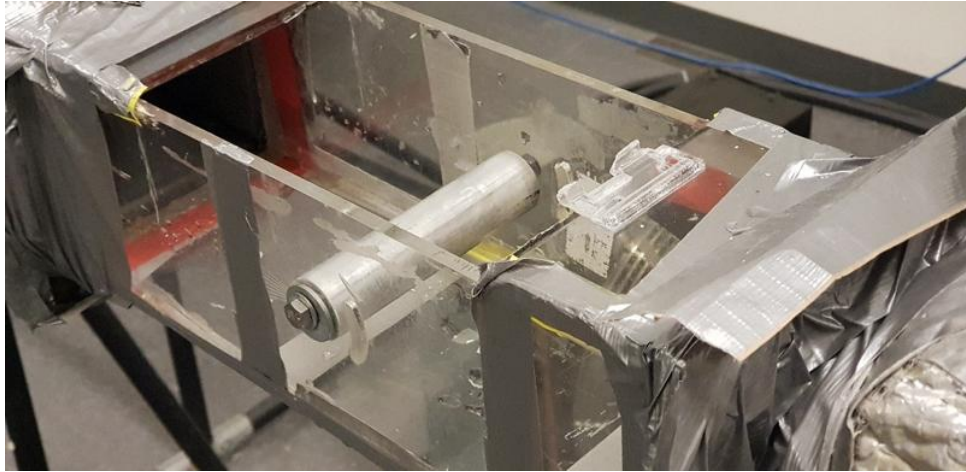


Figure 6.11: Schematic of icing wind tunnel test section.

6.5.1 Ice Accretion Test

Within the capabilities of the testing equipment, the operating condition was designed to estimate ice accretion. In all these conditions, the liquid water content (LWC) was 0.5 g/m^3 , and the median volume diameter (MVD) was $30 \mu\text{m}$, matching the icing risk conditions. The air stream velocity was equal to 25 m/s . We chose temperatures slightly below the freezing point of water (-4 ± 1) $^{\circ}\text{C}$, which typically forms the glaze or clear ice (the most dangerous type of ice). Each ice accretion test was conducted for one minute to assess the delay in ice formation more accurately. We weighed each sample before and after each trial to determine the weight of the ice formed during the test. The tests were repeated six times for each sample to assess the repeatability of the results. The profile of ice formation was also studied. Figure (6.12) illustrates the effectiveness of a passive anti-icing strategy versus uncoated samples under the same icing conditions. Figure (6.12) (a) shows the dynamics of ice accumulation on aluminum (hydrophilic surface) under clear icing conditions without

using any anti-icing strategies. Most of the impinged super-cooled water droplets became frozen into ice as gotten on the surface (mainly near the leading edge). The remaining mass of impacted water formed a thin layer of water. Afterward, they split into multiple rivulets and subsequently became ice at further downstream locations. For comparison purposes, a commercial superhydrophobic product, NeverWet® (Rust-Oleum, Canada), was used to coat the aluminum substrate. It is clearly shown in Figure (6.12) (b) that the ice accretion process on the SHS-coated surface was much less than that of the hydrophilic surface. The accumulated ice structures mainly concentrated near the leading edge instead of covering a much greater area over the hydrophilic model. Moreover, weighing the samples also confirms that the mass of accreted ice on the surface covered by SHS coating is much less than the Aluminum surface. The results of weighing the sample are shown in Table (6.6). All the measurements were recorded after one minute of surface exposure to the icing condition. The critical results that should be given importance, show that ice features were found to be accreted in the region near the stagnation line of the leading edge. The subsequent super-cooled water droplets would impact the surface of the accreted ice. Therefore, these experimental results confirm the claim that the stagnation point is the most critical area that should be protected because it is the first point that ice starts to nucleate.

Table 6.6: Effect of applying SHS on the ice accumulation ratio.

Sample	Weight (g)	Weight (Hydrophilic) (g)	Weight (Superhydrophobic) (g)	Weight decrease (%)
1	105	120	93	22.6
2	104	118	90	23.8
3	105	113	87	23.0
4	104	118	91	23.0
5	105	125	93	25.3
6	106	117	86	26.6

Passive strategy with SHS coating was found capable of reducing ice accretion compared to the bare aluminum surface. However, it is still far from being sufficient to successfully prevent ice formation/accretion. Moreover, durability and humidity tolerance during ice

removal (under severe icing condition) was unsafe. Ice-phobic coatings' durability is a critical issue, mainly in harsh icing conditions that cause severe delamination of the ice-phobic layer.



Figure 6.12: Ice accretion on (a) hydrophilic, and (b) SHS coating.

6.5.2 Heated Anti-icing Test

Thermally-sprayed Heating System

The coating's heating performance was tested by exposing each sample to the harshest icing condition. The first set of experiments were done on the designed structure (thermally-sprayed heating system). Electric currents were applied to the heating element (FeCrAlY coating) at different voltages. FeCrAlY coatings have high electrical resistance, so heat is generated by passing a current through the conductive FeCrAlY layer. All tests were done for enough minutes to see the stabilized temperature on heaters, and then the samples were exposed to the icing condition. The tests aimed to determine the amount of heat required to maintain the surface free from ice. We turned on the heater and allowed enough time for the temperature profile to be stabilized. The steady-state was ensured by reading the temperature from the infrared camera. We conducted the first group of tests by heating one strip 3 mm wide at the center of the substrate (almost at stagnation point). once after the infrared camera displayed a steady-state temperature, water was sprayed. We started the test with the maximum power we could supply. The heater was turned on with 20 W. Formation of ice on the sample's surface means that we did not supply enough power. In the

case of this occurrence, the test was designed was stopped; the sample was deiced, dried, and repeated with higher heat input. On the other hand, if we saw the sample remained free from ice, we decreased the power by 1 W and repeated the test (In the absence of ice on the sample, the process repeated with a 1 W reduction in heating). We continued this cycle to find the least amount of energy in which the surface remained free from ice. The minimum electrical power required to maintain an ice-free surface was measured and recorded acceptably by this trial and error method. There should be a reminder that the surface temperature can vary depending on the external environment and the supplied energy, committing changes in anti-icing modes (dry surface mode, evaporative mode, and runback water mode). The dry surface mode prevents water from entering the protected area, keeping the aircraft relatively safe but consuming massive energy. The water barely evaporates in the runback water mode, and the surface temperature stays a few degrees above freezing. Although it consumes little energy, it risks the formation of runback ice, which cannot be permissible on lifting surfaces or on the air intakes of aircraft. In order to maintain flight safety and conserve energy, thermal anti-icing systems work in an evaporative mode. Evaporative mode indicates that runback water may be allowed but must evaporate entirely within the protected area. This approach has an energy consumption between the dry surface mode and the runback water mode. Therefore this method as the most proper technique was used in our experiments. Published experimental data were used to validate the calculation method. For preserving the surface free of ice, the maximum value of heat load was recorded. Finally, the method was calibrated to verify experimental results based on findings in the literature, aviation industry regulations and standards. Based on the calculations of this study, the necessary power for anti-icing was measured. As anticipated, the total required installed power for our electrical anti-icing system not only was in good agreement but also met our anticipation (introduce more efficient IPS). For example, the Boeing 787 (an airplane with one of the most efficient electrical ice protection systems) requires 3.61 kW/m^2 power for its leading edges ice protection which was also a good benchmark for comparison with our system. Moreover, in the next set of experiments the comparison between these results and the results gained from conventional method was done. Figure (6.13) presents a schematic of the heat generation circuit. The test was started by supplying current in strip 1. These procedures were also

done for 2 and 3 strips at the same time, and finally, the average power intensity required for anti-icing in the harshest icing conditioned was measured. It should be noted that there are various challenges for the optimization of an electro-thermal wing anti-icing system in both running-wet and evaporative regimes, which have not been addressed in this study; however, since they can be effective in some cases, they can not be ignored.

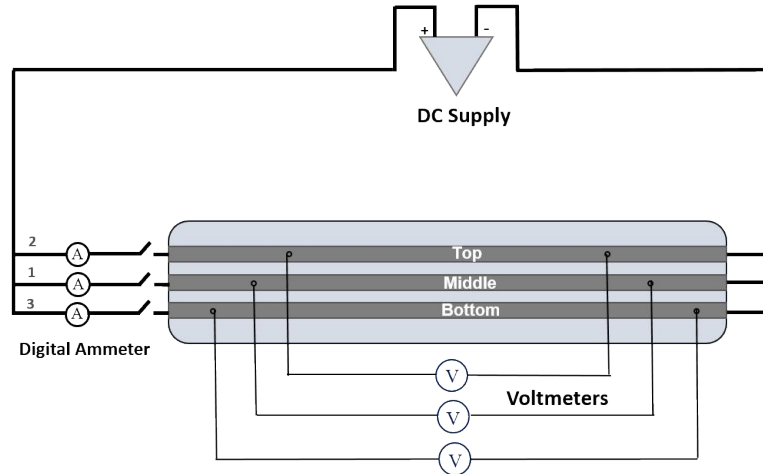


Figure 6.13: Schematic of the heat generation circuit.

The test was conducted on sample number 5, which has coated strips all 3 mm wide. At the beginning, electric potential of 9 V was supplied into the heating element. After 100 s, the surface temperature reached over $150^{\circ}C$, which was deemed okay for starting the experiment. The procedure of calibrating the required power as above-mentioned is shown in Figure (6.14). In this case, the minimum power to keep the surface free from ice was around $(4 \pm 0.5)W$. The surface temperature decreased to $(13 \pm 2)^{\circ}C$ but remained at this temperature, preserving the surface free from ice in 7 minutes duration of icing condition. We could protect the surface against icing with very low power intensity. However, after around 7 minutes, the ice started to form at the back of the substrate (runback ice) and grew downstream because the temperature was approximately $(4 \pm 0.5)^{\circ}C$ in the lower regions which was enough to runback ice formation.

Test	Voltage (V)	Current (A)	Power Density (W/m ²)	Ice Nucleation
1	9	2.21	19.9	✗
2	8	1.9	15.7	✗
3	7	1.7	12.0	✗
4	6	1.4	8.8	✗
5	5	1.2	6.1	✗
6	4	0.9	3.9	✗
7	3	0.7	2.2	✓
8	2	0.4	0.9	✓
9	1	0.2	0.2	✓

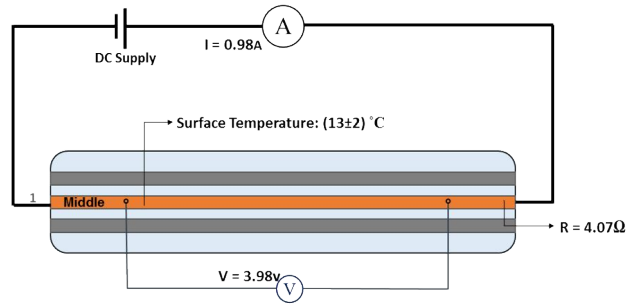


Figure 6.14: Required anti-icing power for heating only the middle strip.

Figure (6.15) shows that, when we warmed up the leading edge insufficiently the ice starts to nucleate on the surface (the area where drop collection is the highest). Therefore we could not avoid ice nucleation. Ice starts to form on the leading edge and get larger by time.



Figure 6.15: Formation of runback ice on the unprotected regions.

Figure (6.16) shows the picture captured by the infrared camera. It is apparent that supplying approximately 4W of power preserve the surface at a temperature around 13°C which was enough for anti-icing performance. However, in the unprotected regions, it was

evident that the surface temperature was as low as necessary, letting runback water being transformed into the solid phase.

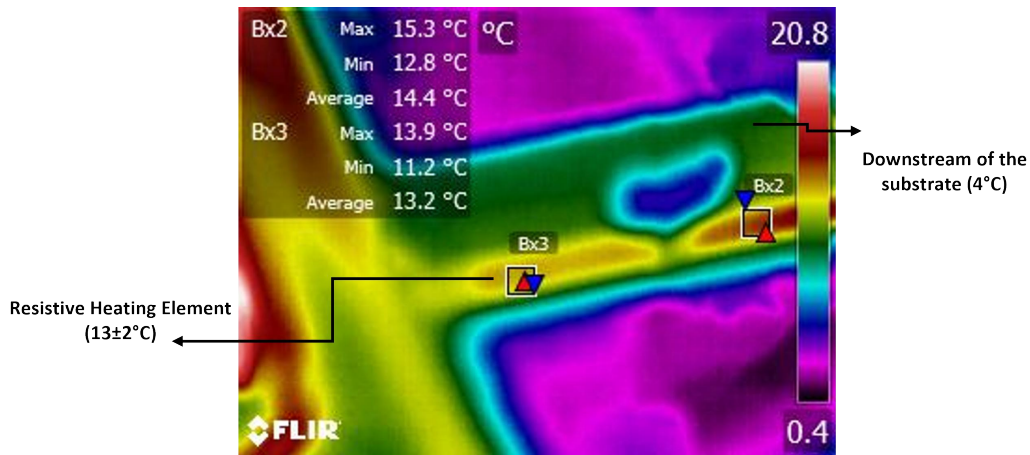


Figure 6.16: Surface temperature while heating only the middle strip under icing condition.

Consequently the experiments were repeated by supplying 20 W power to the two of the heating elements (strip 1 and 2). After the 120 s, the surface temperature of the strips reached over 150°C (proper target temperature to start the water spraying). In this case, the minimum power to keep the whole surface free from ice was around $(3 \pm 1)\text{W}$. The surface temperature decreased to $(11 \pm 0.7)^{\circ}\text{C}$ for both strips but remained at this temperature, and preserved the surface free from ice for 10 minutes duration of icing condition. In this configuration with two heating elements, we could run from runback icing as we protected the downstream regions as well. Moreover, less energy than the previous condition was required to protect the surface against icing. In fact, when we turned on just one heating element, we required more energy to evaporate more water from the leading edge to prevent the formation of runback ice. In other words, we can supply lower energy to the first heating element located at the stagnation point (the region ice initiates to form) to keep the supercooled droplet in the liquid phase. Consequently, the second heating element prevents the ice nucleation in the runback flow. It was also possible to have an interval for using heating elements when needed.

Finally, the test was conducted on the same sample with three strips were connected to the power supply. Again the experiments started with supplying 20 W power into each heating elements. The minimum power to keep the whole surface free from ice was around

Strip	Voltage (V)	Current (A)	Power (W)	Anti-icing Performance
1	9	2.2	19.9	✓
2		2.3	20.8	
1	8	2.0	15.8	✓
2		2.1	16.4	
1	7	1.7	11.9	✓
2		1.8	12.6	
1	6	1.5	9.0	✓
2		1.5	9.0	
1	5	1.2	6.0	✓
2		1.3	6.5	
1	4	1.0	4.0	✓
2		1.0	4.0	
1	3	0.7	2.1	✗
2		0.8	2.4	
1	2	0.5	1.0	✗
2		0.5	1.0	
1	1	0.3	0.3	✗
2		0.3	0.3	

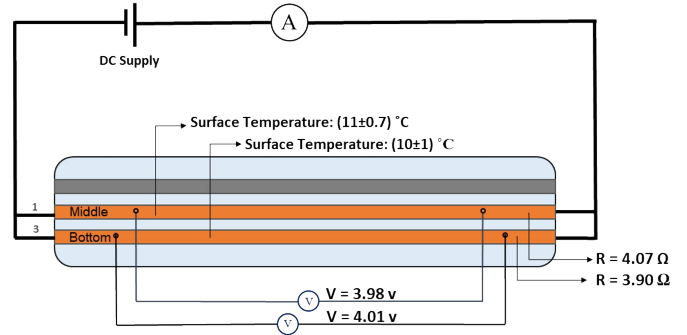


Figure 6.17: Required anti-icing power for heating two strips.

$(2 \pm 1)W$. The surface temperature for all strips decreased to around $(7 \pm 1)^\circ C$ after ten minutes of spraying super-cooled water droplets, but the supplied power was enough to keep the surface free from ice under the harsh icing condition. The procedure of calibrating the required power is shown in Figure (6.18). As we had three heating elements, we could rid of runback icing. In addition, less energy consumption was required to protect the surface against icing. The reason was that three strips enabled us to supply less power for evaporation on the leading edge because more runback liquid water can be avoided, while we used three heating elements.

In other words, we could remain more in the wet-water regime because the second and third heater removed the runback water. We can supply the least energy to the first heating element at the leading edge (the region ice initiates to form) to remain in the liquid phase. In continuing, if the runback ice wants to nucleate, the second and third heaters were turned on and put off the ice formation on the unprotected areas. This was also possible to have an interval for using heating elements. It means that we can turn on the other heating element than the one located at the leading edge right as icing happens on the unprotected regions,

Strip	Voltage (V)	Current (A)	Power (W)	Anti-icing Performance
1	9	2.2	19.8	✓
2		2.3	20.7	
3		2.1	18.9	
1	8	2.0	16.0	✓
2		2.1	16.8	
3		1.9	15.2	
1	7	1.7	11.9	✓
2		1.8	12.6	
3		1.7	11.9	
1	6	1.5	9.0	✓
2		1.5	9.0	
3		1.4	8.4	
1	5	1.2	6.0	✓
2		1.3	6.5	
3		1.2	6.0	
1	4	1.0	4.0	✓
2		1.0	4.0	
3		1.0	4.0	
1	3	0.7	2.1	✓
2		0.8	2.4	
3		0.7	2.1	
1	2	0.5	1.0	✗
2		0.5	1.0	
3		0.5	1.0	
1	1	0.3	0.3	✗
2		0.3	0.3	
3		0.2	0.3	

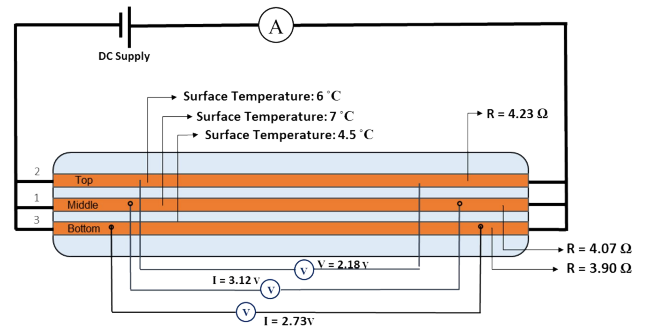


Figure 6.18: Required anti-icing power for heating three strips.

which is an excellent achievement in heating system improvement regarding controllability and energy consumption. Figure (6.19) illustrates the capability of the anti-icing system. In this case, we could completely get rid of ice nucleation either at the leading edge and downstream of the sample. This approach has been proved to require a small amount of energy to be spent on evaporating liquid water on the surface. Recently, there has also been much interest in superhydrophobic and ice-phobic surfaces, which are capable of repelling water and ice, respectively, and may be used to prevent ice accretion. Despite remarkable improvements in this route, there are still some significant problems with such alternatives.

Figure (6.20) presents the matching plot, the surface temperature versus time during spraying of super-cooled water. In graph (a) we turned on just strip one, (b) strips 1 and 2, and (c) three strips at the same time. In all graphs, power of $(3 \pm 1)W$ was supplied to the sample until reaching the steady-state temperature before spraying started.



Figure 6.19: Anti-icing performance of heating system with three heaters on.

Conventional Heating System

In this set of tests, all the icing conditions were performed similar to the previous experiments to have the proper comparison on the performance of the two systems. The only difference between the two tests was the heating type to see the effect of using thermally sprayed resistive heaters. The coating system heating performance was tested by exposing each sample to the harshest icing condition, which was shown in Table (6.7). The set of experiments were done based on conventional heating system from the backside of the substrate. This test provided electric currents to the Hi-density Cartridge Heater with 321 stainless steel sheath and 12.7 mm nominal diameter (DBA OMEGA Environmental, QC, Canada) for different voltages. Various voltages were applied to the system to test the heating performance. This flexible cylindrical heating element was placed inside the sample (Figure (6.21)). The possible space between the sample and the heater should not be left empty because the air breach between the sample and the heater affects the experiment's reliability. Also, the gap disturbed the uniformity of heat transfer from the heater to the substrate. Therefore high temperature and high thermally conductive paste (OT-201-2 OMEGATHERM, DBA OMEGA Environmental, QC, Canada) was used to fill the gap,

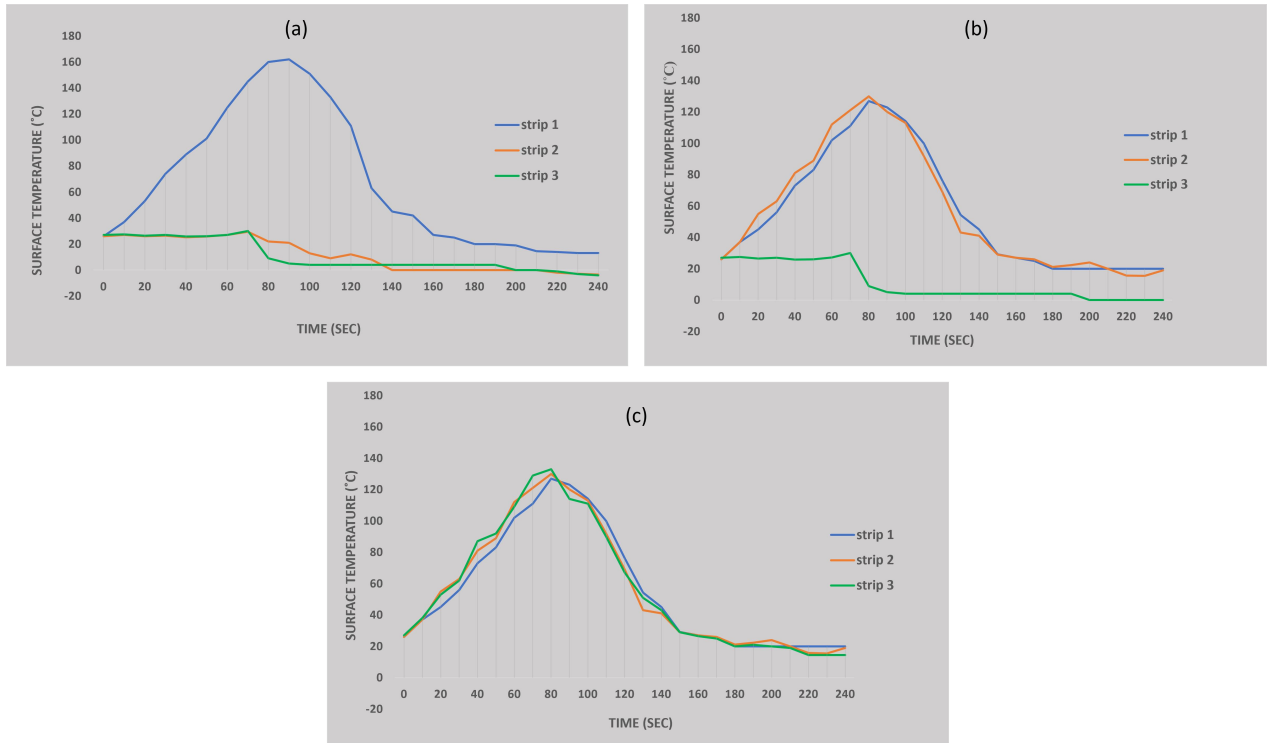


Figure 6.20: Surface temperature under icing conditions when (a) one strip, (b) two strips, and (c) three strips are turned on.

consolidate and unite the heater with the sample. For the first step, like the previous test, 20 W electrical power was supplied to the heater. We waited the surface of the sample was reaches up to the maximum stabilized temperature. Afterward, the spraying started, and the sample remained under the icing condition for 10 minutes. The heating tests were all conducted at the same initial ice temperature of $(-4 \pm 1)^\circ C$. The test aimed to determine the amount of heat required to maintain the surface of the samples free from ice. Figure (6.21) presents a schematic of the experiment’s sample preparation that was used in the icing wind tunnel for anti-icing test. It should be noted again that in this set of tests, all the icing conditions were observed as before for the purposes of comparing the performance of the two systems.

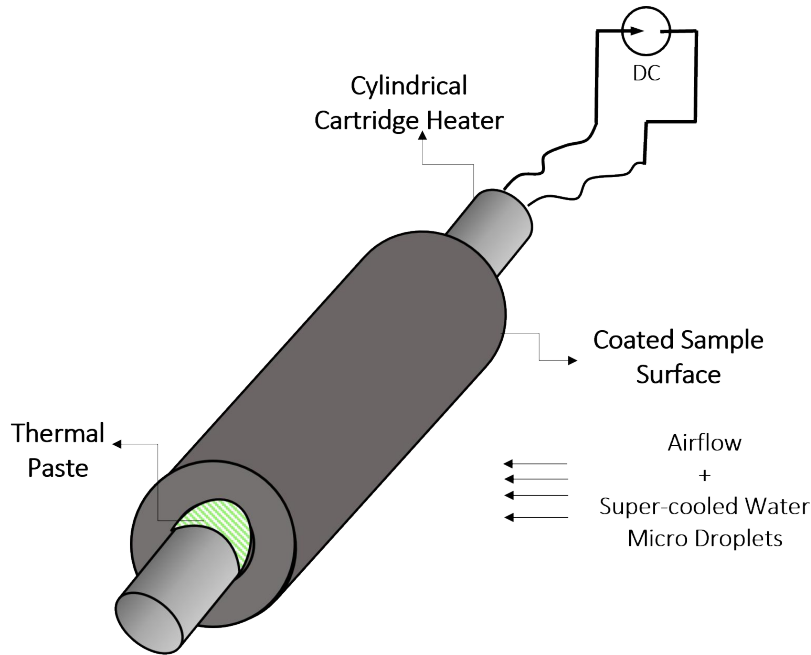


Figure 6.21: Schematic of the prepared sample for the conventional heated anti-icing test.

Figure (6.22) shows the test section and the sample holder used in the icing wind tunnel. The details of these tests are discussed in the following sections.

The test was started by supplying voltage. At first, we supplied 20 W to the heating element. Approximately it took around 15 min to reach the stabilized temperature around 110°C , and was stabilized there, then we start spraying water for 10 minutes. It was shown that ice was started to form on the surface after after around 4 min of start spraying. It was apparent that supplying 20W of power was not suitable for anti-icing in this experiment and after a short while the system will not be able to keep the surface at the required temperature, avoiding ice formation, so we increased power for 1w and repeated this process up to the power that was enough for ice mitigation for the long-enough time. Finally, We reached to this condition by applying around 26W. Then we decreased the power for 1 W and recorded the result as the anti-icing required power. These procedures were done for 6 times, and the average power intensity required for anti-icing in the harshest icing conditioned was measured. It should be noted that there are various rigid challenges for the optimization of an electro-thermal wing anti-icing system in both running-wet and evaporative regimes,

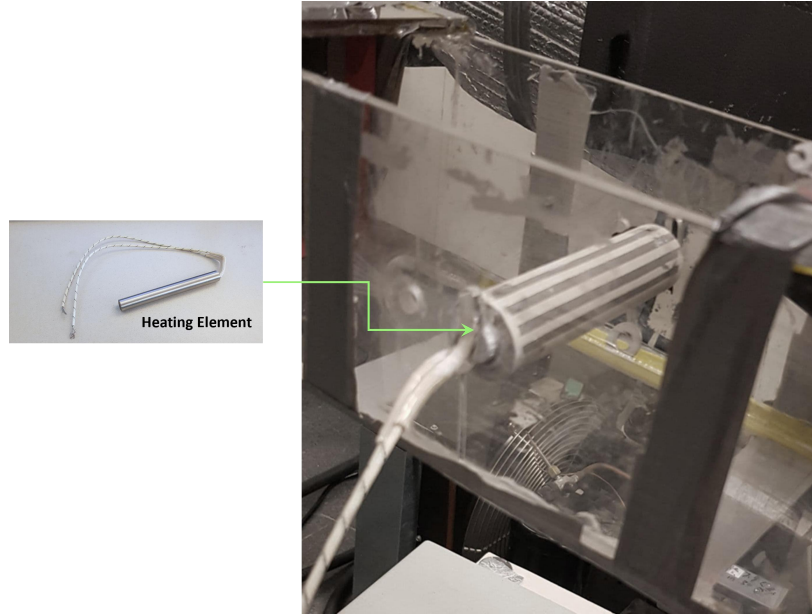


Figure 6.22: Test section and the sample holder used in the icing wind tunnel.

which have not been addressed in this study. The procedure of calibrating the required power as above-mentioned is shown in Table (6.7). In this case, the minimum power to keep the surface free from ice was around $(25 \pm 2)W$. The surface temperature decreased to $(13 \pm 1)^{\circ}C$ but remained at this temperature, and preserved the surface free from ice in 15 minutes in the icing wind tunnel.

Table 6.7: Calibration of the power required for electro thermal anti-icing.

Voltage (V)	Current (A)	Supplied Power (W)	Anti-icing Performance within 15 min
3	0.51	1.53	×
6	0.63	3.6	×
9	0.77	7.2	×
12	0.97	12	×
15	1.01	15	×
18	1.05	19.8	×
21	1.16	25.2	✓
24	1.24	28.8	✓
27	1.64	43.2	✓
30	1.93	57	✓

Figure (6.23) shows the picture captured by the infrared camera. It seems that supplying approximately $(25 \pm 2)W$ of power preserved the surface at a temperature around $(13 \pm 1)^\circ C$ which was enough for anti-icing performance. Figure (6.23) (a) presents the temperature the the surface was reached after 7 min and and was stabilized there which was the point of starting the super-cooled water spraying for 15 minutes to see the occurrence. Figure (6.23) (b) represents the surface temperature after 15 min of spraying which is in the range of $(12\text{to}13)^\circ C$ providing an ice free surface steadily. However, in contrast to the previous case (heating one thermally-sprayed resistive heater), significantly more power was required for the anti-icing process. Another important concern refers to the time that takes for the surface to reach the required temperature for anti-icing which was more than the previous experiment. It was also evident that the surface temperature was enough in the downstream regions, avoiding runback ice formation.

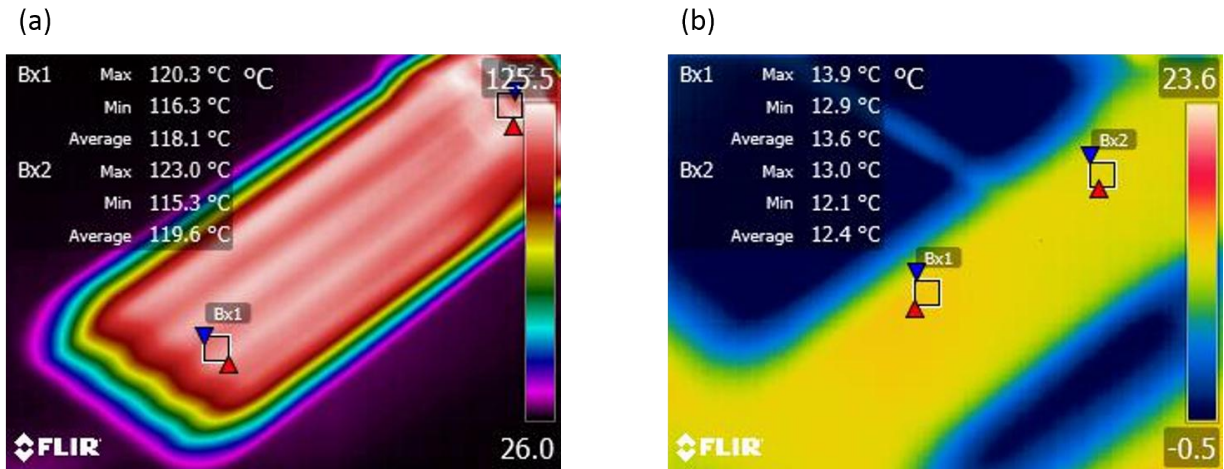


Figure 6.23: Surface temperature while heating: (a) stabilized temperature before water spraying, and (b) stabilized temperature after 15 min of water spraying.

Comparison of the Anti-icing Performance

In the present study, an effective anti-icing operation is defined as no ice could accrete over the surface during the anti-icing process. The thermally sprayed electrical elements with a specific architecture were used as an anti-icing system in the first set of tests. The second set of experiments includes using conventional electrical heating elements located in the back

of the surface. In order to compare the two anti-icing strategies, power consumption was measured for each model. For further assessment, we measured the time it took for the heaters to reach the steady-state temperature. Furthermore, a monotonic distribution of temperature was detected in both experiments. Glaze ice formation was formed throughout all the experiments, which is the most dangerous form of icing. The minimum power required consumption for preventing glaze ice formation over the thermally-sprayed model was found to be $(3 \pm 1)W$ while using an electrical element; we found the minimum power consumption to prevent glaze ice formation is $(25 \pm 2)W$ watts. Moreover, the time for the samples to reach the required temperature enough for anti-icing was significantly different in the two strategies. When using thermally-sprayed FeCrAlY heaters, in the worst case, the temperature reached $150^{\circ}C$ in just 60s while for the heating elements, this time was at least 7 min which was significantly longer. Moreover the temperature in thermally-sprayed heaters reached around $220^{\circ}C$ while the heating element under the best circumstance reached to $120^{\circ}C$. Figure (6.24) presents the comparison of two strategies regarding the time required to reach the steady-state temperature.

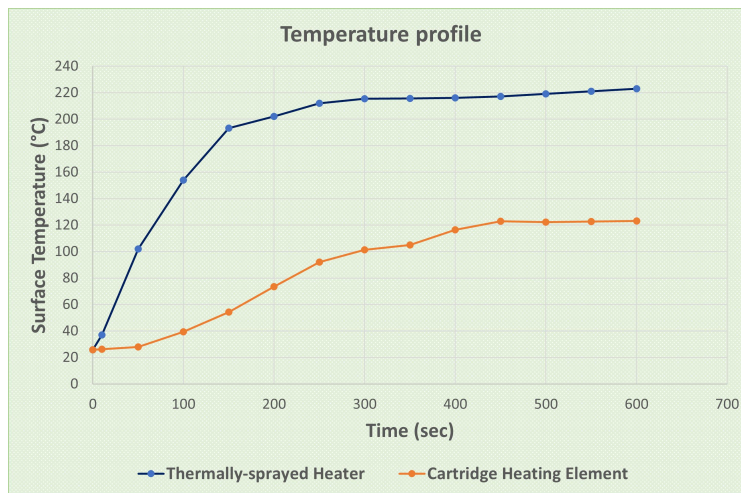


Figure 6.24: Temperature variation versus time for thermally-sprayed heater and cartridge heating element.

Using a commercially available heating element, we consumed more energy to reach the required temperature for anti-icing conditions. A faster heating up requires a considerable amount of energy compared with using thermally-sprayed resistive heaters. Moreover, through the results obtained from the infrared camera, the temperature distribution on the surface was significantly more uniform in the thermally-sprayed resistive heaters. It could be recognized that this study was an achievement in the improvement of the anti-icing system as it yielded the anticipated outcomes. Using this system brings a massive saving in energy consumption and shows a faster response in anti-icing performance, resulting in a more reliable IPS system. In addition, it should be considered that another great advantage of this technique is controllability. Using the proposed heating system, we could heat-up the elements at any time, and wherever required. This improvement is desirable as we could develop a high controllable IPS system that requires a small amount of energy for outstanding performance compare with other prevalent thermal IPS systems. This extraordinary results can be related to several facts. In this connection some of the more prominent reasons can be itemized as follows:

- Typically, conventional thermal ice protection systems are subject to intrinsic limitations associated with heating element geometry and physical location, while thermally-sprayed electrical elements directly on surfaces can overcome these limitations by tailoring the geometry of the heating element to the application.
- Heat transfer rate in thermally-sprayed heating elements becomes maximized by minimizing the distance between the heater and the surface to be heated (intimate contact of heating elements and the to-be-heated surface).
- Thermally sprayed techniques are comparatively cost-efficient compared to the other methods of surface heating because, in this method, the massive heating pieces of equipment are eliminated, and complex installment is preventable.
- This method enables the temperature to reach up to 600°C, which is not reachable in other types of heating elements. Moreover, these type of heating elements is warmed up significantly faster than the other privileged types (very fast warm-up).

- The temperature distribution is more uniform than other heating elements due to far-reaching contact between the thermally-sprayed heating element and the to-be-protected surface.
- Immunity from thermal shocks, which notably affects heaters specially on ceramic

Our study of the anti-icing heat load reduction mechanism provides valuable guidance for designing a beneficial thermal anti-icing system in all aspects. This information can be used to design an effective ice protection system for the aircraft's wings leading edge and wind turbine blades or any other components with an aerodynamic profile. Based on the presented results, it is possible to improve the configuration of the thermal anti-icing system, which will reduce the weight and energy requirements despite particular limitations. In order to meet the anti-icing requirements in practical applications, the margins for both the anti-icing heat load and protected area need to be increased accordingly. In addition, regarding the amount of heating power that can be provided, extra consideration must also be given to the density of this power. It should be mentioned that we anticipate that ice-phobic coatings will improve performance under these conditions. Compared to the conventional ice protection methods (brutally heating the entire hydrophilic surface) to keep the surface free from ice, the hybrid strategy was found that substantially requires less power to provide the same anti-icing performance. However, there is a severe problem with such surfaces regarding their durability under icing conditions. This reason also was applied in our study that we could not use the available commercial superhydrophobic coating in our experiment as its very low durability against icing circumstances. However, some superhydrophobic coatings were found that can tolerate the harsh condition of icing, which will lead us to have a more developed ice protection system.

Chapter 7

Conclusion and Future Works

In this study, the fabrication of a FeCrAlY coating layer on an aluminum substrate for anti-icing application was examined. For the fabrication of the proposed structure the plasma spray technique was used. Then this strategy was compared with the conventional heating strategy to assess the advantages of this technique regarding energy consumption and safety. The first group of experiments comprised ice accretion tests to show the effect of superhydrophobic surfaces on anti-icing performance. Results showed that the ice accretion process on the SHS-coated surface was much less than that of the hydrophilic surface. In the second and the major group of tests, thermally-sprayed resistive heaters' anti-icing performance was compared with conventional heating elements' anti-icing effectiveness. We concluded that in our testing condition, heaters needs to be supplied by an average power of $(4 \pm 1)W$ to have acceptable anti-icing performance while heating the substrate with conventional heating elements required to consume at least $(25 \pm 2)W$ of power which was approximately six times greater than that of thermally-sprayed heaters. In addition, the time required for the to-be-heated surface to reach a stable and high enough temperature for anti-icing was significantly different between the two systems; thermally-sprayed resistive heaters can be reached ($120^{\circ}C$) in just 1 min while this time for the cartridge heating elements takes around 7 min. Moreover, it was also apparent that implementing the thermally-sprayed resistive heaters in functional conditions will be cost-effective as it is much easier to use than the cartridge heater. Also, using thermal spray techniques will let industries use different materials in ice protection systems without any restriction, and at the same time, they will enable the

implementation of their techniques on the complex geometries of to-be-protected surfaces. Controllability of heating strategy regarding the required time and location of protection is another benefit of this method. Although the proposed system is a simple setup, all the results demonstrate that using this strategy can bring significant advantages.

7.1 Future Works

Based on, the findings in this study the following directions for future research can be envisioned.

- Feasibility of developing more efficient multi-functional ice protection system (use thermal spray methods).
- Examine coating adhesion to various aerospace substrates (aluminum, carbon fiber-reinforced polymer (FRPC), glass fiber reinforce polymer (GFRP), and metal composite laminate).
- Coating development on more complex aerodynamic surfaces.
- Investigating the performance of using a durable superhydrophobic surface coating in the icing condition enabling to take advantage of ice-phobicity characteristic of superhydrophobic surfaces under the harsh weather condition.
- Using other metallic materials instead of FeCrAl_y, for the deposition of a heating element coating, and comparing their performances with each other.
- Life cycle assessment and benefit assessment of the system in practical application
- Using thermal spray techniques makes it possible to deposit a wide variety of materials on different substrates. Therefore it would be possible to take advantage of specific material characteristics. For example, deposition the resistive material on the composite structures without damaging such temperature-sensitive materials.

Bibliography

- [1] P. Irajizad, S. Nazifi, and H. Ghasemi, “Icephobic surfaces: Definition and figures of merit,” *Advances in colloid and interface science*, vol. 269, pp. 203–218, 2019.
- [2] L. B. Boinovich and A. M. Emelyanenko, “Anti-icing potential of superhydrophobic coatings,” *Mendeleev Communications*, vol. 1, no. 23, pp. 3–10, 2013.
- [3] P. Nordin and G. Strindberg, “Multifunctional de-icing/anti-icing system,” Jan. 13 2015, uS Patent 8,931,740.
- [4] A. Dolatabadi *et al.*, “Ice-phobic evaluation of super-hydrophobic coatings for aircraft icing protection,” *Montreal: PWC*, 2010.
- [5] J. Steuernagle, K. Roy, and D. Wright, “Aircraft icing,” *Safety Advisor (Weather No. 1)*, Air Safety Foundation, Sponsored by the FAA, Flight Safety Branch, 2008.
- [6] K. R. Petty and C. D. Floyd, “11.2 a statistical review of aviation airframe icing accidents in the us.”
- [7] A. Aventin, F. Morency, and S. Nadeau, “Statistical study of aircraft accidents and incidents related to de/anti-icing process in canada between 2009 and 2014,” 2015.
- [8] M. K. Politovich, “Aircraft icing caused by large supercooled droplets,” *Journal of Applied Meteorology (1988-2005)*, pp. 856–868, 1989.
- [9] —, “Predicting in-flight aircraft icing intensity,” *Journal of aircraft*, vol. 40, no. 4, pp. 639–644, 2003.

- [10] T. A. Talay, *Introduction to the Aerodynamics of Flight*. Scientific and Technical Information Office, National Aeronautics and Space . . . , 1975, vol. 367.
- [11] G. Mingione, M. Barocco, E. Denti, F. G. Bindi, and D. French, “Flight in icing conditions,” *Direction gnrale de l’aviation civile, DGAC, Tech. Rep*, 1997.
- [12] T. Cebeci and F. Kafyeke, “Aircraft icing,” *Annual review of fluid mechanics*, vol. 35, no. 1, pp. 11–21, 2003.
- [13] M. Politovich, “Aircraft icing,” *Encyclopedia of atmospheric sciences*, vol. 358, no. 1776, pp. 68–75, 2003.
- [14] S. G. Cober, G. A. Isaac, and J. W. Strapp, “Characterizations of aircraft icing environments that include supercooled large drops,” *Journal of Applied Meteorology*, vol. 40, no. 11, pp. 1984–2002, 2001.
- [15] H. Ibrahim, L. Ould Rouis, C. Masson, and D. Rouse, “Optimisation par contrôle d’un système de dégivrage électrothermique d’une pale d’éolienne,” 2015.
- [16] L. Gao, Y. Liu, L. Ma, and H. Hu, “A hybrid strategy combining minimized leading-edge electric-heating and superhydro-/ice-phobic surface coating for wind turbine icing mitigation,” *Renewable Energy*, vol. 140, pp. 943–956, 2019.
- [17] T. Strobl, S. Storm, D. Thompson, M. Hornung, and F. Thielecke, “Feasibility study of a hybrid ice protection system,” *Journal of Aircraft*, vol. 52, no. 6, pp. 2064–2076, 2015.
- [18] H. Sojoudi, M. Wang, N. Boscher, G. H. McKinley, and K. K. Gleason, “Durable and scalable icephobic surfaces: similarities and distinctions from superhydrophobic surfaces,” *Soft matter*, vol. 12, no. 7, pp. 1938–1963, 2016.
- [19] X. Huang, N. Tepylo, V. Pommier-Budinger, M. Budinger, E. Bonaccorso, P. Villedieu, and L. Bennani, “A survey of icephobic coatings and their potential use in a hybrid coating/active ice protection system for aerospace applications,” *Progress in Aerospace Sciences*, vol. 105, pp. 74–97, 2019.

- [20] C. Antonini, M. Innocenti, T. Horn, M. Marengo, and A. Amirfazli, “Understanding the effect of superhydrophobic coatings on energy reduction in anti-icing systems,” *Cold Regions Science and Technology*, vol. 67, no. 1-2, pp. 58–67, 2011.
- [21] K. Al-Khalil, “Energy-efficient electro-thermal ice-protection system,” May 4 2010, uS Patent 7,708,227.
- [22] C. Stenroos, “Properties of icephobic surfaces in different icing conditions,” Master’s thesis, 2015.
- [23] Z. Goraj, “An overview of the deicing and anti-icing technologies with prospects for the future,” in *24th international congress of the aeronautical sciences*, vol. 29, 2004.
- [24] K. Greenly, “Recent developments in aircraft ice protection systems,” *Aircraft Engineering and Aerospace Technology*, 1963.
- [25] O. Fakorede, Z. Feger, H. Ibrahim, A. Ilinca, J. Perron, and C. Masson, “Ice protection systems for wind turbines in cold climate: characteristics, comparisons and analysis,” *Renewable and Sustainable Energy Reviews*, vol. 65, pp. 662–675, 2016.
- [26] K. Lum, D. Chandler, and J. D. Weeks, “Hydrophobicity at small and large length scales,” 1999.
- [27] T. Young, “Iii. an essay on the cohesion of fluids,” *Philosophical transactions of the royal society of London*, no. 95, pp. 65–87, 1805.
- [28] X. Wu, V. V. Silberschmidt, Z.-T. Hu, and Z. Chen, “When superhydrophobic coatings are icephobic: Role of surface topology,” *Surface and Coatings Technology*, vol. 358, pp. 207–214, 2019.
- [29] S. Kulinich and M. Farzaneh, “How wetting hysteresis influences ice adhesion strength on superhydrophobic surfaces,” *Langmuir*, vol. 25, no. 16, pp. 8854–8856, 2009.
- [30] M. J. Kreder, J. Alvarenga, P. Kim, and J. Aizenberg, “Design of anti-icing surfaces: smooth, textured or slippery?” *Nature Reviews Materials*, vol. 1, no. 1, pp. 1–15, 2016.

- [31] J. T. Simpson, S. R. Hunter, and T. Aytug, “Superhydrophobic materials and coatings: a review,” *Reports on Progress in Physics*, vol. 78, no. 8, p. 086501, 2015.
- [32] M. Nosonovsky and V. Hejazi, “Why superhydrophobic surfaces are not always icephobic,” *ACS nano*, vol. 6, no. 10, pp. 8488–8491, 2012.
- [33] T. M. Schutzius, S. Jung, T. Maitra, P. Eberle, C. Antonini, C. Stamatopoulos, and D. Poulikakos, “Physics of icing and rational design of surfaces with extraordinary icephobicity,” *Langmuir*, vol. 31, no. 17, pp. 4807–4821, 2015.
- [34] N. Alegre, “Full-scale runback ice: accretion and aerodynamic study,” 2010.
- [35] M. Sinnott, “787 no-bleed systems: saving fuel and enhancing operational efficiencies,” *Aero Quarterly*, vol. 18, pp. 6–11, 2007.
- [36] K. Al-Khalil, “Energy-efficient electro-thermal and electro-mechanical ice-protection method,” Apr. 30 2013, uS Patent 8,430,359.
- [37] E. Celia, T. Darmanin, E. T. de Givenchy, S. Amigoni, and F. Guittard, “Recent advances in designing superhydrophobic surfaces,” *Journal of colloid and interface science*, vol. 402, pp. 1–18, 2013.
- [38] M. Farzaneh, C. Volat, and A. Leblond, “Anti-icing and de-icing techniques for overhead lines,” in *Atmospheric icing of power networks*. Springer, 2008, pp. 229–268.
- [39] J. G. Duman, “Animal ice-binding (antifreeze) proteins and glycolipids: an overview with emphasis on physiological function,” *Journal of Experimental Biology*, vol. 218, no. 12, pp. 1846–1855, 2015.
- [40] S. AMS, “1428 air-craft deicing/anti-icing fluids,” 2007.
- [41] T. Bharathidasan, S. V. Kumar, M. Bobji, R. Chakradhar, and B. J. Basu, “Effect of wettability and surface roughness on ice-adhesion strength of hydrophilic, hydrophobic and superhydrophobic surfaces,” *Applied Surface Science*, vol. 314, pp. 241–250, 2014.

- [42] T. C. Government, “Aircraft critical surface contamination training for aircrew and ground-crew,” <https://tc.canada.ca/en/aviation/publications/when-doubt-small-large-aircraft-aircraft-critical-surface-contamination-training-tp-10643s>, Dec. 2004.
- [43] M. Davies, *Standard handbook for aeronautical and astronautical engineers*. McGraw-Hill Education, 2003.
- [44] J. Jordan, “Overview of designing a freezing point depressant ice protection system,” <https://www.cav-systems.com/>, 2020.
- [45] I. D. Inc, “Runway and aircraft weather sensing technology,” <https://icesight.com/index.php>, 2020.
- [46] K. Al-Khalil, T. Ferguson, D. Phillips, K. Al-Khalil, T. Ferguson, and D. Phillips, “A hybrid anti-icing ice protection system,” in *35th Aerospace Sciences Meeting and Exhibit*, 1997, p. 302.
- [47] L. J. Adams, N. A. Weisend Jr, and T. E. Wohlwender, “Attachable electro-impulse de-icer,” Jul. 14 1992, uS Patent 5,129,598.
- [48] R. J. Shaw, J. J. Reinmann, and T. Miller, “Nasa’s rotorcraft icing research program,” *NTRS 19880007258, NASA, Washington, DC*, pp. 802–832, 1988.
- [49] D. W. Newton, *Severe weather flying*. Aviation Supplies & Academics, 2002.
- [50] L. A. Haslim and R. D. Lee, “Electromagnetic repulsive deicer for aircraft,” 1987.
- [51] a. E. Francis, Khawar, “Aircraft anti-icing and deicing systems,” <https://www.slideshare.net/ErangaJrABW/aircraft-anti-icing-deicing-sytems-project-report>, 2014.
- [52] SKYbrary, “Ice and rain protection, control systems,” https://www.skybrary.aero/index.php/Aircraft_Ice_Protection_Systemst, 2019.
- [53] C. . Company, “Electro-mechanical expulsion deicing system,” <https://www.coxandco.com/index.html>, 2019.

- [54] G. R. C. in NASA, “Ultra-sound deicing system,” <https://technology.grc.nasa.gov/>, 2019.
- [55] B. Canada, “General pneumatic and hot air ice protection techniques,” <https://studylib.net/doc/18082442/10th-stage-and-14th-stage-bleed-air.-the-10th-stage>, 2019.
- [56] J. P. Lewis and D. T. Bowden, “Preliminary investigation of cyclic de-icing of an airfoil using an external electric heater,” 1952.
- [57] J. Sloan, “787 integrates new composite wing deicing system,” *High Performance Composites*, vol. 17, no. 1, pp. 27–29, 2009.
- [58] D. Briand, F. Beaudoin, J. Courbat, N. F. de Rooij, R. Desplats, and P. Perdu, “Failure analysis of micro-heating elements suspended on thin membranes,” *Microelectronics Reliability*, vol. 45, no. 9-11, pp. 1786–1789, 2005.
- [59] M. Prudenziati, G. Cirri, and P. Dal Bo, “Novel high-temperature reliable heaters in plasma spray technology,” *Journal of thermal spray technology*, vol. 15, no. 3, pp. 329–331, 2006.
- [60] J.-M. Lamarre, P. Marcoux, M. Perrault, R. C. Abbott, and J.-G. Legoux, “Performance analysis and modeling of thermally sprayed resistive heaters,” *Journal of thermal spray technology*, vol. 22, no. 6, pp. 947–953, 2013.
- [61] C. Mayer, “Système électrothermique de dégivrage pour une pale d’éolienne: simulations en soufflerie réfrigérée et impact sur la puissance produite,” Ph.D. dissertation, Université du Québec à Rimouski, 2007.
- [62] C. C. Ryerson, “Assessment of superstructure ice protection as applied to offshore oil operations safety ice protection technologies, safety enhancements, and development needs,” 2009.
- [63] G. C. Botura and J. Hu, “Ice phobic material to reduce runback ice,” Dec. 29 2020, uS Patent 10,875,632.

- [64] Q. Liu, Y. Yang, M. Huang, Y. Zhou, Y. Liu, and X. Liang, “Durability of a lubricant-infused electrospray silicon rubber surface as an anti-icing coating,” *Applied Surface Science*, vol. 346, pp. 68–76, 2015.
- [65] T. A. Rickard and O. C. Ralston, *Flotation*. Mining and Scientific Press, 1917.
- [66] J. W. Gibbs, “Art. lii.—on the equilibrium of heterogeneous substances,” *American Journal of Science and Arts (1820-1879)*, vol. 16, no. 96, p. 441, 1878.
- [67] R. N. Wenzel, “Resistance of solid surfaces to wetting by water,” *Industrial & Engineering Chemistry*, vol. 28, no. 8, pp. 988–994, 1936.
- [68] A. Cassie, “Contact angles,” *Discussions of the Faraday society*, vol. 3, pp. 11–16, 1948.
- [69] W. Barthlott and C. Neinhuis, “Purity of the sacred lotus, or escape from contamination in biological surfaces,” *Planta*, vol. 202, no. 1, pp. 1–8, 1997.
- [70] C. E. Carraher Jr, *Introduction to polymer chemistry*. CRC press, 2012.
- [71] A. Ulman, “Formation and structure of self-assembled monolayers,” *Chemical reviews*, vol. 96, no. 4, pp. 1533–1554, 1996.
- [72] T. Onda, S. Shibuichi, N. Satoh, and K. Tsujii, “Super-water-repellent fractal surfaces,” *Langmuir*, vol. 12, no. 9, pp. 2125–2127, 1996.
- [73] J. Aizenberg, M. Aizenberg, S. H. Kang, T. S. Wong, and B. Kim, “Slippery surfaces with high pressure stability, optical transparency, and self-healing characteristics.” 2013, uS Patent 9-121-307. [Online]. Available: <https://patents.google.com/patent/US9121306B2/en>
- [74] B. Bhushan, “Biomimetics inspired surfaces for drag reduction and oleophobicity/philicity,” *Beilstein journal of nanotechnology*, vol. 2, no. 1, pp. 66–84, 2011.
- [75] D. Anderson, A. Reich, D. Anderson, and A. Reich, “Tests of the performance of coatings for low ice adhesion,” in *35th Aerospace Sciences Meeting and Exhibit*, 1997, p. 303.

- [76] W. M. Leary, *We Freeze to Please: A History of NASA's Icing Research Tunnel and the Quest for Flight Safety*. National Aeronautics and Space Administration, 2002, vol. 4226.
- [77] X. Sun, V. G. Damle, S. Liu, and K. Rykaczewski, "Bioinspired stimuli-responsive and antifreeze-secreting anti-icing coatings," *Advanced Materials Interfaces*, vol. 2, no. 5, p. 1400479, 2015.
- [78] C. Urata, G. J. Dunderdale, M. W. England, and A. Hozumi, "Self-lubricating organogels (slugs) with exceptional syneresis-induced anti-sticking properties against viscous emulsions and ices," *Journal of Materials Chemistry A*, vol. 3, no. 24, pp. 12 626–12 630, 2015.
- [79] M. Sinnett, "Saving fuel and enhancing operational efficiencies," *vol. AERO Q*, vol. 4, p. 6, 2007.
- [80] M. Ruan, W. Li, B. Wang, B. Deng, F. Ma, and Z. Yu, "Preparation and anti-icing behavior of superhydrophobic surfaces on aluminum alloy substrates," *Langmuir*, vol. 29, no. 27, pp. 8482–8491, 2013.
- [81] M. Pourbagian and W. G. Habashi, "Surrogate-based optimization of electrothermal wing anti-icing systems," *Journal of aircraft*, vol. 50, no. 5, pp. 1555–1563, 2013.
- [82] A. G. Aissaoui and A. Tahour, *Wind Turbines: Design, Control and Applications*. BoD–Books on Demand, 2016.
- [83] L. Gao, Y. Liu, C. Kolbakir, and H. Hu, "An experimental investigation on an electric-thermal strategy for wind turbines icing mitigation," in *2018 Atmospheric and Space Environments Conference*, 2018, p. 3658.
- [84] M. Papadakis, G. ZUMWALT, J. KIM, R. Elangovan, and G. FREUND, JR, "An experimental method for measuring droplet impingement efficiency on two-and three-dimensional bodies," in *24th Aerospace Sciences Meeting*, 1986, p. 406.

- [85] R. M. Waldman, H. Li, and H. Hu, “An experimental investigation on the effects of surface wettability on water runback and ice accretion over an airfoil surface,” in *8th AIAA Atmospheric and Space Environments Conference*, 2016, p. 3139.
- [86] Y. Liu, L. Li, H. Li, and H. Hu, “An experimental study of surface wettability effects on dynamic ice accretion process over an uas propeller model,” *Aerospace Science and Technology*, vol. 73, pp. 164–172, 2018.
- [87] S. Struggl, J. Korak, and C. Feyrer, “A basic approach for wing leading deicing by smart structures,” in *Sensors and Smart Structures Technologies for Civil, Mechanical, and Aerospace Systems 2011*, vol. 7981. International Society for Optics and Photonics, 2011, p. 79815L.
- [88] T. Strobl, S. Storm, and S. Ameduri, “Synergic effects of passive and active ice protection systems,” in *Morphing Wing Technologies*. Elsevier, 2018, pp. 841–864.
- [89] K. R. Khedir, *Superhydrophobic nanostructured coating for anti-icing applications*. University of Arkansas at Little Rock, 2012.
- [90] K. Morita, S. Kimura, and H. Sakaue, “Hybrid system combining ice-phobic coating and electrothermal heating for wing ice protection,” *Aerospace*, vol. 7, no. 8, p. 102, 2020.
- [91] H. M. Ali, M. A. Qasim, S. Malik, and G. Murtaza, “Techniques for the fabrication of super-hydrophobic surfaces and their heat transfer applications,” *Heat Transfer-Models, Methods and Applications*, vol. 1, pp. 284–315, 2018.
- [92] D. Tejero-Martin, M. R. Rad, A. McDonald, and T. Hussain, “Beyond traditional coatings: A review on thermal-sprayed functional and smart coatings,” *Journal of Thermal Spray Technology*, vol. 28, no. 4, pp. 598–644, 2019.
- [93] D. E. Crawmer, “Introduction to coatings, equipment and theory,” *Hand book of thermal spray technology*, ASM International, Materials Park, OH, USA, pp. 43–46, 2004.
- [94] J. R. Davis *et al.*, *Handbook of thermal spray technology*. ASM international, 2004.

- [95] P. Fauchais, “Understanding plasma spraying,” *Journal of Physics D: Applied Physics*, vol. 37, no. 9, p. R86, 2004.
- [96] M. Prudenziati and M. L. Gualtieri, “Electrical properties of thermally sprayed ni and ni20cr-based resistors,” *Journal of Thermal Spray Technology*, vol. 17, no. 3, pp. 385–394, 2008.
- [97] G. R. S. Techn, “Selected patents related to thermal spraying,” 2009.
- [98] T. I. I. P. L. S. F. H. . SENSING), “Industrial heaters,” <https://tempsens.com/>, 2020.
- [99] H. Herman, S. Sampath, and R. McCune, “Thermal spray: current status and future trends,” *MRS bulletin*, vol. 25, no. 7, pp. 17–25, 2000.
- [100] B. Group, “In-flight aircraft ice protection with a proprietary technology based on resistive heating coating,” <https://www.battelle.org/government-offerings/national-security/payloads-platforms-controls/deicing-technology/article-the-science-of-corrosion-busting-smart-coatings>, 2020.
- [101] O. Metco, “Metco materials e-guide,” <https://mymetco.oerlikon.com/en-us/category/materials>, 2021.
- [102] M. Zimbru, M. D’Aniello, A. D. Martino, M. Latour, G. Rizzano, and V. Piluso, “Investigation on friction features of dissipative lap shear connections by means of experimental and numerical tests,” *The Open Construction & Building Technology Journal*, vol. 12, no. 1, 2018.
- [103] V. Msomi, “Vanadium dioxide thermochromic thin films correlation between microstructure, electrical and optical properties,” Ph.D. dissertation, 2008.
- [104] N. Sharifi, A. Dolatabadi, M. Pugh, and C. Moreau, “Anti-icing performance and durability of suspension plasma sprayed tio2 coatings,” *Cold Regions Science and Technology*, vol. 159, pp. 1–12, 2019.
- [105] A. Ganvir, “Design of suspension plasma sprayed thermal barrier coatings,” Ph.D. dissertation, University West, 2018.